UNIVERSITÀ DI PISA

Scuola di Dottorato in Ingegneria “Leonardo da Vinci”
Stefano Bennati (Direttore)

Programma di Dottorato in Automatica Robotica e Bioingegneria
Andrea Caiti (Presidente)

PRESENT AND FUTURE PERVASIVE HEALTHCARE METHODOLOGIES: INTELLIGENT BODY DEVICES, PROCESSING AND MODELING TO SEARCH FOR NEW CARDIOVASCULAR AND PHYSIOLOGICAL BIOMARKERS

PhD Thesis
SSD: ING-INF/06

Tutor:
Dr. Giovanni PIOGGIA

Doctoral Dissertation of:
Gennaro TARTARISCO

June 2013

Summary

In order to face the new healthcare challenges, Personal Health Systems (PHS) are envisioning a new generation of devices and applications dedicated to embody the most recent and evidence-based knowledge and to transform the collected information into a valuable intelligence support. The aim of the PHS is to improve the quality of the healthcare services for all of the stages of an individual's care cycle assisting in the provision of a continuum of care for subjects with chronic conditions and older adults in the home and community settings and reducing both the number of hospitalizations and caregivers. In the modern concept of PHS-based models focused on the user empowerment, the ownership of the care service is fully taken by the individual. Under this model, the technological innovations can help each person to self-engage and manage his/her own health status, minimizing any interaction with other health care actors. Even if, in the clinical practice this model has not been yet implemented, it can be considered as a target to be reached achieving at the same time the empowerment of the users and the reduction of workload and costs, as well as the preservation of the quality and safety of care. The main reasons for the lack of effective implementations of PHS range from legal and societal obstacles, issues related to the real application of wearable devices,

inappropriate use of decision support systems and the skepticism of many healthcare professionals. Wearable devices need to be non-intrusive, easy to use, and comfortable to wear, efficient in power consumption, privacy compliant, with very low failure rates and high accuracy in triggering alarms, especially if used for diagnostic purposes.

The aim of this thesis is focused on emerging personal unobtrusive technologies and new methodologies for early diagnosis and personalized treatment and rehabilitation for individuals with cardiovascular and neurophysiological diseases, integrating the current clinical efforts.
The investigation on physiological processes has been focused on:

- Innovation in personal on body devices (miniaturization and unobtrusiveness, accuracy, specificity, sensitivity and power management) to acquire, monitor and communicate physiological parameters and other health related context of an individual (e.g., vital body signs, activity, emotional and social state)
- Signal processing, feature extraction and use of pattern recognition techniques such as learning algorithms based on artificial neural networks of the acquired information and coupling of it with expert biomedical knowledge to derive important new insights about individual's health status

The proposed bioengineering approach in the first part of the thesis is focused on early diagnosis. Special attention was paid to the valvular heart diseases and to the study of muscular fatigue, an important symptom of neuromuscular diseases (EU project OASIS). The second part is dedicated to the bioengineering support to improve the personalization of the treatment. The research activity was focused on the clinical assessment of a wearable sensing set for long term monitoring of the ECG signals (EU project CHIRON) and studies of heart rate variability assessment and the characterization of a novel sensing technology for lower limb rehabilitation of patients after stroke (at Spaulding Rehabilitation Hospital, Harvard MIT division).

Heart murmurs were investigated developing a digital stethoscope for the automatic classification and screening of cardiac valve disease in developing countries. In the last century, many efforts have been made in order to develop sophisticated techniques for the early diagnosis of cardiac disorders but the screening of cardiac valve disease in these places is limited by costs and by the necessity to train skilled sonographers. Even if during last ten years some works provided interesting results about the automatic classification of heart valve disease, we still suffer the lack of heart sound screening methods and results for a practical contextualized use. The aim of the study was to develop a new body device mechanically designed to reject the environmental noise, easy to use, integrated with a new pattern recognition approach based on both hierarchical and the fusion of neural networks with fuzzy rules for the automatic classification of heart murmurs to be used for clinical screening purposes. The digital stethoscope developed to achieve this goal uses the front-end board and one high sensitive microphone integrated into a Littmann Stethoscope to capture the acoustic sound waves of the heart. This board contains the necessary circuitry for signal conditioning and acquisition from the sensor. The analog signals are amplified and digitized before transmitting them to the digital signal processing unit (DSP) for further processing, analysis, and display. The DSP is the nucleus of the system. DSP produced by Texas Instruments (TI) is a high performance and low power fixed-point DSP. It has plentiful on-chip peripheral interfaces and among these, the Universal Asynchronous Receive/Transmitter (UART) interface was used both to provide signal between microphone and DSP and to the PC application for display. The firmware of DSP was developed using Code Composer Studio. The participants of the study were 120 patients with heart valve diseases and 40 control subjects both validated by ecodoppler. The heart sounds were recorded in sequence with the digital stethoscope from two sites of auscultation: the first at the third left intercostal space, and the second on the mitral space in supine position for 2 minutes. Each cardiac cycle was then digitally segmented into two parts: the systolic period (S1-S2) and the diastolic period (S2-S1). Signals were then processed to

extract relevant features in time and frequency domain of each segmented signal. In order to extract these knowledge about stenosis and regurgitation in time domain was extracted the distance between S1 and S2, which was obtained after the peak detection with the homomorfing filter, the entropy and the root mean square (RMS) of the heart cycle. In frequency domain, considering that the signal is not stationary, the discrete Wavelet transform was applied to extract features from the segmented phonocardiogram signals. Wavelet coefficients were extracted using Daubechies-2 wavelet. After the feature extraction, two models of classification were implemented:

1- A neural network model based on a hierarchical architecture of self-organizing Kohonen maps was realized (1st level: to recognize healthy or valve disease; 2nd level: aortic or mitral valve disease; 3rd level: stenosis or regurgitation)

2- A neural network model based on a self-organizing Kohonen map combined with fuzzy rules to improve the performances of classification.

The distributed adaptable parameters of the models were modified through a learning process according to a dataset consisting of signal features and Eco Doppler scores. In order to check the generalization capability of the neural network, the leave one subject out validation process was carried out. The hierarchical model recognized at the 1st level with 89% sensitivity and 85% specificity. The second model implemented has shown increased sensitivity and specificity of 95% and 91%

respectively. Moreover a success rate of about 80% for recognition of combined aortic and mitral diseases was achieved.

In the second study dedicated to early diagnosis, an architecture to monitor symptoms of muscular fatigue at home, to motivate the subjects to perform training exercises and to provide a report to the physicians about muscular strengthening was designed. The whole architecture consists of three main components: the sEMG acquisition sensor platform, the mobile acquisition system and the remote database integrating the decision support system. These three components interact with each other through wireless connections. The algorithm is organized as follows:

1. Acquisition of data from the mobile module
2. Transmission of data to the central database
3. Processing of data by the support system
4. Sending the report to the physicians

The system introduces an innovative ontology enabling and facilitating interoperability for the patient and physicians. The function of the mobile device is to implement the measurement protocol acquiring and processing sEMG data, while displaying data gathered by the sEMG sensor platform and the movement of the subject through an avatar. The EMG signal is acquired using a dedicated small wireless sensor platform that can record and transmit physiological data in real-time. The firmware of the microcontroller is programmed using the open-source research platform TinyOS. Forty volunteers (age range 66.56 ± 7.03 years; height 167.8 ± 5.03 cm; weight 74.18 ± 12.82 kg) were enrolled. All subjects were healthy with sedentary lifestyle; they had no known neuromuscular or cardiovascular disease. Most participants' (98%) were normal weight with a BMI >=20 and <25 followed by 2% being overweight with a BMI >=25 and <30. The majority of subjects were women (55%). All subjects were asked to use the device providing training, a tablet with the software application pre-installed and a user manual with experimental instructions. The software application asks a subject to wear the sensor following dedicated instructions and to perform an exercise, based on isometric knee extension while seating, in order to investigate the muscular fatigue of the vastus medialis. The sEMG data are acquired using bipolar configuration of two Ag–AgCl surface electrodes, placed over the right vastus medialis muscle with inter-electrode distance of 20 mm. During the test, the subject's upper body is firmly secured to the seat with the hip and knee joint angles at 90º from full extension. During the task, each subject is asked to maintain a maximal voluntary contraction for approximately 5 s and a rest position for approximately 1 s up to exhaustion. The wearable wireless platform, the stream of information and the data processing techniques are managed by the application. In order to train the support system, the Borg ratio scale is simultaneously measured during the endurance task, i.e. the application asks the user each minute to rate the perceived exertion ranging from 0 to 10 values. Endurance tasks are interrupted when the subject is no longer able to perform the exercise. Data are segmented extracting only the knee extensions intervals in order to assess the sEMG signal during isometric contractions. The Kohonen Self Organizing predictive model (KSOM) was used to assess six levels of muscular fatigue: none, weak, moderate, strong, very strong, extremely strong, respectively extracted from the Borg scale. The sEMG monitoring system was used to monitor and infer indexes of muscular performance during exercises of the subjects at home, focusing on the analysis and investigation of the correlation between the extraction of sEMG parameters such as the average rectified value (AVR), the root mean square (RMS) and the instantaneous median frequency (IMDF) and the level of muscular fatigue. Three series of measurements were performed for each subject one time per week for a total of 120 acquisitions. In order to check the generalization capability of the KSOM, a 10-fold cross-validation was applied in this work; each fold consisted of randomly selected samples, at least one for each category index was included in each fold. In this work, a 6 x 6 neuron KSOM with the parameters a(T) = 0.8 and a training of 800 epochs was adopted, which allowed the model to obtain its best performance. The KSOM map at the end was able to identify all the six classes with accuracy rates of 93.6%, 82.36%, 88.52%, 85.79%, 87,51% and 90.72%, respectively.

The first study to improve the personalization of treatment was focused on clinical assessment of a wearable ECG monitoring solution for long term monitoring and studies of heart variability assessment. Several ECG systems have been proposed to date. All of them use some form of electrodes that must make electrical contact with the subject's skin surface. This necessitates the use of sticky pads, pastes or gel. While this method works for stationary patients, it suffers from several problems. First, the material used to construct the electrode or the paste could cause skin irritation and discomfort, especially if the subject is performing rigorous physical exercise and may be sweating. Another problem is that most of time they are not ergonomic, with motion artefact and not suitable for long term monitoring studies outside the hospital setting. The proposed ECG chest belt is a wearable device based on the Shimmer® wireless sensor platform CE certified and equipped with several peripherals such as digital I/O, analog to digital converters, bluetooth radio, and a microSD slot. The electronic board and his enclosure was redesigned to collect one lead ECG and to be easily plugged on the common cardio-fitness chest straps (i.e. Polar®, Adidas®), which are fully washable, integrate dry electrodes applied directly to the patient's skin for single-lead acquisitions without skin preparation, gels, or adhesives. Moreover it guarantees an optimal and comfortable contact with the thorax for a long-term monitoring, adapting itself to the body shape. The first block of the ECG daughterboard is the low power front-end data acquisition circuit composed by analog amplifiers and filters able to reduce the artifacts of movement, breath and muscle contraction and to reach the desired dynamic range. The digitized data are passed to a microcontroller for processing and storage. To maintain the low-power usage capabilities of the electronic board a power management system optimizes the power utilization by putting un-used circuits into sleep mode. The core element of the system is the low power microcontroller (MSP430 family made by Texas Instrument) which has been widely used in wireless sensors. The device uses TinyOS, an open-source research platform for the design, implementation, testing and validation of the embedded firmware. TinyOS provides off-the-shelf components to interface with the hardware at higher abstraction level and is optimized for limited resources of wireless nodes, in terms of memory and CPU. Firmware developed on the sensor platform provides local processing of the sensed data, local storage of the data when required and communications of that data to a higher level application for advanced signal processing, display and data persistence. After the firmware implementation, 10 healthy volunteers (age 30 ± 3) were enrolled in the study to test the performances of the ECG chest strap. The ECG was acquired from 5 freely moving nurses at work and 5 subjects at bedside for 3 hours. All the subjects wore both the developed chest strap with the smartphone and a clinical holter (ELA). The resulting waveform confirmed the signal quality was comparable to that acquired by the ELA holter. Moreover, the ECG chest strap provided readable signal for more than 95% and 99% of the time of acquisition while the subjects where on working and lying supine at bedside respectively. Finally special attention was focused on the capability of the system to extract the features of cardiac rhythm. The high correlation between the two trends indicates a correct estimation of RR interval and of the average beat-by-beat heart rate from the ECG chest strap. The error between the heart rate of ECG chest strap and the gold standard system was lower than 10% (maximum value established by the CEI ISO60601-2-47 regarding HR calculation) during the entire whole validation. The second part of this study was focused on the system's ability to extract heart rate variability (HRV) features in time and frequency domain. It is based on evaluation of consecutive RR intervals extracted from ECG chest-strap; thus, HRV belongs to a group of non-invasive diagnostic methods. HRV reflects behavior of both parts of autonomous nervous system: sympathetic and parasympathetic. It is well accepted that conditions such as assuming an upright position, mental stress, and exercise are associated with an increase of the sympathetic tone. In contrast, vagal tone is high during resting conditions. An ECG data analysis interface was developed to extract all HRV parameters in time and frequency domain following the Heart Rate Variability Guidelines. The tool was tested on a study on HRV assessment in anorexia nervosa adolescents compared to controls in a resting condition. 27 adolescent girls (mean age: 14.6 ± 2.2 years) with ANR complete form in line with DSM-4TR standards and a sample of

15 healthy adolescent girls as control group (mean age: 14.5 ± 1.5 years) were enrolled to be part of the experimental group in the Child and Adolescent Eating Disorders Unit of the IRCCS Stella Maris. The electrocardiographic signals were acquired with the developed and validated ECG chest strap for 15 min while the patients lay in a supine position on an ambulatory bed in a quiet, darkened room. The patients were asked to relax. ECG signals were sampled at 250 Hz and HRV parameters were extracted with the developed tool. The comparison of the individual temporal features showed that in AN patients mean HR was decreased (AN mean: 62.05 ± 13.84, controls mean: 77.97 ± 10.31, $p < 0.001$). RRmean (AN mean: 1000 ± 250 ms, controls mean: 790 ± 90 ms, $p = 0.002$), diffRR (AN mean: 270 ± 70 ms, controls mean: 210 ± 30 ms, $p = 0.006$), RMSSD (AN mean: 130 ± 110 ms, controls mean: 50 ± 20 ms, $p = 0.008$) and RRdevstd (AN mean: 77(45-13) ms, controls mean: 60(40-70) ms, $p = 0.028$) were increased in AN with respect to controls. The comparison between AN and controls of the frequency features showed that the ratio between LF and HF was lower in AN than in controls (AN mean: 0.69(0.43-0.27), controls mean: 2.07(0.85-5.29), $p = 0.002$). The results of this study showed that compared to controls, young ANR adolescent girls have significantly lower heart rate (HR) and higher heart rate variability (HRV), lower low-frequency components, elevated high-frequency components, and decreased low- to high-frequency power ratio when compared to controls. Therefore, AN

patients showed a reduced cardiovascular sympathetic nervous responsiveness and an increased parasympathetic responsiveness when compared with healthy controls.

The second study of long term monitoring and personalized treatment was focused on a wearable system for the monitoring of activity and knee kinematics. The assessment and characterization of the system were performed at Spaulding Rehabilitation Hospital Harvard-MIT Division of Health Sciences and Technology. The system consists of a detachable device for tracking knee flexion/extension movements and an off-the-shelf knee sleeve with embedded sensors for compliance monitoring. The detachable device includes a low-cost rotary potentiometer for measuring knee flexion/extension, a 3-axis accelerometer for activity monitoring and a wireless platform for data logging and communication. A smartphone application has been developed to interact with the device using Bluetooth communication. The application allows users to check device status, visualize raw sensor data, and perform sensor calibration and configuration. In addition, the smartphone can also be used as an information gateway for remote access to data gathered by the wearable system. Tests were performed to compare the accuracy of the knee sensor with respect to the Vicon motion analysis system enrolling 6 health subjects. Each subject was setup with a lower body marker configuration to have the estimation of the joint kinematics and walked on a treadmill 3 times for over a period of 2-3hrs at comfortable and increased walking speed. Each walk on the treadmill at different self-selected speed was performed for a period of 2 minutes to observe effects due to knee sleeve migration. This allowed to collect data from Vicon and knee sensor simultaneously. First, was performed a calibration of the rotatory potentiometer at bench. A 3rd order polynomial model was derived by fitting the knee sensor data to the knee flexion angle obtained from Vicon. Comparing the knee angle derived from the rotary potentiometer and the Vicon system the results were very close and the corresponding root mean square error of the range of motion was 2.72 degrees. In the second part of this study a multilayer perceptron model was applied for the accelerometer for recognition of ambulatory activity as well as sitting, standing, walking, Up_Stairs and Dwn_Stairs. In this study 6 healthy subjects were enrolled. Each of them was asked to wear the knee tracker system and two times per day he/she had to follow a script with a defined protocol of the activities of 20 minutes. Signals were collected at 25 Hz, processed and extracted features in time domain as well as mean, variance, root mean square, entropy, peak to peak acceleration, correlation and frequency domain as well as dominant frequency and energy ratio dominant frequecy. The Relief method was used to rank the features and Davies Bouldin index criteria was applied to quantitatively analyze the clustering data and to select a subset of features. We demonstrated that implementing an artificial neural network with the integrated tri-axial accelerometer and using the leave one subject out method we achieved the classification of physical activities with accuracy more than 98%. More than 90% was achieved also with the selected subset of features making reliable the integration of the model into the wearable platform.

The purpose of this PhD work has been the development and characterization of PHS and knowledge based models for early diagnosis and long term personalized treatment with special attention paid to heart murmurs, muscular fatigue and stroke. In order to achieve this goal an innovative large scale screening methodology for heart sound classification, a wireless architecture and methodology to evaluate the muscular fatigue, novel ergonomic devices for long term monitoring of patients with cardiovascular diseases and lower limb injuries have been designed and characterized. The focus on enhanced body devices supported by knowledge-based approach represents an important milestone to gain the continuity of care and a new person centric model. The collected information combined with the current clinical findings and physiological clues can be used to provide a deeper understanding of medical problems and the impact of novel screening methodologies and personalized interventions.

Chapter 1

The potential impact of Personal Healthcare Systems

Recent advances of digital world technologies such as ubiquity of smart phones, tablets, bandwidth, pervasive connectivity have led to the evolution of revolutionary paradigms for computing models in the 21st century. Tremendous developments in Micro-Electro-Mechanical Systems (MEMS) technology, integrated circuits, small and power efficients devices, and wireless communication have allowed the realization of pervasive healthcare systems (PHS). In this chapter we will focus on the potential role of PHS. They promise to improve the chronic disease management programs, early diagnosis and long-term rehabilitation to gain the continuity of care and improve the people well-being.

1.1 Introduction

The medical knowledge is frequently updated and re-evaluated comprising new risk factors identification, new diagnostic tests, new evidences from clinical studies [1]. The challenges faced today are to incorporate the most recent and evidence-based knowledge into personal health systems [2,3] and to transform collected information into valuable knowledge and intelligence to support the decision making process [4,5]. Several expert systems tailored to specific diseases are nowadays available in clinical research [6,7,8,9,10,11], often covering the topics addressed by European priorities [12]. Technology can play a key role to gain the continuity of care and a person-centric model, focusing on a knowledge-based approach integrating past and current data of each patient together with statistical evidences. In currently applied care practices, the emergence of clinical symptoms allows a disease to be discovered. Only then, a diagnosis is obtained and a treatment is provided. Currently, different healthcare practice models are used [12,13,14]. In some models, the hospital is the core of the care and any level of technology available at the patient site may help in providing information useful for both monitoring, early diagnosis and preventive treatments. In other models dedicated call centers or point of care act as an intermediary between hospital/health care professional and patients. Many of the solutions available today on the market follow the above-mentioned model and call center services or point of care are used by the patients just as a complement to the hospital-centred healthcare services [12,13,14,15]. In the more advanced Personal Health Systems [16,17,18,19,20] model focused on the empowerment, the ownership of the care service is fully taken by the individual. This model is suitable for any of the stages of an individual's care cycle, providing prevention, early diagnosis, personalized rehabilitation and chronic disease management. Under this model, the technological innovations can help each person to self-engage and manage his/her own health status, minimizing any interaction with other health care actors. Solutions fully led by the patients are the overwhelming majority of those developed by research efforts covering chronic disease management, lifestyle management and independent living. Even if, in the clinical practice this model has not been yet implemented, it can be considered as a target to be reached achieving at the same time the empowerment of the users and the reduction of workload and costs, preserving the quality and safety of care. The main reasons for the lack of effective implementations of Personal Health Systems range from legal and societal obstacles, issues related to the real application of wearable devices, inappropriate use of decision support systems and the skepticism of many healthcare professionals. In particular wearable and portable devices need to be easy to use and comfortable to wear, efficient in power consumption, privacy compliant, with very low failure rates and high accuracy in triggering alarms, especially if used for diagnostic purposes [18,19,20,21]. The decision support system must infuse clinical knowledge into methodology and technology, thus enhancing the reliability of high-level processing systems customized to his/her personal needs represents the next critical step. The currently used approaches are based on values of health-related parameters, often monitored instantaneously during a check-up [21,22]. Moreover, the correlations across physiological, psycho-emotional, environmental and behavioural parameters, to evaluate prognostic marker of cardiovascular, pulmonary risk, stress levels, patient’s physical activities, are difficult to explore.

1.2 The concept of pervasive technologies

The pervasive technologies envisions a new generation of applications. These tools are based on the increasing convergence between information and communication technologies (ICT) and other technologies such as: biomedical sensors, micro- and nano- systems, user interfaces and digital signal processing and intelligent algorithms. They assist in the provision of continuous, quality controlled, and personalized health services to empowered individuals regardless of location. Unobtrusive, body-worn devices providing ease of data gathering and processing capabilities are essential to achieve the objective of making the leap between the preliminary results obtained as part of the research carried on so far and the daily clinical practice of medicine and rehabilitation. Three areas of work are essential to achieve this objective: 1) the development of sensors that unobtrusively and reliably record physiological data, movement and other relevant data to provide an early diagnosis and an objective evaluation of rehabilitation progress; 2) the design and implementation of systems that integrate multiple sensors, record data simultaneously from body-worn sensors of different types, and relay sensor data to a remote location at the time and in the way that is most appropriate for the clinical application of interest; and 3) the development of soft computing methodologies that starting from a wide range of data acquired and preprocessed by the related embedded systems are able to personalizes their analysis according to the specific case and to the specific patient and defines a reduced set of key parameters / information able in a simple and robust way to assess the clinical situation of the patient and to support the doctor in his decision process. Pervasive system for monitoring health may be in the form of wearable, implantable or portable systems. Wearable systems in particular are convenient platforms for monitoring an individual's health-related parameters. These systems are able to collect signals through unobtrusive interfaces, even on a continuous basis, and for processing and feeding relevant information to their users and/or medical professionals. They achieve this by integrating sensing, processing, and communicating devices in body-worn systems (e.g., wrist-worn devices, patches, or even clothes [23]), which are also linked to health information systems and electronic health records. Presently, personal health systems for the unobtrusive biomonitoring of body-kinematics and physiological and behavioural signals are continuously improving. They integrate smart sensors together with on-body signal conditioning and pre-elaboration, as well as the management of the energy consumption and wireless communication systems. Integrated wearable systems are able to transduce heart rate and electrocardiographic signals (ECG), as well as electromiographic signals (EMG), electrodermal response (EDR), respiratory values and arterial oxygen saturation. Acquired information is correlated to evaluate heart sounds, blood pressure, body temperature, hearth rate variability (HRV), end tidal CO2 and thoracic impedance pneumographic values. The aim of smart pervasive technologies is to match the living environment with the abilities of subjects affected by diseases or suffering from disabilities in order to reduce as much as possible the risks for those patients, to enhance their abilities and to support their independent living and their rehabilitation.

1.3 The impact of pervasive technologies in medicine and rehabilitation

The need for development of pervasive technology has been increasing in the scientific and industrial world. The rise in the percentage of elderly population has been changing the needs of the society, being age-related diseases more and more present in the actual society. Such conditions rise the need for care and assistance and are more likely to be admitted to a hospital or nursing home. Permanent admission to a care home is an expensive way of providing care for elderly, most of whom would prefer to remain in their own home [24, 25, 26]. It’s estimated that, nowadays, between 2 and 5% of elderly people reside in nursing homes [27], representing a not negligible cost for national sanitary systems. In 2011, USA spent the 17.6% of their gross domestic product (GDP) on healthcare delivery, according to data provided by the Organization for Economic Cooperation and Development (OECD), behind is the Europe with 11.6% for

France and Germany, 9.3% Italy [28]. Healthcare issues are faced by employing innovative models of care, such as telehealth, telemedicine and telecare, for which several industrial products and laboratory prototypes have been realized [29,30]. In this scenario the role of smart monitoring systems is to match the living environment with the physical and cognitive abilities and limitations of those suffering from disabilities or diseases, thereby enhancing performance and minimizing the risk of illness, injury, and inconvenience. Supporting independent living for the elderly, understanding the impact of clinical interventions on the real life of individuals following postoperative rehabilitation for patients to expedite recovery, is an essential component of medicine and rehabilitation [31, 32]. While assessments performed in the clinical setting have value, it is difficult to perform thorough, costly evaluations of impairment and functional limitation within the time constraints and limited resources available in outpatient units of rehabilitation hospitals. Furthermore, it is often questioned whether assessments performed in the clinical setting are truly representative of how a given clinical management program affects the real life of patients. Researchers and clinicians have looked at recent advances in wearable technology intrigued by the possibility offered by this technology of gathering sensor data in the field [33,34]. Likely to be complementary to outcome measures, the use of wearable systems in the clinical management of individuals with chronic diseases is very attractive because it provides the opportunity of recording quantitative data in the settings that matter the most, i.e. the home and the community. Capabilities such as remote, automated patient monitoring and diagnosis, may make pervasive technologies a tool advancing the shift towards home care, and may enhance patient self-care and independent living. Automatic reports of key physiological parameters and activities as supplied by pervasive technologies are expected to increase the effectiveness as well as efficiency of health care providers. 'Anywhere and anytime' are becoming keywords – a development often associated with 'pervasive healthcare' [35, 36]. In addition to these patient-centric medical benefits, such framework will also provide economic benefits for public health systems, by reducing the frequency and severity of hospitalization episodes and by potentially improving the relationship and interaction between patient and doctors.

1.4 The role of ICT solutions in chronic disease management programs

Observational and randomized controlled trials have generally shown that disease management programs reduce hospitalization and can improve quality of life and functional status. In addition, non-pharmacologic management strategies represent an important contribution to chronic disease therapies. They may significantly impact patient stability, functional capacity, mortality, and quality of life. Thus, some of the most cost-effective entry points into a disease-management program are: multi-factorial interventions (both from pharmacological and non-pharmacological therapies, also based on the patient lifestyle), in order to attack different barriers to behavioral change of the patient, and multidisciplinary disease-management programs for patients at high risk for hospital admission or clinical deterioration. Non-compliance with diet and medications can rapidly and profoundly affect the clinical status of patients; increases in body weight and some minor changes in symptoms commonly precede the major clinical episodes that require emergency care or hospitalization. Poor or non-adherence to medication, diet or symptom recognition is common and may be responsible for over one-third of the hospital readmission. Patient education and close supervision, with a watchful surveillance by the patient itself of by his/her family is critical for the out-of-hospital follow-up. Regular visits in the outpatient clinic cannot monitor the changes of hemodynamic and clinical status of the patient, which can be subtle. Management programs have to be structured as a multidisciplinary care approach that coordinate the continuum of care and throughout the chain of care delivered by various services within the healthcare systems. If possible, patients should learn to recognize symptoms and practice self-care measures. Remote-monitoring with pervasive technologies may be a form of management that allows daily monitoring of symptoms and signs measured by patients, family, or caregivers at home while allowing patients to remain under close supervision.

To reach this goal, is necessary to:

- deliver a new multi-parametric, feedback based, user centered disease management system, considering both technological and socio-psychological aspects by using the analysis and the correlation of multiple parameters to design a complete and personalized health monitoring system.
- enable the collection of large quantities of fine-grained, continuous data, which medical researchers can mine to develop new prevention algorithms and techniques/policies to identify which variables should be monitored for maximum impact for predicting degenerative episodes.
- develop new equipments with additional monitoring parameters and more sophisticated technology should be developed to permit unobtrusive, long-term patient monitoring.

Due to the complex nature of each chronic disease, several factors have to be studied to obtain relevant advances both in medical and ICT fields. In Table 1 are resumed the main clinical needs and the ICT role to improve the chronic disease management programs.

Table 1 Summary of the main clinical needs and the proposed ICT solutions

Clinical needs	ICT support
Chronic diseases are linked to multiple interacting risk factors and risk management requires attention to all modifiable risk factors.	To develop a multi-parametric monitoring system.
Each patient is unique. Several differences are present at country level, between male and female, between age, categories and each individual has his own risk pattern.	To develop a personalized system.
To prevent one single degenerative event it is necessary to intervene in many subjects with no apparent benefit to them (the "prevention paradox").	To study many subjects and correlate their data to better act on a single patient.
Current available data are still poor: hospital statistics reveal only the tip of the iceberg since sudden cardiac death occurring outside the hospital still represents a large proportion of all cardiovascular deaths.	To develop an integrated network able to collect a large quantity of data for statistical analysis and develop new model to support clinical decisions
Tele-monitoring and educational approaches have to cope with serious difficulties such as accuracy and reliability of the measurements, acceptance by the people, psychological attitude of the individuals and all of them can generate false alarms, excessive anxiety and sometimes unjustified requests of a direct intervention of the medical professionals. The ultimate risk to be avoided is the paradox that technological solutions, aiming at reducing the medical burden, generate overload without achieving the goal of a better quality of care and a more effective prevention approach	To develop systems minimally invasive, very reliable and accurate in order to really improve the quality of care.

1.5 References

[1]. Peleg M, Tu S. Decision Support, Knowledge Representation and Management in Medicine. Methods of Information in Medicine. 2006 45 (Suppl 1), 72-80.

[2]. Miles A, Loughlin M, Polychronis A. Evidence-based healthcare, clinical knowledge and the rise of personalised medicine. J Eval Clin Pract. 2008 Oct;14(5):621-49.

[3]. Lester WT, Zai AH, Grant RW, Chueh HC. Designing healthcare information technology to catalyse change in clinical care. Inform Prim Care. 2008;16(1):9-19.

[4]. Song B, Marschollek M, Wolf KH, Gietzelt M, Franken T, Haux R. A home-centered ICT architecture for health-enabling technologies. Stud Health Technol Inform. 2010;160(Pt 1):48-52.

[5]. Lugovkina T, Richards B. Clinical events classification for using the EHR to provide better patient care. Stud Health Technol Inform. 2010;156:167-70.

[6]. Mago VK, Mago A, Sharma P, Mago J. Fuzzy logic based expert system for the treatment of mobile tooth. Adv Exp Med Biol. 2011;696:607-14.

[7]. Kubben PL, van Santbrink H, Cornips EM, Vaccaro AR, Dvorak MF, van Rhijn LW, Scherpbier AJ, Hoogland H. An evidence-based mobile decision

support system for subaxial cervical spine injury treatment. Surg Neurol Int. 2011 Mar 23;2:32.

[8]. Spjuth O, Eklund M, Ahlberg Helgee E, Boyer S, Carlsson L. Integrated decision support for assessing chemical liabilities. J Chem Inf Model. 2011 Jul 20.

[9]. Fossum M, Alexander GL, Ehnfors M, Ehrenberg A. Effects of a computerized decision support system on pressure ulcers and malnutrition in nursing homes for the elderly. Int J Med Inform. 2011 Jul 21.

[10]. Ohlsson M, “perfusion images using artificial neural networks”, Artificial Intelligence in Medicine, 30(1), 2004, 49-60.

[11]. Narasingarao MR, Manda R, Sridhar GR, Madhu K, Rao AA, “A clinical decision support system using multilayer perceptron neural network to assess well being in diabetes”, J Assoc Physicians India, 57, 2009, 127-33.

[12]. Hansen J, Schäfer W, Black N, Groenewegen P. “European priorities for research on health care organizations and service delivery”. J Health Serv Res Policy. 2011 Jul;16 Suppl 2:16-26.

[13]. van Sambeek JRC, Cornelissen FA, Bakker PJM, Krabbendam JJ, "Models as instruments for optimizing hospital processes: a systematic review", 2010, International Journal of Health Care Quality Assurance, Vol. 23 Iss: 4, pp.356 - 377

[14]. Nguyen YL, Kahn JM, Angus DC., Reorganizing adult critical care delivery: the role of regionalization, telemedicine, and community outreach., Am J Respir Crit Care Med. 2010 Jun 1;181(11):1164-9. Epub 2010 Mar 11.

[15]. Mechanic D., Replicating High-Quality Medical Care Organizations, JAMA. 2010;303(6):555-556.

[16]. Bardram JE, "Pervasive Healthcare as a Scientific Discipline," Methods of Information in Medicine, vol. 47, no. 3, 2008, pp. 178–185.

[17]. Orwat C, Graefe A, Faulwasser T, "Towards Pervasive Computing in Health Care: A Literature Review," BMC Medical Informatics and Decision Making, vol. 8, no. 26, 2008; www.biomedcentral.com/1472-6947/826.

[18]. Delmastro F, Conti M, “Wearable Computing and Sensor Systems for Healthcare”, in Pervasive Computing and Networking (eds M. S. Obaidat, M. Denko and I. Woungang), John Wiley & Sons, Ltd, Chichester, UK. 2011, doi: 10.1002/9781119970422.ch8

[19]. Hansen TR, Bardram JE, Soegaard M, "Moving Out of the Lab: Deploying Pervasive Technologies in a Hospital," IEEE Pervasive Computing, vol. 5, no. 3, 2006, pp. 24–31.

[20]. Rigby M, "Applying Emergent Ubiquitous Technologies in Health: The Need to Respond to New Challenges of Opportunity, Expectation, and Responsibility," Int'l J. Medical Informatics, vol. 76, no. 3, 2007, pp. S349–S352.

[21]. Pantelopoulos A, Bourbakis NG “A Survey on Wearable Sensor-Based Systems for Health Monitoring and Prognosis”. IEEE Transactions on Systems, Man and Cybernetics, 2011, 41(1):1-12

[22]. Auricchio A, Brugada J, Ellenbogen KA, Gold MR, Leyva F, “CLEPSYDRA investigators, Assessment of a novel device-based diagnostic algorithm to monitor patient status in moderate-to-severe heart failure: rationale and design of the CLEPSYDRA study”, Eur J Heart Fail. 2010 Dec;12(12):1363-71. Epub 2010 Oct 14.

[23]. A. Lymberis and S. Olsson, “Intelligent biomedical clothing for personal health and disease management: State of the art and future vision,” Telemed. J. e-Health, vol. 9, pp. 379–386, Dec. 2003.

[24]. Hedda Agüro-Torres H, von Strauss E, Viitanen M, Winblad B, Fratiglioni L. Institutionalization in the elderly: the role of chronic diseases and dementia. Cross-sectional and longitudinal data from a population-based study. Journal of Clinical Epidemiology 2001;54:795–801.

[25]. McCann M, Donnelly M, O'Reilly D. Living arrangements, relationship to people in the household and admission to care homes for older people. Age and Ageing 2011;40:358–63.

[26]. Eloranta S, Arve S, Isoaho H, Routasalo P. Home care from the perspective of older clients and their professional.

[27]. Ribbe MW, Ljunggren G, Steel K, Topinková E, Hawes C, Ikegami N, et al. Nursing homes in 10 nations: a comparison between countries and settings. Age and Ageing 1997;26(S2):3–12.

[28]. http://www.oecd-ilibrary.org/ [accessed 06.03.12].

[29]. Stowe S, Harding S. Technology applied to geriatric medicine, telecare, telehealth and telemedicine. European Geriatric Medicine 2010;1:193–7.

[30]. Moehr JR, Schaafsma J, Anglin C, Pantazi SV, Grimm NA, Anglin S. Success factors for telehealth—a case study. International Journal of Medical Informatics 2006;75:755–63.

[31]. Gatzoulis L, Iakovidis I. Wearable and portable eHealth systems. IEEE Engineering in Medicine and Biology Magazine 2007;September/October:51–6.

[32]. Tröster G. The agenda of wearable healthcare. In: Haux R, Kulikowski C, editors. IMIA yearbook of medical informatics 2005: ubiquitous health care systems. Stuttgart: Schattauer; 2004. p. 125–38.

[33]. Frontera W: The importance of technology in rehabilitation. IEEE Eng Med Biol Mag 2003, 22(3):25.

[34]. Stein J: Wearable sensor technology for functional assessment after stroke. IEEE Eng Med Biol Mag 2003, 22(3):26-27.

[35]. Varshney U: Pervasive healthcare. IEEE Computer 2003, 36(12):138-140.

[36]. Korhonen I, Bardram JE: Guest Editorial Introduction to the Special Section on Pervasive Healthcare. IEEE Transactions on Information Technology in Biomedicine 2004, 8(3):229-234.

Chapter 2

A knowledge-based approach for the automatic classification of heart valve disease

The study presented in this chapter is aimed at the development of a cardiac prescreening device based on pattern recognition models for automatic classification of heart murmurs to be used by non-medical personnel. The adopted methodology is both experimental and computational. In this chapter the preliminary part is focused on a brief description about the physiology of the heart and the state of art of methods of automatic classification of heart sounds. Then follows a detailed description about the design and configuration of the embedded hardware potentially suitable for data collection and the campaign of acquisition of cardiac signals. The last part of the work is focused on signal-processing, segmentation, feature extraction and use of combined knowledge-based models for acquisition, denoising, segmentation and classification of heart sounds and murmurs. Each cardiac cycle was segmented using homomorphic filtering and K-means clustering. Features were extracted and selected in time and frequency domain using wavelet transform and new hierarchical and multimodal models based on self-organizing maps (SOM) and fuzzy logic were described and results were presented.

2.1 Introduction

Although sophisticated medical technology like ultrasound imaging and Eco-Doppler techniques is already available in healthcare, cardiac auscultation continues to be the professional's primary tool to evaluate cardiac functions and distinguish between innocent and pathological heart murmurs. For medical persons to acquire high-quality auscultation skills requires the guidance of an experienced instructor using a sizable number of patients along with frequent practice [1]. Moreover the development of new diagnostic modalities has experienced a gradual decline of their skill to appreciate many of the subtleties of heart sounds. Since some years the advances in digital signal processing are focused on the analysis of acoustic cardiac signals combined with knowledge-based models for automatic classification of heart murmurs. This approach could play an important role in terms of use and cost-effectiveness and making phonocardiogram-based diagnostic techniques available to every doctor, would reduce the referral of patients to unaffordable and expensive tests. In particular in developing countries, where they still suffer a lack of medical facilities, this cost effective way of providing medical care would improve the life expectancy of patients with valvular pathologies. Many pathological conditions that cause murmurs and aberrations of heart sounds manifest much earlier in phonocardiography than are reflected by symptoms. Thus by proper interpretation of the phonocardiogram (PCG) signal, corrective measures can be taken. In most cases, the activities in the PCG signal relating to a given disease are contained in a single interval of cardiac cycle. Efforts to date have provided interesting results about the automatic classification of heart valve disease, in terms of performance of classification but we still suffer the lack of emphasis on developing reliable algorithms differentiating pathological murmurs and results for a practical contextualized use.

2.1.1 Heart sounds and murmurs

The heart is an organ consisting of four separated chambers, whose main function is to provide a pulsatile blood stream to both the pulmonary (oxygenation) and systemic circulation (nutrients, etc.). From the anatomical point of view, the heart consists of a muscular bundle (myocardium), properly structured and divided by a partition (or septum) into two halves: each half, on its turn, is divided into two chambers, the atrium and ventricle as showed in Figure 1. The pumping function is achieved by a complex electro-mechanical system providing the rhythmic contraction of the myocardium (or heart cycle) and the increase of the blood pressure within the ventricular chambers. During the heart cycle, each ventricle exchanges blood with the corresponding atrium and the corresponding artery through natural orifices. In order to maintain unidirectional flow, each orifice is occupied by special structures called heart valves (HV). The heart valves are passive structures, opening and closing the valvular orifices according to the transvalvular pressure drop. In the opening, the blood pressure pulls apart the leaflets and the blood flow rate crosses the orifice. The act of opening and closing of the HV cause thuds, the heart beats or sounds. The Wiggers diagram is shown in Figure 2. The left heart cycle, which is represented by atrial, ventricular, aortic pressure-time curve, and the electrocardiograph (ECG) traces with the heart sounds is plotted: the time scale of the graph highlight that the valve transition from open to close configuration and vice versa occurs in fraction of the heart cycle (i.e. 0:1 s). The pressure drops exerted on the closed leaflets spans from 5 to 120 mmHg, during regular heart cycles. Unlike the other biological tissues, leaflets pass from a fully unloaded to fully loaded state each heartbeat.

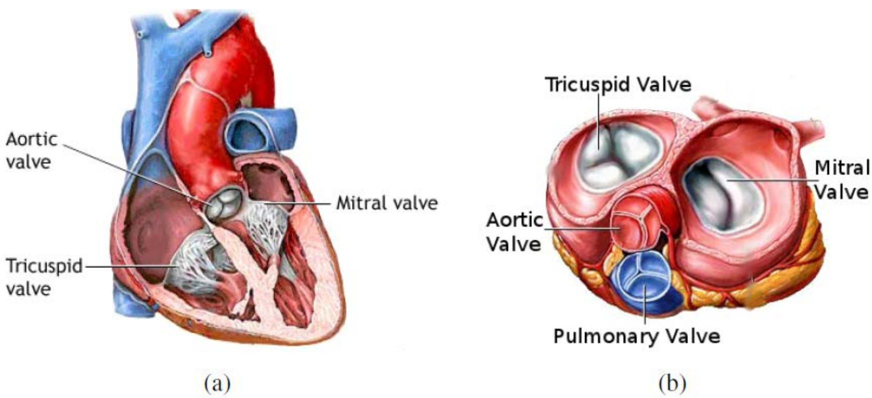

Figure 1: Heart Anatomy. a) frontal section b) transversal section

Looking at the anatomy, two kinds of heart valves can be identified: atrioventricular HV and semilunar HV. The atrio-ventricular (the mitral and tricuspid valve) prevent blood from flowing back from the ventricles to the atria and the semilunar valves (aortic and pulmonary valves) prevent blood from flowing back into the ventricles once being pumped into the aorta and the pulmonary artery. In the beginning of ventricular systole, all the valves are closed resulting in an isovolumic contraction. When the pressure in the ventricles exceeds the pressure in the blood vessels, the semilunar valves open allowing blood to eject out through the aorta and the pulmonary trunk. As the ventricles relax the pressure gradient reverses, the semilunar valves close and a new heart cycle begins.

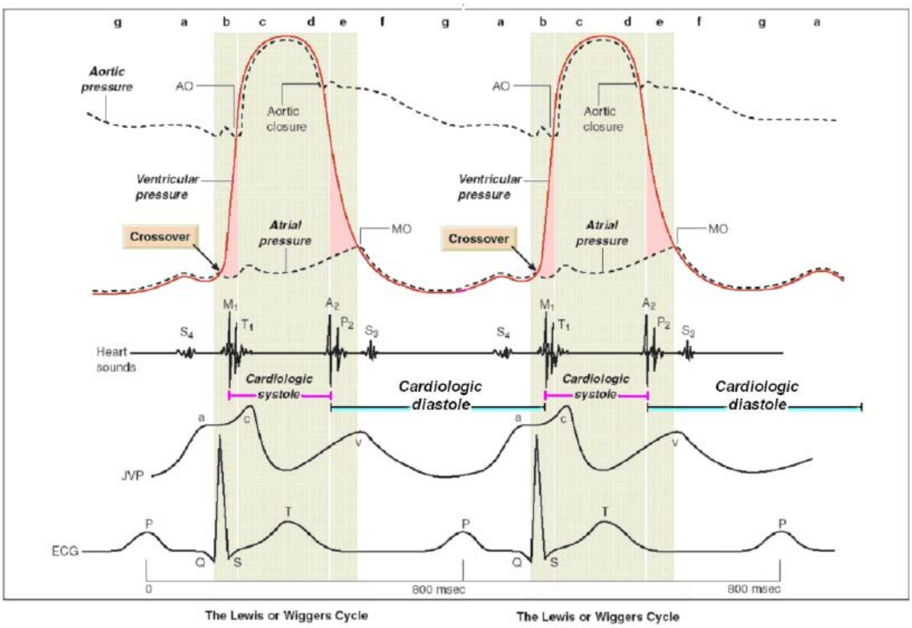

Figure 2: Wiggers diagram: the cycle of the left heart is illustrated in terms of synchronous pressure in the atrial, ventricular and aortic zone; the heart sounds, the Electrocardiograph (ECG) and the Jugular Venus Pressure (JVP) traces are also represented

The relationship between blood volumes, pressures and flows within the heart determines the opening and closing of the heart valves. Normal heart sounds occur during the closure of the valves, but how they are actually generated is still debated. The valvular theory states that heart sounds emanate from a point sources located near the valves, but this assumption is probably an oversimplification [2]. In the cardiohemic theory the heart and the blood represent an interdependent system that vibrates as a whole [2]. Both these theories originate from a time when the physiological picture was based on a one-dimensional conception of flow. Recent research provides means to visualize the actual three-dimensional flow patterns in the heart [3], and this new knowledge will probably clarify our view on the underlying mechanisms of heart sounds. The blood's pathway through the heart is far from fully understood, but the induced vortices seem optimized to facilitate flow and thereby increase the efficiency of the heart as a pump. The impact of this new knowledge on the understanding of heart sounds and their origin is yet to be investigated. Awaiting this new insight, the cardiohemic theory will be assumed valid. Normally, there are two heart sounds. The first sound (S1) is heard in relation to the closing of the atrioventricular valves, and is believed to include four major components [4]. The initial vibrations occur when the first contraction of the ventricle move blood towards the atria, closing the AV-valves. The second component is caused by the abrupt tension of the closed AV-valves, decelerating the blood. The third component involves oscillation of blood between the root of the aorta and the ventricular walls, and the fourth component represents the Processing of the Phonocardiographic Signal vibrations caused by turbulence in the ejected blood flowing into aorta. The second sound (S2) signals the end of systole and the beginning of diastole, and is heard at the time of the closing of the aortic and pulmonary valves [5]. S2 is probably the result of oscillations in the cardiohemic system caused by deceleration and reversal of flow into the aorta and the pulmonary artery [6]. There is also a third and a fourth heart sound (S3 and S4). They are both connected with the diastolic filling period but they will not be treated further. Murmurs are produced by turbulent blood flow as a result of narrowing or leaking valves or from the presence of abnormal passages in the heart. More specifically, heart murmurs occur when the blood flow is accelerated above the Reynolds number. The resulting blood flow induces non-stationary random vibrations, which are transmitted through the cardiac and thoracic tissues up to the surface of the thorax. There are five main factors involved in the production of murmurs [5]:

- High rates of flow through the valves.
- Flow through a constricted valve (stenosis).
- Backward flow through an incompetent valve (insufficiency or regurgitation).
- Abnormal shunts between the left and right side of the heart (septal defects).
- Decreased viscosity, which causes increased turbulence.

Heart murmurs are graded by intensity from I to VI. Grade I is very faint and heard only with special effort while grade VI is extremely loud and accompanied by a palpable thrill. Grade VI murmurs are even heard with the stethoscope slightly removed from the chest. When the intensity of systolic murmurs is crescendo-decrescendo shaped and ends before one or both of the components of S2, it is assumed to be an ejection murmur (S2 is composed of two components, one from the aortic valve and one from the pulmonary valve). Murmurs due to backward flow across the atrioventricular valves are of more even intensity throughout systole and reach one or both components of S2. If the regurgitant systolic murmur starts with S1 it is called holosystolic and if it begins in mid- or late systole it is called a late systolic regurgitant murmur. Besides murmurs, ejection clicks might also be heard in systole. They are often caused by abnormalities in the pulmonary or aortic valves. Different murmurs, snaps, knocks and plops can also be heard in diastole, but such diastolic sounds are beyond the scope of this thesis.

2.1.2 Heart Sound auscultation

Auscultation is the technical term for listening to the internal sounds of the body. The loudness of different components varies with the measurement location. For instance, when listening over the apex, S1 is louder than S2. Also, the location of a heart murmur often indicates its origin, e.g. mitral valve murmurs are usually loudest at the mitral auscultation area. The traditional areas of auscultation, see Figure 3, are defined as [5]:

- Mitral area: The cardiac apex.
- Tricuspid area: The fourth and fifth intercostal space along the left sternal border.
- Aortic area: The second intercostal space along the right sternal border.

- Pulmonic area: The second intercostal space along the left sternal border.

Even though the definition of these areas came to life long before we had much understanding of the physiology of the heart, they are still good starting points. Revised areas of auscultation, allowing more degrees of freedom, have however been adopted [5].

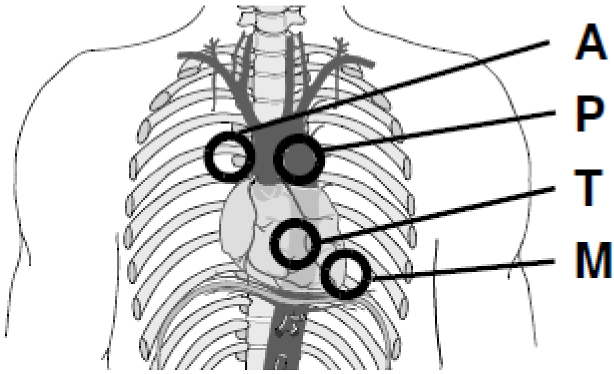

Figure 3: Traditional areas of auscultation (M refers to the mitral area, T the tricuspid area, P the pulmonic area, and A the aortic area).

2.1.3 Related works of automatic classification of heart sounds

In the last few decades several approaches have been proposed to analyze heart murmurs. The main efforts starts from 2001 on Circulation with DeGroff et al [7] who proposed the use of an artificial neural network (ANN) able to classify innocent and pathological murmurs in 69 children isolating three characteristic beats. The features were extracted from the energy spectrum of the entire signal. Using this approach, false positive and false negative rates of 0% were claimed for the system even if this tends to be an easier problem since murmurs can generally be heard more clearly in children because the chest walls in children typically have less fat and muscle than in adults [8]. Moreover the beats were isolated manually by highly trained individual with the ability to detect the disorder that the system is trying to diagnose. Andrisevic et al. [9] proposed the use of ANN extracting features from spectrogram images of cardiac cycle, denoising the data using Wavelet analysis and selecting input features using Principal Component Analysis. The ANN was tested on 15 subjects obtaining a sensitivity of 64,7%; a specificity of 70,5%; and an accuracy of 70,2%. De Vos et al. [10] acquired ECG synchronized with heart sound and extracted features using wavelet analysis from each cardiac cycle. The study included 50 pathological and 113 functional cases and reached a sensitivity and specificity of 90% and 96,46% respectively. Pretorius et al (2010) [11] developed a decision support system to screen children in developing countries without the need of expensive equipment or specialist skills. Both heart sound and ECG data were collected for single cardiac cycle segmentation and ANN was trained for each specific murmur type. The study enrolled 381 patients of which 99 had no murmurs validated by Ecodoppler. They collected the data from all the four sites of auscultation and demonstrated that aortic and tricuspid location had the best sensitivity and specificity, 82%

and 92% respectively even if they miss to consider subjects with mitral stenosis and with combined pathologies. Kwak et al. [12] classified heart murmurs using hidden Markov models obtaining an accuracy of 80% using a database of 160 subjects. In some works, the analysis was performed on auscultation skill training CD [13],[14]. The results are good but is not clear exactly which method has been applied for data collection and cleaning. In other studies, raw data analyzed comes from clinical databases that usually miss subjects with combined pathologies. Moreover, in literature, reference of devices for cardiac prescreening and diagnosis using Heart Sounds are rare.

2.2 Material and methods

2.2.1 Requirements of the system for automatic heart sound classification

The primary system requirements are that the device must be unobtrusive reliable and based on a simple and fast procedure of use to guarantee a wide dissemination in developing countries where they still suffer a lack of medical facilities. The main objective of our developed system is to be used by non-medical personnel for cardiac pre-screening. The developed tool will be used also to give an useful support to the doctor for diagnosis outside the hospital. The system must be ergonomic, should last a monitoring period of several days without requiring a battery recharge, and designed to don't be unaffected by external noise. The audio recording chain involves a sequence of transformations of the signal: a sensor to convert sound or vibrations to electricity, a pre-amplifier to amplify the signal, a pre-filter to avoid aliasing and an analogue to digital converter to convert the signal to digital form which can be stored permanently. Electronic stethoscopes make use of sensors specially designed to suit cardiac sounds. Compared to classic stethoscopes, electronic stethoscopes tries to make heart and lung sounds more clearly audible using different filters and amplifiers. Some also allow storage and the possibility to connect the stethoscope to a computer for further analysis of the recorded sounds.

2.2.2 Hardware of the digital stethoscope

In this study we chose to develop the digital stethoscope using the hardware of Texas Instrument. It is composed of three main components, the digital signal processing unit, the front end board and the sensor of auscultation. The TMS320C5515 digital signal processor (DSP) has been suited for the development of the digital stethoscope [15]. In particular has been used the medical development kit (MDK) based on the C5515 DSP. It uses an analog front end to capture the acoustic sound waves of the heart. The analog signals are amplified and digitized before transmitting them to the DSP for further processing and data transmission using Bluetooth interface as showed in Figure 4.

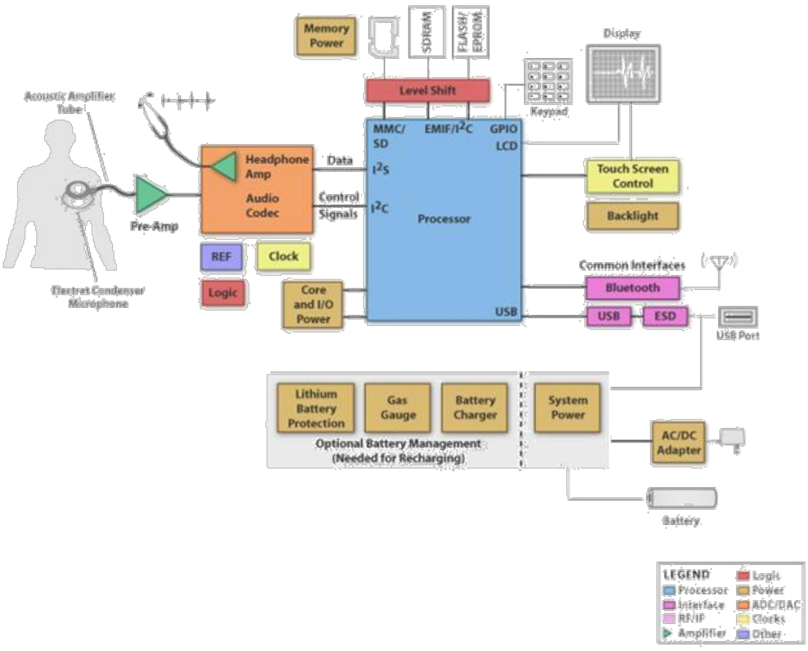

Figure 4: Block diagram of digital stethoscope

The DSP C5515 operates using a + 5 V battery and is designed to be programmed using TI's Code Composer Studio which communicates with the board through an esternal emulator. The DSP reads the digitized signals from the audio codec via the I2S interface and processes it. Then, the signal is decimated to 3 KHz and provided to the PC application over the UART interface for display. The front-end board contains the necessary circuitry for signal conditioning and acquiring from the sensors. In particular it contains the pre-amplifier stage that increase the input signal with a gain factor of 31, a low pass filter with cut-off frequency of 2.5 KHz to remove the high-frequency noise and also to act as an anti-aliasing filter, capacitive coupling block to isolate the DC bias and the audio codec with the sampling frequency of 12KHz. The front-end board has three 2.5mm mono jack connectors to connect the microphones and one 2.5 mm stereo jack to connect the head phone. The front-end board is interfaced with the C5515 board through a universal front-end connector using I2C and I2S interfaces. The first interface is used for configuring the codec on the front end board while I2S interface is used for codec data transfer. In Figure 5 is reported the front end board of digital stethoscope.

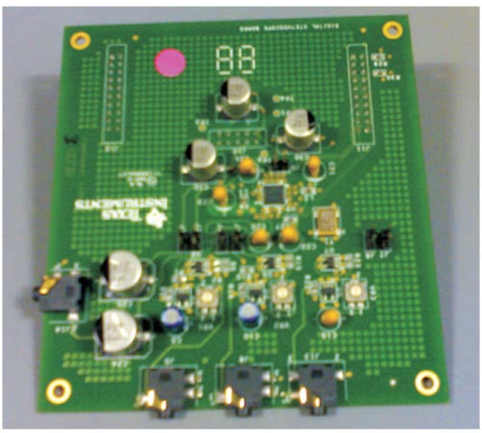

Figure 5: Front-end board digital stethoscope

The last component is the sensor of auscultation which is mainly composed of three blocks: diaphragm, condenser microphone and 2.4 mm audio plug. Sound waves from the acoustic amplifier (diaphragm) are fed to the condenser microphone. The sound waves hitting the condenser microphone change its capacitance by changing its impedance, which produces a voltage swing proportional to the amplitude of the input sound waves. The voltage swing of the signal also depends on the bias voltage given for the microphone. A microphone bias voltage of 1.25 V is produced by the audio codec. The coupling of the microphone with the acoustic stethoscope diaphragm 3M Littman as shown in Figure 6 was critical to pick up noise free sound signals from the human body.

Figure 6: Acoustic stethoscope head coupled with microphone

The microphone was placed close as possible to the diaphragm and was connected to a 2.5 mm jack to plug it with the front-end board. The electric wire that connects the microphone to the plug was made long enough to ensure that there is sufficient length to place the sensor on the subject.

2.2.3 Subjects selection and experimental procedure

The study was conducted in collaboration with the cardiologists of the Institute of Clinical Physiology of Pisa and with the Department of Medical and Surgical Critical Care, University of Florence. Digital heart sounds recording were obtained with the developed digital stethoscope from 160 subjects (mean age 50±10) and all diagnosis were confirmed by Ecodoppler.

Heart sounds were recorded from three sites of auscultation: aortic, third intercostal space and mitral in supine position. For each patient, three separated heart sound recordings of one minute were acquired. Under Internal Review Board protocol, all participants and/or parents gave written, informed consent to participate in this study. In Table 2 is reported the number of subjects for each pathology collected and validated by Echography.

Table 2 Number of subject for each collected pathology

Classes	N. of subjects
Normal	40
Aortic Stenosis	20
Aortic Regurgitation	10
Mitral Stenosis	5
Mitral Regurgitation	12
Mitral + Aortic Stenosis	13
Mitral + Aortic Regurgitation	18
Mitral Stenosis + Aortic Regurgitation	10
Mitral Regurgitation + Aortic Stenosis	32
TOTAL	**160**

2.2.4 Pre-processing and segmentation

The first step of implementation of automatic analysis is based on signal pre-processing and signal segmentation. The original signal down sampled to 3000 Hz was first normalized by setting the variance of the signal to a value of 1. A low pass Chebyshev type I filter with 3-dB cutoff frequency at 750 Hz was used to filter the heart sounds, considering that higher frequencies are not of clinical significance for analysis and diagnosis. After filtering the segmentation was performed with cardiac cycle detection, identifying respectively systolic between S1 and S2 and diastolic cardiac phases between S2 and S1. The prerequisite to identify each cardiac cycle is based on envelope. This is important to find the locations of S1 and S2 peaks. The homomorfing filtering tipically used for envelope of speech has been implemented [16]. This technique converts a non-linear combination of signals into a linear by applying logarithmic transformation. Steps performed are given below:

1. Extraction of energy E(n) from phonocardiogram signal:

   $$E(n)=s(n)*f(n) \quad (1)$$

   where s(n) represents the slow varying part of the S1 and S2 main components of the signal and f(n) is the fast varying part mainly due to the murmurs contribute.
2. Logarithmic transformation to convert operation to addition:

   $$z(n)=\log(E(n)) \quad (2)$$

   thus:

   $$z(n)= \log s(n) + \log f(n) \quad (3)$$
3. Low-pass filter, L to filter the unwanted components:

   $$L[\log s(n)] + L[\log f(n)] \approx \log s(n) \quad (4)$$

   Applying the exponential transformation, we arrived at:

   $$\exp[\log s(n)] = s(n)$$

After some preliminary experimentation, a low pass filter (L) was applied with a transition bandwidth from 10 to 20 Hz. The exponentiation enabled to obtain the envelope of signal. After this analysis the peaks S1 and S2 were extracted applying some empirical rules with the support of the physicians: (i) all the peaks values > 0.35 of maximum value of envelope were considered; (ii) spikes < 0.5 of the mean peak width were removed; (iii) the maximum width of S1-S2 peak was fixed at 120 ms. After fixed this empirical thresholds, K-mean cluster of the distances between the peaks was applied to discriminate 2 classes: systolic (S1-S2) and dystolic (S2-S1) intervals, which consecutively indicates a single cardiac cycle. K-mean is a non-hierarchical partitioning method that partitions the observations in the data into K mutually exclusive clusters, and returns a vector of indices indicating to which of the K clusters it has assigned each observation. It uses an iterative algorithm that minimizes the sum of distances from each object to its cluster centroid, over all clusters. This algorithm moves objects between clusters until the sum cannot be decreased further.

2.2.5 Feature extraction

Auscultation is an old science where a lot of information and experience have been gathered over the years. All this domain knowledge is incorporated in the features that can be extracted from the signal to perform the classification task. These parameters were extracted to quantify the available information into a few descriptive measures extracted from each signal. In phonocardiograpic classification, the features were derived on a heart cycle basis. Knowledge about the accurate timing and frequency of events in the heart cycle are thus of great importance. In healthy subjects, the frequency spectrum of S1 contains a peak in the low frequency range (10-50 Hz) and in the medium frequency range (50-140 Hz) [17]. S2 contains peaks in low- (10-80 Hz), medium- (80-220 Hz) and high-frequency ranges (220-400 Hz) [18]. S2 is composed of two components, one originating from aortic valve closure and one originating from pulmonary valve closure. Normally, the aortic component (A2) is of higher frequency than the pulmonary component (P2) [19]. The peaks probably arise as a result of the elastic properties of the heart muscle and the dynamic events that causes the various components of S1 and S2 [18], [20]. When the aortic or pulmonary valves becomes narrowed or constricted, blood has to be forced through the valve opening. In this case we have a stenosis condition. The arising turbulent blood flow causes vibrations in the cardiac structure which are transmitted through the tissue and perceived as a murmur. The murmur peaks in mid-systole at the time of maximal ejection and produces a crescendo-decrescendo shape in the phonocardiographic signal. The severity of the stenosis influences the shape of the murmur, where the intensity will increase and the peak will occur later in systole as the stenosis becomes more severe. In case of regurgitation, the backward flow through the mitral or tricuspid valves causes a murmur that begins as soon as the atrioventricular valves closes and continues up to the semilunar valve closure. Because the pressure gradient between ventricle and atrium is large throughout systole, the murmur tends to have a constant intensity throughout systole. In order to extract these knowledge about stenosis and regurgitation in time domain was extracted the distance between S1 and S2, which was obtained after the peak detection with the homomorfing filter, the entropy and the root mean square (RMS) of the heart cycle. In frequency domain, considering that the signal is not stationary, the discrete Wavelet transform was applied to extract features from the segmented phonocardiogram signals. Wavelet coefficients were extracted using Daubechies-2 wavelet. These coefficients were obtained through a single cycle of PCG signal and wavelet detail coefficients at the second decomposition level were seen to have the distinguishing features as in [21].

2.2.6 Feature selection

Feature selection was performed in two steps. First, we used the ReliefF [22] algorithm which ranks the features in decreasing order of importance. The ReliefF feature selection algorithm is an extension of the original Relief algorithm proposed by Kira et al. [23]. The ReliefF algorithm iterates through every instance updating the weights assigned to a feature at each iteration. For every instance, it searches for K nearest neighbors from the same class (called nearest hits H), and K nearest neighbors from each of the other classes (called nearest misses M). Then, it updates the quality of estimation W[A] for each attribute A and moves to the next instance. The number of nearest neighbors K was set to 10 as suggested by Robnik-Sikonja and Kononenko [24]. The ReliefF algorithm is computationally simple. It is more robust compared to the original Relief algorithm, since it can deal with incomplete and noisy data. The second step of the feature selection procedure consisted of selecting an appropriate number of top ranked features provided by the ReliefF algorithm in step 1. We adopted the criterion of selecting the top N ranked features that provided the maximum class separation among classes associated with different clinical scores defined in the reduced feature space. This was achieved by calculating the Davies-Bouldin (DB) cluster validity index [25]. Instead of utilizing the DB index to assess cluster quality, we applied it to assess the discriminatory ability of our candidate feature subsets for distinguishing the different classes. The DB index measures how well-separated data samples belonging to different classes are and how similar samples in the same class are. It is a function of the ratio of the sum of within-class scatter to between-class separation. Thus, smaller values of the DB index indicate better class separation and vice versa. The DB index was calculated by incrementally adding, one at a time, features ranked according to the ReliefF algorithm. We determined an optimal cutoff point for the discrimination of classes beyond which adding more features led to no significant improvement in the DB index.

2.2.7 Classification

The recognition of health outcomes from clinical datasets is a very important problem in biomedical research and health risk management. The techniques based on machine learning, such as artificial neural networks (ANN) are based on inductive inference rather than on classical statistics [26]. Machine learning algorithms can achieve superior predictions than the only statistical protocols and can be used for clinical decision support. For the implementation of machine learning classification a number of steps are needed:

- Initialization of parameters of selected neural network.
- Training of the machine learning model with the features selected and extracted in order to avoid dependencies between variables which can decrease the classifier accuracy. In this step the architecture of the model and its hyper-parameters are optimized.
- Validation: the leave one subject out cross validation is performed in order to guarantee good predictive properties of the machines learning.

The results of heart murmurs classification obtained by the model were validated with Eco-doppler scores. In this study, we choose to use of the self-organizing map (SOM) due to the success of this approach in several classification problems. The SOM is a network structure which provides a topological mapping [27]. The main difference with the artificial neural network is that it is based on unsupervised learning. In contrast to supervised learning, which is based on an external supervision who presents a training set to the network, an unsupervised or self-organizing network during the training session receives a number of different input patterns, discovers significant features in these patterns and learns how to classify input data into appropriate categories. This type of learning tend to follow the neuro-biological organization of the brain which is dominated by the cerebral cortex, a very complex structure of billions of neurons and hundreds of billions of synapses. The cortex includes areas that are responsible for different human activities (motor, visual, auditory, somatosensory, etc.) and associated with different sensory inputs. We can say that each sensory input is mapped into a corresponding area of the cerebral cortex. The cortex is a self-organizing computational map in the human brain. It places a fixed number of input patterns from the input layer into a higher-dimensional output or Kohonen layer as showed in Figure 7. Training in the Kohonen network begins with the winner's neighborhood of a fairly large size. Then, as training proceeds, the neighborhood size gradually decreases.

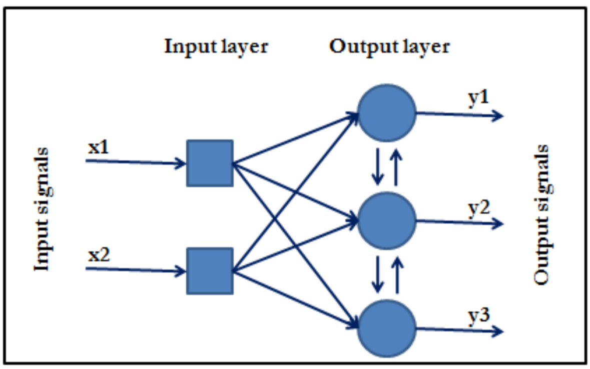

Figure 7: Architecture of a simple Kohonen self-organized map

The lateral connections are used to create a competition between neurons. The neuron with the largest activation level among all neurons in the output layer becomes the winner. This neuron is the only neuron that produces an output signal. The activity of all other neurons is suppressed in the competition. The lateral feedback connections produce excitatory or inhibitory effects, depending on the distance from the winning neuron. This is achieved by the use of a Mexican hat function (Figure 8) which describes synaptic weights between neurons in the Kohonen layer.

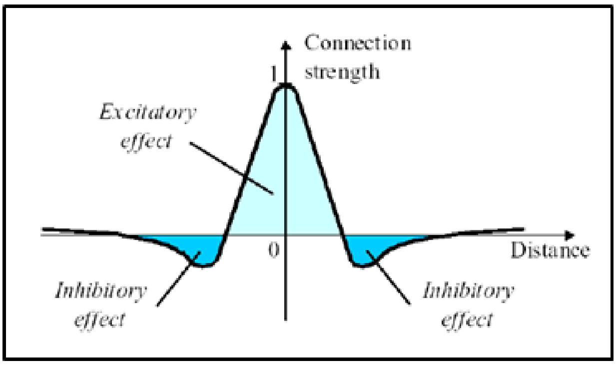

Figure 8: Mexican hat shaped competition function among neurons

In the Kohonen network a neuron learns by shifting its weights from inactive connections to active one. Only the winning neuron and its neighborhood are allowed to learn. If a neuron does not respond to a given input pattern, then learning cannot occur in that particular neuron. The competitive learning rule defines the change Δw_{ij} applied to synaptic weight w_{ij} as

$$\Delta w_{ij} = \begin{cases} \alpha\left(x_i - w_{ij}\right) & \text{if neuron j wins the competition} \\ 0 & \text{if the neuron j loses the competition} \end{cases}$$

where x_i is the input signal and α the learning parameter. The overall effect of the competitive learning rule resides in moving the synaptic weight vector w_j of the winning neuron j towards the input pattern X. The matching criterion is equivalent to the minimum Euclidean distance between vectors. During the model fine-tuning design, two different types of SOM models were tested using registrations and features extracted both from the third left intercostal and mitral space:

1) a hierarchical SOM based model
2) a combined SOM model with fuzzy rule base

Both the models are totally self-organizing and adaptive, but their performance will strictly depend on the “goodness” of the features extracted and selected in the training dataset.

2.2.8 The hierarchical SOM

The hierarchical SOM developed is shown in Figure 9 a component-based description of the system is given in the following description.

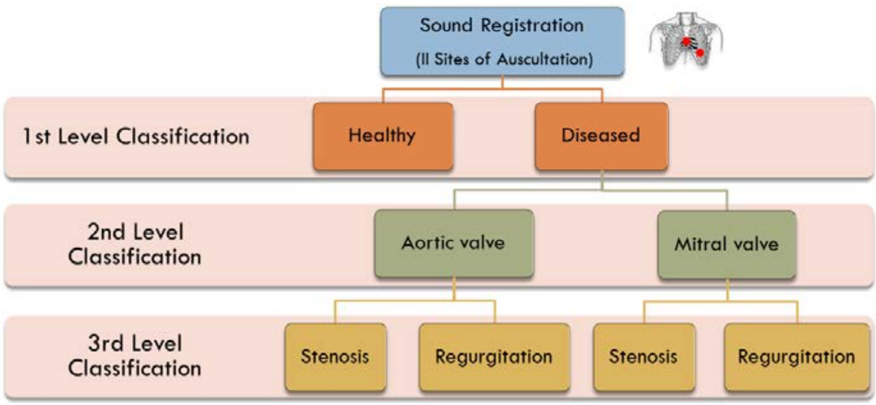

Figure 9 Hierarchical model with one site of auscultation in the third intercostal space

The input of the network were the features extracted and selected from the third intercostal and the mitral spaces. The first level of the SOM network was developed to perform if the subject was healthy or with disease. At The second level one SOM was trained using only the dataset of diseased subjects to recognize if the problem is for the aortic or mitral valve and finally at the third level two SOM were trained for two separates diseases: SOM to recognize stenosis or regurgitation for aortic valve and SOM to recognize stenosis or regurgitation for mitral valve. Each SOM is composed of one layer two-dimensional in which all the inputs are connected to each node in the network. A topographic map is autonomously organized by a cyclic process of comparing input patterns to vectors at each node. The node vector to which inputs match is selectively optimized to present an average of the training data. Then all the training data are represented by the node vectors of the map. Starting with a randomly organized set of nodes, and proceeding to the creation of a feature map representing the prototypes of the input patterns, the training procedure is as follows:

1. Initialization of the weights w_{ij} (1≤*i*≥ nF, 1≤*j*≥ m) to small random values, where nF is the total number of selected features (input) and m is the total number of nodes in the map. Set the initial radius of the neighbourhood around node j as $N_j(t)$.
2. Present the inputs $x_1(t)$, $x_2(t)$ . . . . . $x_{nF}(t)$, where $x_i(t)$ is the *ith* input to node j at time t.
3. Calculate the distance d_j between the inputs and node j by the Euclidean distance to determine j* which minimizes d_j:

$$d_j = \left|\left|W_j(t) - X(t)\right|\right| \qquad (1)$$

   Every node is examined to calculate which one's weights are most like the input vector. The winning node is commonly known as the Best Matching Unit (BMU). The radius of the neighborhood of the BMU is then calculated. This is a value that starts large, but diminishes each time-step. Any nodes found within this radius are deemed to be inside the BMU's neighborhood.

4. Update the weights w_{ij} of the winning neuron j* and of its neighborhood neurons $N_{j*}(t)$ at the time t, for the input vector X, are modified according to the following equation (2) to make them more like the input vector:

$$w_{ij}(t) = w_{ij}(t-1) + \alpha(t)[X(t) - w_{ij}(t-1)] \tag{2}$$

   where α(t) is the learning rate. Both α (t) and $N_{j*}(t)$ are controlled so as to decrease in t.

5. If the process reaches the maximum number of iterations, stop; otherwise, go to (2).

As expected, the prototypes of the same class (or classes with similar feature characteristics) are close to one another in the feature map. Those labels are then used in classifying unknown patterns by the nearest neighbor SOM classifier. At the end of the training process, the testing phase is performed. Even if the SOM are unsupervised learning model, the final outputs were compared with the scores provided by Eco-doppler. The final performances of the classification task were evaluated using the leave one subject out validation process, where each fold consists of one subject left-out. This method is an iterative process in which one subject is recruited each time for validation. Each level of hierarchical SOM classifier was trained using the remaining data and validated on the single, left-out validation point. This ensures that the validation is unbiased, because the classifier does not see the validation input sample during its training. One by one, each available subject was recruited for validation.

2.2.9 Combining SOM and fuzzy logic

The results provided in terms of sensitivity and specificity of the hierarchical model were encouraging, but considering that several data collected from subjects had combined pathologies, we decided to improve the results combining the SOM with fuzzy rules. The SOM was trained with the features extracted from the sounds collected from the third intercostal space and the mitral sites of auscultation and labeling performed with Ecodoppler score as shown in Figure 10.

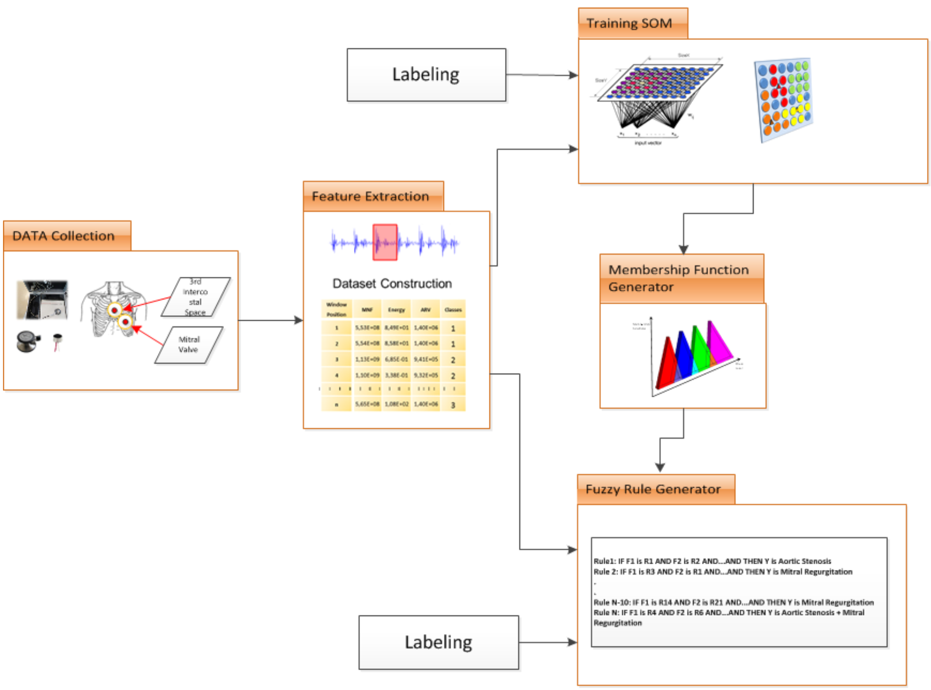

Figure 10 Training phase of SOM model with Fuzzy rules

In this learning phase, the SOM was used to produce a prototype of the training set and then, for each input variable x_i we generated the fuzzy membership function using triangular functions with the center in the corresponding weight w_{ij} of the map and the corresponding variance $v_{ij,}$ where ì is the *ith* input and j represents the *jth* node of the map. The centers of the triangular membership functions in the *ith* input are (w_{i1} w_{i2} ..... w_{im}). The corresponding regions were set to [w_{i1}-2v_{i1}, w_{i1}+2v_{i1}], [w_{i2}-2v_{i2}, w_{i2}+2v_{i2}],…, [w_{im}-2v_{im}, w_{im}+2v_{im}], as is shown in Figure 11 where m is the last node of the map.

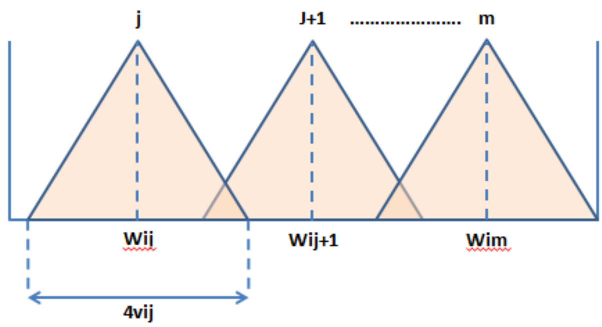

Figure 11 Generation of the fuzzy membership function for the *ith* input. The number of triangular functions is the equal to the SOM nodes

In order to reduce the number of fuzzy rules and to improve the system reliability, narrowly separated regions were combined to become a single region. Let the positions of the four corners of region j be ll_j, lh_j, rh_j and rl_j (for a triangular membership function, lh_j = rh_j). Two neighboring regions j-1 and j were merged if they satisfied the following equation (3):

$$\frac{\mathrm{lh_j} + \mathrm{rh_j}}{2} - \frac{\mathrm{lh_{j-1}} + \mathrm{rh_{j-1}}}{2} \leq \mathrm{thr} \qquad (3)$$

where thr is pre-specified threshold (set to 0.1 in our experiments). This process continued until all regions were well separated in terms of the threshold. Accordingly, some fuzzy regions had trapezoidal shapes instead of triangular ones as is shown in Figure 12.

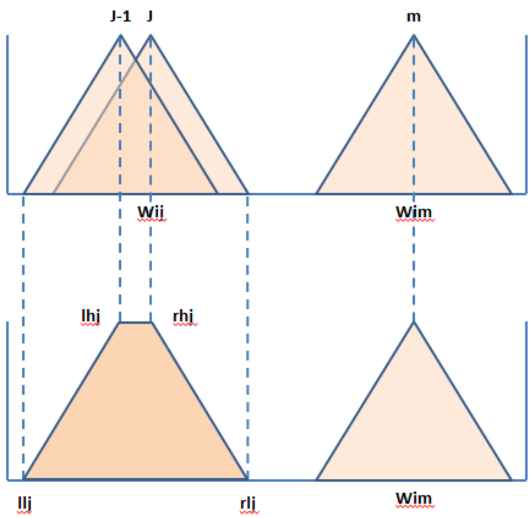

Figure 12 Trapezoidal function obtained for neighboring regions

After that, we generated fuzzy rules as a set of associations of the form “if antecedent conditions hold, then consequent conditions hold”. Each feature was normalized to the range of

[0.0,1.0] and each region of fuzzy membership function was labeled as R1, R2,…RN. An input was assigned to the label of a region where the maximum membership value was obtained. Apparently each training sample produced a fuzzy rule. An example of rule generated is listed below:

IF

feature1 is R1 AND feature2 is RN AND feature3 is R2 AND feature4 is R3 AND feature5 is R6, AND feature6 is R8 …. AND feature M is R3

THEN

it is Aortic Stenosis

Finally, the number of all the fuzzy rules was the same order of the training samples. The problem was that a large number of training patterns may lead to repeated or conflicting rules. To deal with this problem, we recorded the number of rules repeated during the learning process. Those rules supported by a large number of examples were saved. A centroid defuzzification formula was used to determine the output for each input pattern (valvulopaties):

$$Z = \frac{\sum_{i=1}^{k} D_p^i O^i}{\sum_{i=1}^{k} D_p^i} \qquad (4)$$

Where Z is the output, k is the number of rules, O^i is the class generated by rule i and D_p^i measures how the input vector fit the ith rule. D_p^i is given by the product of degrees of the pattern in the regions which the *ith* rule occupies. The output is within [0,9] for numeral recognition of valvulopaties (0=unknown, 1=healthy, 2=aortic stenosis, 3=aortic regurgitation, 4=mitral stenosis, 5=mitral regurgitation, 6=mitral + aortic stenosis, 7=mitral + aortic regurgitation, 8=mitral regurgitation + aortic stenosis, 9=mitral stenosis + aortic regurgitation). The output Z was adapted taking the nearest smaller integer value. Fuzzy rules do not necessarily occupy all fuzzy regions in input space. There could be some regions where no related rule exists. This is the case when the denominator in equation (4) is zero. We label the corresponding input subject as unknown. After training the model was designed to be able to discriminate until nine different classes as presented in the bottom part of Figure 13 during recognition phase with the trained fuzzy classifier.

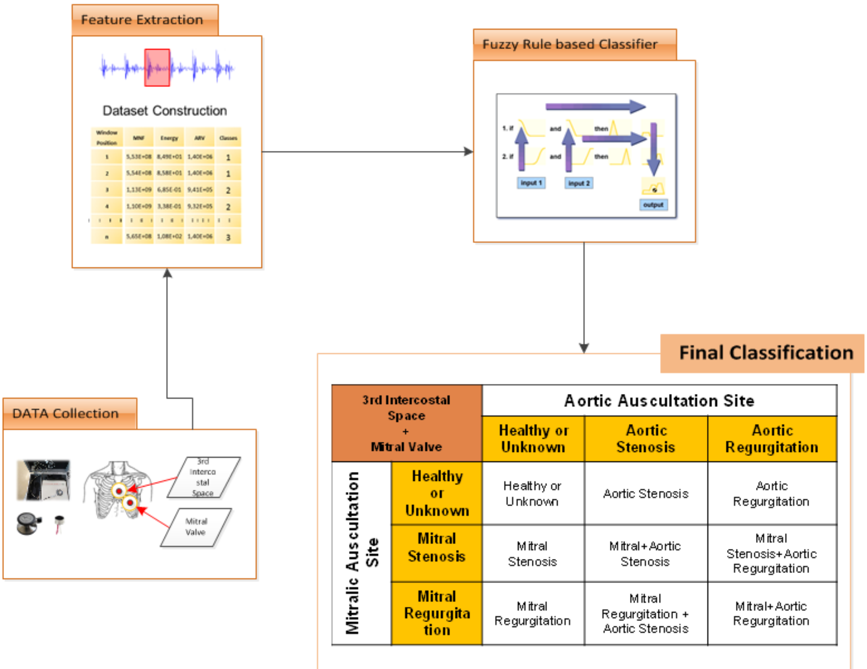

Figure 13 Recognition phase with the trained fuzzy classifier

2.3 Results and Discussion

The signals were collected from the two sites of auscultation (third intercostal space and mitral) and then 35 features were extracted for each site of auscultation extracting totally 70 parameters. The features were extracted from the segmented cardiac cycle applying the homomorfing filtering technique described in section 2.2.5 which allowed a good peak detection as is shown in Figure 14 and Figure 15.

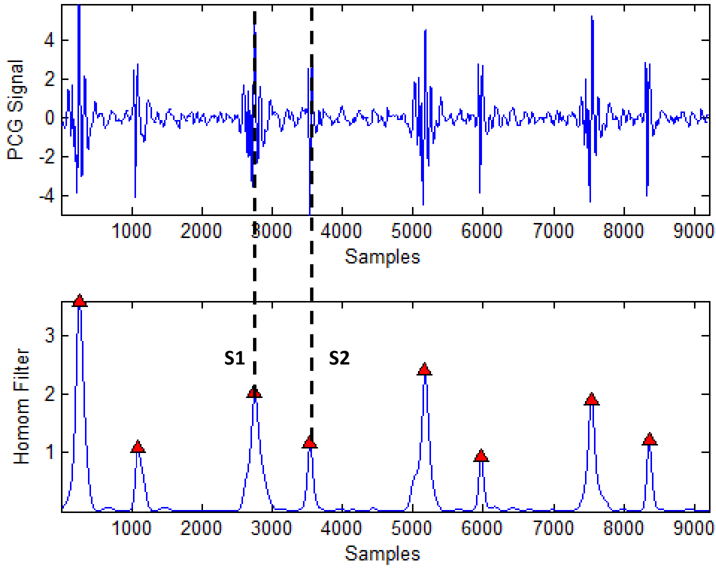

Figure 14 Peak detection for PCG signal (Normal)

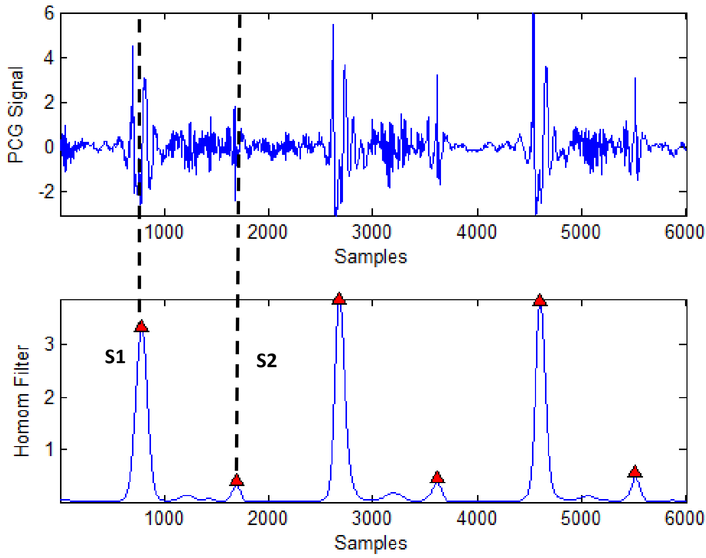

Figure 15 Peak detection for PCG signal (Aortic stenosis)

After peak detection in time domain was extracted the distance between S1 and S2, the entropy and the root mean square (RMS) of all the heart cycle, while in frequency domain the wavelet coefficients were extracted using Daubechies-2 wavelet as is shown in Figure 16 and applying the powers of the signal at the second decomposition level with each window containing 16 discrete data values and obtaining 32 parameters as is shown in Figure 17. Finally were extracted 35 features for each site of auscultation.

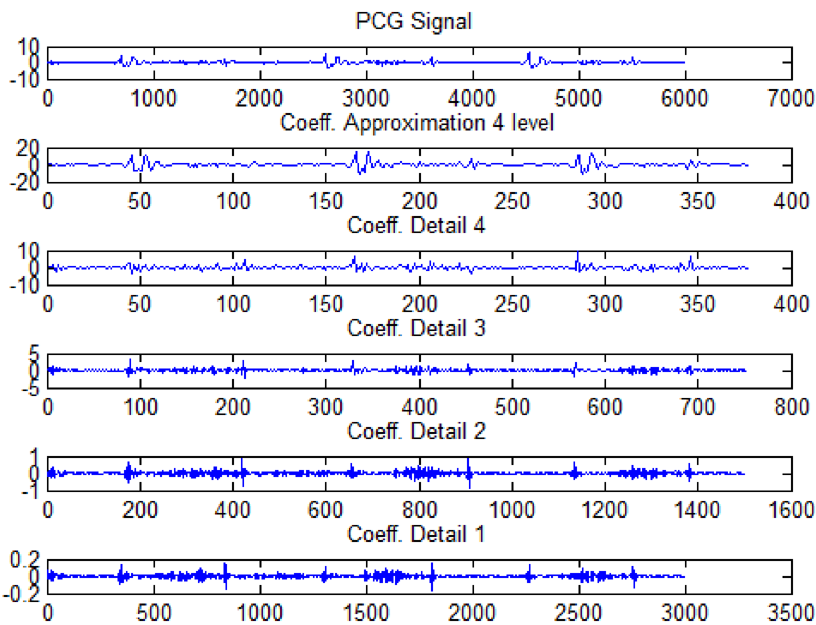

Figure 16 Wavelet detail coefficients at the first four levels (d1–d4) and wavelet approximation coefficient at the fourth level (a4) for PCG signal (Aortic stenosis).

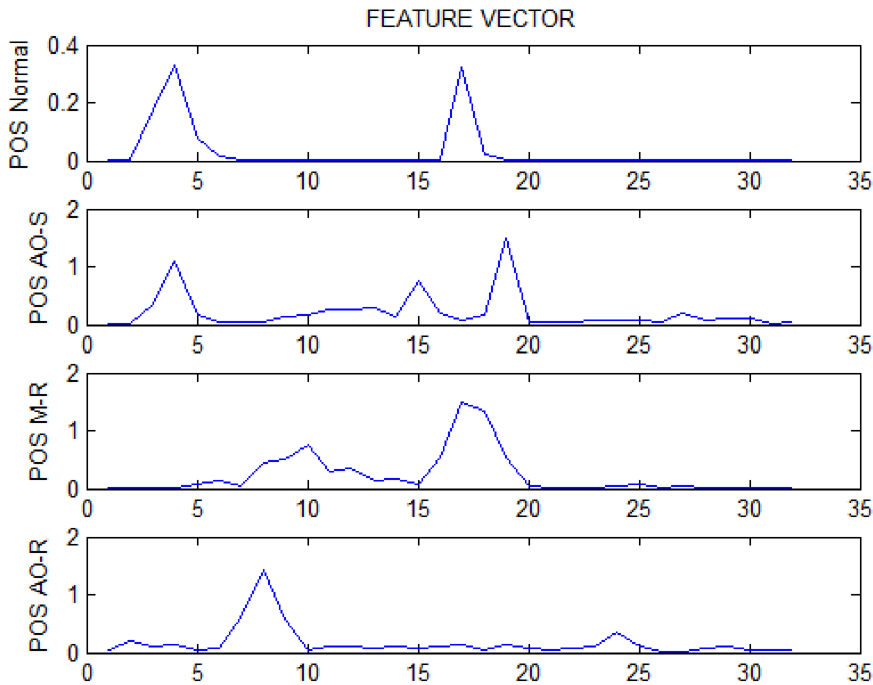

Figure 17 Vector of features extracted applying the power of signal of wavelet coefficients for five cases: (a) Normal, (b) Aortic Stenosis (AO-S), (c) Mitral Regurgitation (M-R), (d) Aortic Regurgitation (AO-R)

Then, features were first ranked using the Relief algorithm and the DB index rejecting both less discriminant and redundant features for the classification avoiding over-training effects and allowing diminished computational costs. In Figure 18 is reported the DB index. For the study were selected 30 features. This choice indicates that optimal separation among the classes associated with different clinical scores can be achieved by using the first 30 features selected with the ReliefF algorithm.

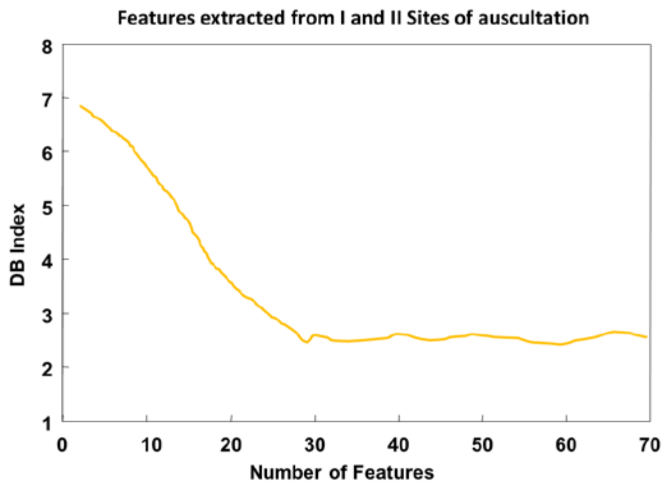

Figure 18 DB index extracted from ranked features

Among the 30 most significant features selected we had the distance between S1 and S2, the RMS, the entropy of the heart cycle while as regards the 32 parameters related to the powers of the signal extracted from the wavelet detail coefficients extracted from the second decomposition level, the most discriminant features were selected from 4th to 9th and 15th to 20th power spectral sub-windows of both sites of auscultation. The selection of these components in frequency domain is not surprising because most of murmurs are systolic and most of information is located in that sub-window. After feature selection the last stage to perform was the classification. In particular, in this study Kohonen self-organizing maps were used. Two different classifiers were developed and tested. The first is based on a hierarchical structure, while the latter is combined with fuzzy logic rules. For both classifiers, the input was the feature vector Xi that represent the 30 selected features extracted and selected of each cardiac cycle. The output of the hierarchical SOM was a binary variable representing healthy or diseased at the first level; if the subject was diseased the second level recognized the binary output atrial or mitral and then the third level identify if the recognized valve was affected by stenosis or regurgitation. After input selection, different square self-organizing maps were examined. The best compromise was obtained selecting a 10x10 self-organizing Kohonen map. The percentage classification of error for each class and across all tasks appeared to reach a plateau when the SOM 10x10 and a learning rate equal to 0.9 were used. The improvement in percentage classification error compared to when 5x5 or 8x8 maps were used appeared to be substantial, but no further substantial improvement was observed when 20x20 were used. Based on this observation, we chose to use SOM with 10x10 nodes. This choice is also justified by the observation that unnecessarily increasing the number of nodes could potentially lead to increasing the correlation among nodes thus affecting the classifier performance. For pattern recognition problems and training of the SOM, the mean squared error was used to approximate the posterior probabilities of class membership, conditioned on the input variables. This is carried out by means of the back-propagation. In this study, we set the training algorithm to stop when the norm of the objective function gradient falls below 0.05. That means that the necessary condition for a minimum has been satisfied. During the training process the mean squared error decreases until those stopping criteria is satisfied (about 700 epochs). The evaluation of the initial guess is 0.1; after training this value falls to 0.021 Figure 19 shows the mean squared error and its max error versus the training epochs.

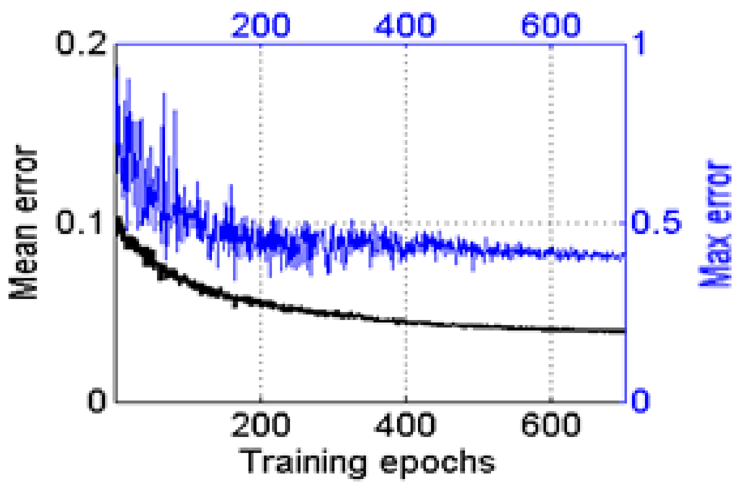

Figure 19. Training of neural network showing mean squared error evaluation and max error as a function of the training epoch

After training of the KSOM by means of the data set collected, the performance of the classification task was evaluated. In order to check the generalization capability of the neural network, the leave one subject out validation process was carried out. The approach measured the power of the classification approach rather than of one specific classifier. To validate the prediction model each output provided by the left-out sample of dataset was compared with the gold standard Eco-doppler scores. The prediction quality of classification model was defined as the ratio between correct and wrong classifications. In Table 3 is reported the true positive percentage for each level of classification with mean and standard deviation of all the subjects tested with the neural network.

Table 3 Classification results of hierarchical SOM model with selected features. For each level of classification is reported the efficiency evaluated by the true positive percentage.

	% CORRECT CLASSIFICATION	
1st Level of Classification	Healthy: 85±3%	Diseased: 89±2%
2nd Level of Classification	Dis_Aortic: 75.1±3%	Dis_Mitral: 73.3±9%
3rd Level of Classification	Ao_Stenosis: 86.2±7% Ao_Regurgit.: 79.2±1%	Mit_Stenosis: 75.2±8% Mit_Regurgit.: 69.3±5%

As showed, the mean sensitivity and specificity of the model were respectively of 85% and 89%, but it’s efficiency fell within the second and third level of classification. Even if the proposed model achieved good capability of generalization up to the second level of classification, it was not able to recognize combined valvulopaties. To further improve the performances a second model of SOM combined with fuzzy rules was developed. In this case the output was a one target variable from

0 to 9 representing respectively the classes: 0=unknown, 1=healthy, 2=aortic stenosis, 3=aortic regurgitation, 4=mitral stenosis, 5=mitral regurgitation, 6=mitral + aortic stenosis, 7=mitral + aortic regurgitation, 8=mitral regurgitation + aortic stenosis, 9=mitral stenosis + aortic regurgitation. After training of the map with 80 subjects selected from all the classes, the fuzzy membership functions were extracted from each node (10x10 map), building totally 30 membership functions. Using the combination technique and starting from 100 fuzzy regions, applying the threshold equal to 0.1, we had a different number of fuzzy regions for each input. In Figure 20 is reported the final number of fuzzy regions for each membership function (input) generated from the 10 x 10 SOM nodes after the combination threshold.

1 **15**	2 **13**	3 **20**	4 **10**	5 **9**	6 **7**
7 **12**	8 **6**	9 **14**	10 **13**	11 **12**	12 **11**
13 **15**	14 **10**	15 **13**	16 **11**	17 **16**	18 **18**
19 **9**	20 **12**	21 **11**	22 **15**	23 **12**	24 **14**
25 **14**	26 **15**	27 **6**	28 **13**	29 **10**	30 **7**

Figure 20 Number of Fuzzy regions generated from 10x10 SOM for each input (membership function)

Altogether 50 fuzzy rules were generated from all the training patterns of the database and 80 subjects were used to validate the model. The combination of SOM with fuzzy rules was the key to reduce the percentage classification error. In Figure 21 is shown that a significant reduction in percentage classification error values was achieved using the SOM combined with fuzzy model respect to the use of the single SOM.

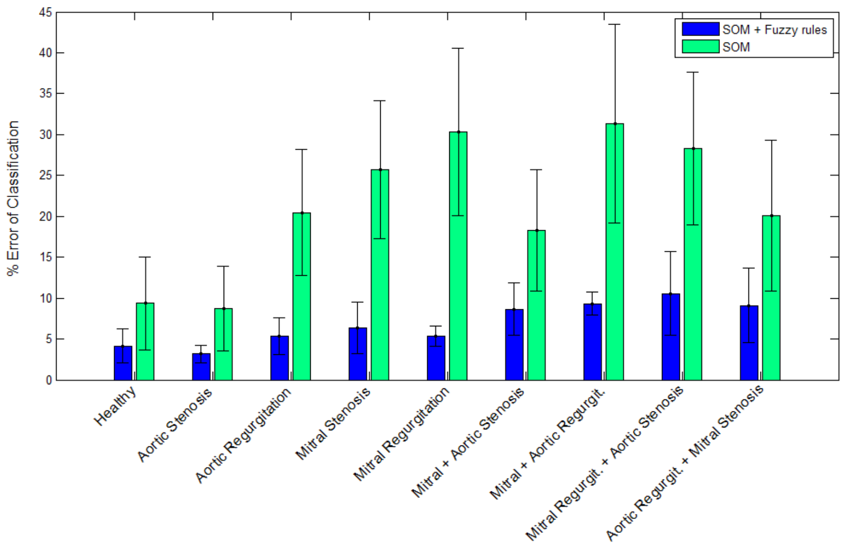

Figure 21 Comparison of error of classification (%) between SOM and SOM combined with fuzzy model

The sensitivity obtained was of 95% and the specificity of 91%. The average error of classification was around 5% for the classes affected by a single pathology and about 10% for combined valvulopaties. Moreover the classification error was reduced by approximately 60% when we used the SOM combined with fuzzy model compared with the SOM. Finally we found that the combined SOM and fuzzy rules system was able to classify most of pathologies correctly, achieving good test accuracy also for combined classes.

2.4 Conclusions

Cardiac auscultation continues to be the healthcare professional's primary tool for distinguishing between innocent and pathological heart murmurs. In this study a new heart sound recognition model using the SOM and the combination with fuzzy rules was presented. Features about the health of heart valves were extracted from a single cycle of phonocardiogram signal using distance between the two sounds, RMS, entropy and wavelet transform. We proposed a methodology to segment phonocardiogram signal into single cycle using Homomorphic filtering and Kmeans clustering for the entire sequence of phonocardiogram signal recording. The first algorithm based on SOM has shown sensitivity of 85% and specificity of 89%, but the capability to discriminate the different pathologies was less efficient. The introduction in the second model of the fuzzy membership functions generated from the nodes of the SOM has been proved to improve the performances especially for combined valvulopaties obtaining an error of classification of 10%. In this model, fuzzy rules can be learned continuously, so such a system can easily be designed to be adaptive. Moreover, this fuzzy rule based classifier provides a framework for us to integrate the rules based on human experience with those learned from the training data. Future work will focus on the optimization of fuzzy membership functions and fuzzy rules for further improvement in classification performances. Such a device is not seen as replacing the need for a clinician's assessment in a patient found to have a heart murmur. Such a device may, however, assist a clinician in rendering an opinion concerning a murmur. The stethoscope's main usage will be in the primary health care, when deciding who requires special care. In addition, this technology offers great promise for the development of a device for high-volume screening of subjects for heart disease. Eventually, this work is expected to lead to an automatic screening device with additional capabilities of predicting selected heart conditions.

2.5 References

[1]. Garson A, Bricker J, McNamara D. The Science and Practice of Pediatric Cardiology. Philadelphia, Pa: Lea & Febiger; 1990:2203–2212. 2. Pelech A. The cardiac murmur. Pediatr Clin North Am. 1998;45:107–122.

[2]. D. Smith and E. Craige, "Heart Sounds: Toward a Consensus Regarding their Origin," Am. J. Noninvas. Cardiol., vol. 2, pp. 169-179, 1988.

[3]. L. Wigstrom, T. Ebbers, A. Fyrenius, M. Karlsson, J. Engvall, B. Wranne, and A. F. Bolger, "Particle trace visualization of intracardiac flow using time-resolved 3D phase contrast MRI," Magn Reson Med, vol. 41, pp. 793-799, 1999.

[4]. S. Persson and J. Engqvist, Kardiologi: hjärtsjukdomar hos vuxna, 5., rev. ochutök. uppl. / ed. Lund: Studentlitteratur, 2003.

[5]. A. G. Tilkian and M. B. Conover, Understanding heart sounds and murmurs: with an introduction to lung sounds, 4. ed. Philadelphia: Saunders, 2001.

[6]. D. Smith and E. Craige, "Heart Sounds: Toward a Consensus Regarding their Origin," Am. J. Noninvas. Cardiol., vol. 2, pp. 169-179, 1988.

[7]. DeGroff, C. G., Bhatikar, S., Hertzberg, J., Shandas, R., Valdes-Cruz, L., & Mahajan, R. L. (2001). Artificial neural network–based method of screening heart murmurs in children. Circulation, 103(22), 2711-2716.

[8]. Dewan, S et al. “Heart Murmurs”, Good Health Magazine, Feb/Mar 1998.(http://www.seton.net/Wellness/GoodHealthMagazine/GoodHealthMagazineAr0A67/HeartMurmurs.asp).

[9]. Andrisevic, N., Ejaz, K., Rios-Gutierrez, F., Alba-Flores, R., Nordehn, G., & Burns, S. (2005). Detection of heart murmurs using wavelet analysis and artificial

neural networks. Journal of biomechanical engineering, 127(6), 899.

[10]. De Vos, J. P., & Blanckenberg, M. M. (2007). Automated pediatric cardiac auscultation. Biomedical Engineering, IEEE Transactions on, 54(2), 244-252.

[11]. Pretorius, E., Cronje, M. L., & Strydom, O. (2010, August). Development of a pediatric cardiac computer aided auscultation decision support system. In Engineering in Medicine and Biology Society (EMBC), 2010 Annual International Conference of the IEEE (pp. 6078-6082). IEEE.

[12]. Kwak, C., & Kwon, O. W. (2012). Cardiac disorder classification by heart sound signals using murmur likelihood and hidden Markov model state likelihood. IET signal processing, 6(4), 326-334.

[13]. Chen, Y., Wang, S., Shen, C. H., & Choy, F. K. (2012). Matrix decomposition based feature extraction for murmur classification. Medical engineering & physics, 34(6), 756-761.

[14]. Mason, D. 'Listening to the heart: a comprehensive collection of heart sounds and murmurs' (F. A. Davis Company, Philadelphia, 2000).

[15]. TMS320C5515 Fixed-Point Digital Signal Processor, http://www.ti.com.

[16]. J.R. Deller, J.G. Proakis, J.L. Hansen, Discrete Time Processing of Speech Signals, Prentice Hall, 1993.

[17]. A. P. Yoganathan, R. Gupta, F. E. Udwadia, J. W. Miller, W. H. Corcoran, R. Sarma, J. L. Johnson, and R. J. Bing, "Use of the fast Fourier transform for frequency analysis of the first heart sound in normal man," Med Biol Eng, vol. 14, pp. 69-73, 1976.

[18]. A. P. Yoganathan, R. Gupta, F. E. Udwadia, W. H. Corcoran, R. Sarma, and R. J. Bing, "Use of the fast Fourier transform in the frequency analysis of the second heart sound in normal man," Med Biol Eng, vol. 14, pp. 455-460, 1976.

[19]. M. S. Obaidat, "Phonocardiogram signal analysis: techniques and performance comparison," J Med Eng Technol, vol. 17, pp. 221-227, 1993.

[20]. A. P. Yoganathan, R. Gupta, F. E. Udwadia, J. W. Miller, W. H. Corcoran, R. Sarma, J. L. Johnson, and R. J. Bing, "Use of the fast Fourier transform for frequency analysis of the first heart sound in normal man," Med Biol Eng, vol. 14, pp. 69-73, 1976.

[21]. T. Olmez, Z. Dokur, Classification of heart sounds using an artificial neural network, Pattern Recognit. Lett. 24 (January) (2003) 617–629.

[22]. ReliefF M. Robnik-Sikonja and I. Kononenko, BTheoretical and empirical analysis of ReliefF and RReliefF, Mach. Learn. J., vol. 53,pp. 23–69, 2003.

[23]. K. Kira and L. A. Rendell, BA practical approach to feature selection, in Proc. Int. Conf. Mach. Learn., 1992, pp. 249–256.

[24]. M. Robnik-Sikonja and I. Kononenko, BTheoretical and empirical analysis of ReliefF and RReliefF, Mach. Learn. J., vol. 53,pp. 23–69, 2003.

[25]. J. C. Bezdek and N. R. Pal, BSome new indexes of cluster validity, IEEE Trans. Syst., Man, Cybern., vol. 28, pp. 301–315, 1998.

[26]. Vapnik V.N. The Nature of Statistical Learning Theory, 2nd ed. Springer, New York, 2000.

[27]. Kohonen T. Self-Organizing Maps. Springer Verlag, 1995

Chapter 3

A novel pervasive architecture for the intelligent monitoring of muscular fatigue in elderly

Muscle fatigue and exercise intolerance are common and frequent symptoms complained by patients with neuromuscular disease. Muscle fatigue would occur when the intended physical activity can no longer be continued or is perceived as involving excessive effort and discomfort. Except for several rare myopathies with specific metabolic derangements leading to exercise-induced muscle fatigue, most studies fail to identify precise pathogenic mechanism of fatigue in this population of patients. On the other, apart from canonical examples of neuromuscular diseases, a number of conditions in which muscle apparatus can be involved is known to occur with high prevalence among certain people categories, such as elderly or people undergoing immobilization. In these cases exercise intolerance and muscle fatigue can be severely invalidating in the daily common activities. An objective and smart unobtrusive techniques able to objectively measure fatigue phenomenon would be useful in monitoring muscle function in both NMD patients and patients with secondary skeletal muscle involvement. Emerging personal assistive and unobtrusive monitoring technologies can help to automatically identify and address major deficits. In this study, we report a novel assistive architecture for the elderly able to non-invasively assess muscle fatigue by biomedical sensors (surface electromyography) using a wireless ergonomic platform during exercise.

3.1 Introduction

3.1.1 Related works about muscular fatigue

Muscle fatigue is considered a typical symptom of neurological diseases [1]. It is present in more than 60% of patients with a neuromuscular disorder [2], but also in diseases affecting central nervous system, as in Parkinson's disease where increased fatigue is associated with less physical fitness, and lower functional capacity [3]. Among the different classifications of fatigue reported in literature, one refers to experienced fatigue, defined as difficulty to sustain voluntary activities [1] and physiological fatigue, defined as the loss of capacity to generate a maximum force during an exercise [4]. Aging is associated with the progressive degeneration of organs and tissues and the loss of several abilities, including cognition and memory, but also of the functional reserve of the body's systems, particularly in neuromuscular apparatus, which varies in type and severity. The muscular strength decline is due to qualitative changes of muscle fibers, such as selective atrophy, and neuronal changes, such as lower activation of the agonist muscle and higher coactivation of the antagonist muscles, reduce the capacity to carry out basic daily life activities and put people at risk of falls and dependence [5]. The decline of the functional reserve of the body's systems may impair an individual's ability to perform physical activities, and in general to cope with external challenges. Maintaining physiological function in an aging population is of utmost importance in order to reduce the burden on medical services and systems, as well as to promote social inclusion. To this regard, the American Physical Activity Guidelines [6] maintain that regular physical activity is essential for healthy aging, mainly focusing on two types of activity, aerobic and muscle-strengthening. Assistive and monitoring technologies can help to automatically identify and address major muscular deficits. In particular, surface electromyography (sEMG) can be useful in recognizing reduced motor performances of a subject. Examples of muscle-strengthening activities include lifting weights, working with resistance bands, doing calisthenics using body weight for resistance (such as push-ups, pull-ups, and sit-ups), climbing stairs and carrying heavy loads. All these activities require a moderate to high level of intensity and often are included as part of a therapy or rehabilitation programs for neuromuscular diseases. The aim of our study is to develop an ergonomic, personal sEMG monitoring architecture for the elderly at home, which is able to extract relevant features for a remote clinical report to the doctor in order to monitor muscular fatigue and coach physical exercises for rehabilitation purposes.

3.1.2 Mobile pervasive architecture for patient-centered systems

From a general point of view, a mobile pervasive architecture consists of different wireless modules cooperating in order to perform data acquisition from multiple sensors, data analysis and decision through several techniques and data redirection and feedbacks. The architecture here proposed addresses the design of a flexible instrument for data acquisition, management, elaboration and decision suitable for those systems which are equipped with distributed remote wearable devices, where a particular attention is paid to the heterogeneous medical information flow and inter-process communication as showed in Figure 22. Moreover, the possibility to operate in real time imposes critical efficiency requirements to each single module.

The core of the architecture is the Personal Digital Assistant (PDA), which collects data from the Personal Mobile Sensing Platform using a configurable time resolution and dedicated Bluetooth communication channels. A data pre-processing step is performed on the sensor electronic board, so that the wireless communication with the PDA is significantly reduced. The PDA is able to integrate the time-aligned wearable sensor information and to store relevant data in its own local database (DB). The PDA performs a provisional analysis of device-mediated responses (Lite Processing), being able to take into account context information (GPS, motion activity) and physiological data (e.g. hearth rate, breath rate, muscular fatigue) to obtain a provisional score (Mobile Reasoning Module). The provisional score triggers a more accurate analysis in order to perform the local feedback strategy and allows the user to get as feedback the output of the analysis. In the case of a provisional score higher than a fixed (configurable) threshold, the PDA is able to establish a connection with the remote central DB and to upload the collected data for further and more accurate analysis. The remote central DB I/O communication layer is implemented through a Web Services Description Language (WSDL) interface. The WSDL interface design pays attention to the management and the synchronization of data and processes. Pattern recognition algorithms, knowledge-based and rule-based models are defined as running processes inside the Analysis Module.

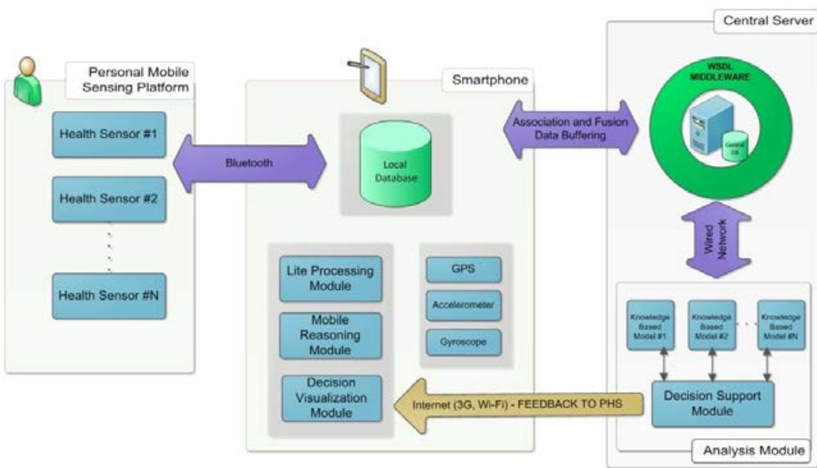

Figure 22 The mobile pervasive architecture

In the PDA a data fusion approach is implemented in order to act as a buffer for the flow of information coming in from different sensors. With this strategy sensor data fusion is gained enabling an abstraction with respect to the specific technology of the transducers. Signals coming from the sensors are gathered in parallel and encoded according to a dedicated protocol. A specific filter for each sensor receives the encoded information. The information available in the PDA data fusion module is encoded in order to set up a common communication language between the sensor interfaces and the Analysis Module. This guarantees an increased flexibility thanks to the presence of interfaces performing the function of interpreters for the specific hardware and filters which specify the way the communication framework senses and communicates the information. Analysis and decision modules run asynchronously in respect of the PDA. The server analysis module is realized on modular knowledge basis enabling an objective and quantitative assessment of physiological data and the decision support provides warnings and motivating feedback. At fixed (configurable) time steps or following the request of the user, the modules will: i) retrieve relevant data from the remote central DB; ii) apply the analysis algorithms; iii) store the analysis results in a specific report within the remote central DB. The PDA can be configured to poll the analysis report at fixed time steps or at the request of the user. In this way the PDA always works as client system in respect of the server analysis modules.

3.2 Materials and Methods

3.2.1 Requirements of the architecture for monitoring of muscular fatigue

The architecture should be designed to monitor symptoms of muscular fatigue at home, to motivate the subjects to perform training exercises and to provide a report to the physicians about muscular strengthening. The whole architecture should consists of three main components: the wireless sEMG acquisition sensor, the mobile acquisition system and the remote database integrating the decision support system. These three components interact with each other through wireless connections. The developed algorithm has to be organized as follows:

- Acquisition of data from the mobile module
- Transmission of data to the central database
- Processing of data by the decision support system
- Sending the report to the physicians

The system will introduces an innovative ontology enabling and facilitating interoperability for the patient and physicians. The data have to be acquired in real-time and analyzed under lite processing on a PDA using Bluetooth connection. All the data are managed and collected with a software running in the tablet, which collects digital sEMG signals and provides i) data synchronization, ii) data storage, and iii) data communication to the WSDL interface. Additional devices for recording other parameters can also be added. A portable device compliant with the following features should be adopted:

- High level operating system (Windows)
- Large screen for elderly user-interface (3-9 inches)
- Touch screen
- Internal memory + SD card (2 GBs)
- Powerful internal CPU (400-600MHz)
- WiFi/3G connection for communication with remote servers
- Bluetooth/Zigbee connection for communication with sEMG sensors
- Long-life Battery (1 day autonomy at least)
- Ergonomics.

The portable device should communicate with the server at the end of the performed task of fatigue to upload the amount of data requested by the remote analysis module. Data compression is essential to limit the upload time. Moreover, encryption is mandatory to grant privacy of sensible/personal data. Continuous authentication may be avoided using authorized certificates.

3.2.2 Hardware for fatigue monitoring

The EMG signal is acquired using a dedicated small wireless sensor platform (Shimmer, http://www.shimmer-research.com/) that can record and transmit physiological data in real-time. The wireless sensor platform has low size and a good autonomy using a battery of 450 mAh; it transfers physiological data to the mobile platform using a Bluetooth connection under the store and forward principle, i.e. data are stored and sent under request of the mobile platform. The wireless sensor platform includes a wearable EMG sensor node while offering high storage capacity by means of a 2 GB Secure Digital (SD) memory card. The sEMG signal is collected using positive, negative and neutral electrodes and amplified with a gain of 682 to enhance the signal. Then the signal is analog-to-digital converted with 12 bit accuracy and the output signal range is adjustable from differential (-3 to 3 V) to single-ended (0–3 V). The core of the system is a microcontroller MSP430 of Texas Instrument and the firmware is developed using the open-source research platform TinyOS [7]. The firmware adopts a configurable sampling rate of 1000 Hz and an appropriate interrupt management strategy for real-time data streaming. The MSP430 used the serial communication port (baud rate: 115,200) to connect to the Bluetooth module. Because the A/D converter of the MCU is 12 bits, the sample data were separated into low and high bytes. The communication protocol is realized through a serial communication using the packet format reported in Figure 23, very powerful for detecting byte or packet losses because it is check summed and sequenced.

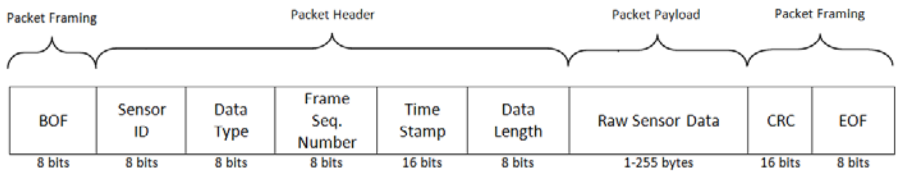

Figure 23 Packet format

3.2.3 Software for fatigue monitoring

The application developed on tablet, provides the visual interface to the elderly user, allowing him/her to access to the service of monitoring muscular fatigue. A C# user interface was designed to collect the data from the Bluetooth sensor at home during exercise. The interactions among the different components are reported in Figure 24. As it can be noticed, the user interaction does not require further workload than the use of the sensors in contact on the body, whereas the system performs a multiple step interaction involving three logical entities: wearable sensors, bio-monitoring application installed on PDA, remote Central server connected to the Decision support system (DSS).

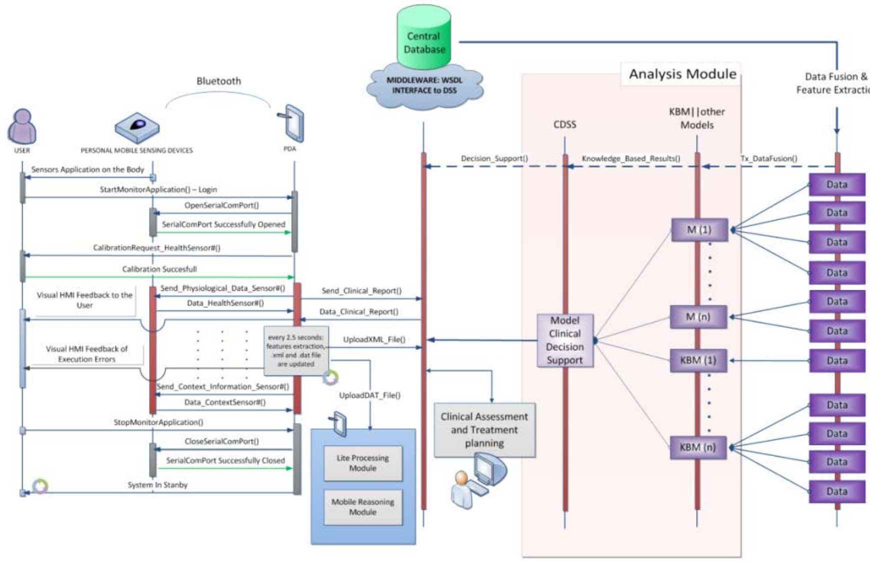

Figure 24 Interactions among the different components of the fatigue monitoring architecture

In Table 4 are reported the main functions developed for the communication between the three entities. The main functions manages the connection and data streaming between the tablet and sEMG sensor. Some functions manages the connection between the tablet and a remote server with user's health profile able to process collected data and to infer a personal muscular model of her/his fatigue monitoring, while other functions are able to provide a feedback to the user in terms of "risk ranges" in order to empower her/him to take a more proactive role in prevention of fatigue, and a detailed report to the doctor available in terms of historical data combined with health profiles to be used for individual treatment planning aimed to continuous monitoring and long-term outcomes.

Table 4 Developed functions

Function	Description	Flow
StartMonitorApplication(); OpenSerialComPort();	The PDA issues the start of sensor data acquisition and open serial communication	user -> PDA -> devices
StopMonitorApplication(); CloseSerialComPort();	The PDA issues the device to stop data acquisition and streaming	user -> PDA -> devices
StartDataAcquisition();	Data streaming will start at the specified frame time interval.	device -> PDA
Req Physiological Data Sensor#();	The PDA ask the device (request) to send Physiological Signals from the specific sensor#	PDA -> devices
Data_HealthSensor#()	The device sends to the PDA the data from the specific sensor#.	device -> PDA
Req Context Information Sensor#()	The PDA ask the device (request) to send motion localization signals from the specific sensor#	PDA -> devices
Data_ContextSensor#()	The device sends to the PDA the data from the specific motion localization sensor#.	devices -> PDA
Req_Clinical_Report()	The PDA sends a request of clinical reports to central database	PDA -> remote Central DB
Data_Clinical_Report()	The central database responses to the request of PDA	remote Central DB -> PDA
Tx_DataFusion()	Fusion of sensor data coming from PDA	remote server -> PDA -> devices
Knowledge_based_results()	Interpretation of features using knowledge based models	remote server -> PDA -> devices
Decision_Support()	Extraction of feedback to the user	remote server -> PDA -> devices

The DSS makes use of information provided by tablet (PDA) and subsequently stored in the central database:

- The PDA exports data acquired by sEMG sensor and stores them into the database (through WSDL functions) together with the *PatientID*, the *TimeStamp* information and the *SensorID* information.
- A questionnaire is filled by the therapist for a given *PatientID*, providing the clinical evaluation of the *FatigueLevel* extracted applying the Borg ratio scale during performed exercise together with the *TimeStamp* information.

The DSS interacts with the architecture through WSDL functions defined as an interface between the central database:

- **Input:** Given the *PatientID*, a *TimeStamp_Begin*, a *TimeStamp_End*, and the *SensorID,* the DSS retrieve the data acquired by the sEMG sensor together with the *FatigueLevel* evaluated by the therapist with Borg ratio scale for that patient for each muscular contraction. These data are used for training of the DSS.
- **Output:** After training, the DSS acts as an expert system and send back to the therapist (through WSDL functions) a *DSSReport* containing the *PatientID*, the *TimeStamp_Begin*, the *TimeStamp_End* and the

FatigueLevel automatically extracted after sEMG processing.

When the user runs the application, a simple tutorial starts automatically explaining how to connect the device and how to perform the task. The muscular fatigue is evaluated applying the sEMG wireless sensor over the right vastus medialis muscle during isometric contractions. To reduce the variability of the exercise, an avatar was added together with the real-time emg data collection. In Figure 25 is shown the application developed on tablet and the isometric knee extension of the avatar to follow during exercise.

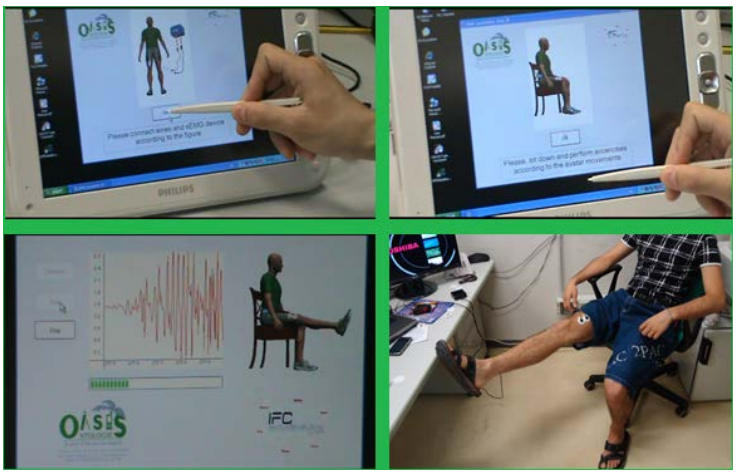

Figure 25 Tablet sEMG application collects data from a wireless sensor on the vastus medialis muscle and shows its performance through avatar movement

3.2.4 Subject selection and experimental procedure

The data were collected from 40 healthy subjects (age range 66.56 ± 7.03 years; height 167,8 ± 5.03 cm; weight 74,18 ± 12.82 kg) all non-smokers with sedentary lifestyle; they had no known neuromuscular or cardiovascular disease. Most participants' (98%) were normal weight with a BMI ≥20 and <25. followed by 2% being overweight with a BMI ≥25 and <30. The majority of subjects were women (55%). Before data collection, participants received a short briefing about the objectives of the experiment and filled out a consent form. All subjects were asked to use the device providing training, a tablet with the software application pre-installed and an user manual with experimental instructions. The software application asks to the subject to wear the sensor following dedicated instructions and to perform an exercise, based on isometric knee extension while seating, in order to investigate the muscular fatigue of the vastus medialis. A simple tutorial starts automatically explaining how to connect the device and to perform the exercise. The sEMG data are acquired using bipolar configuration of two Ag-AgCl surface electrodes with a diameter of 20 mm, placed, after scrubbing the skin with alcohol, over the right vastus medialis muscle with inter-electrode distance of 20 mm. During the test, the subject's upper body is firmly secured to the seat with the hip and knee joint angles at 90° from full extension as is shown in Figure 26.

Figure 26 Knee exercise performed to infer muscular fatigue

During the task, each subject is asked to maintain a maximal voluntary contraction for approximately 5 s and a rest position for approximately 1s up to exhaustion. The wearable wireless platform, the stream of information and the data processing techniques are managed by the application. In order to train the decision support module, the Borg ratio scale (CR-10) was simultaneously measured during the endurance task, i.e. the application asks the user each minute to rate the perceived exertion ranging from 0 to 10 values [8]. Endurance tasks are interrupted when the subject is no longer able to perform the exercise. Data are segmented extracting only the knee extensions intervals in order to assess the sEMG signal during isometric contractions.

3.2.5 Pre-processing and feature extraction

The myoelectric signals recorded from two channels is band-pass filtered with bandwidth of 5Hz to 500Hz and divided into segments corresponding to each contraction. Once the sEMG signal is collected, it is sent to the remote server and the feature extraction module is activated. Each segment is analyzed to extract relevant features in time and frequency. Many algorithms have been described in literature for the extraction of relevant features from the sEMG signal during voluntary contractions [9]. They have been used in different application areas for the non-invasive assessment of muscle functions and in particular on muscular fatigue. It is known that the EMG spectrum changes during a sustained contraction due to fatigue because the signal is not-stationary. Among the different possible approaches to the analysis of non-stationary signals, Cohen class transformations [10] was considered to estimate instantaneous frequency parameters. This class of time-frequency representations is particularly suitable to analyze surface myoelectric signals recorded during dynamic contractions, which may be modeled as realizations of non-stationary stochastic processes [11], [12], [13], [14]. The definition of the class of Cohen time–frequency distributions is as follows:

$$C_x\left(t, f\right) = \int_{-\infty}^{\infty}\int_{-\infty}^{\infty} A_x\left(\eta,\tau\right)\Phi\left(\eta,\tau\right)\exp\left(j2\pi(\eta t-\tau f)\right)d\eta d\tau \qquad (1)$$

where $A_x(\eta,\tau)$ is the ambiguity function:

$$A_x(\eta,\tau)=\int_{-\infty}^{\infty} x(t+\tau/2)\cdot x^*(t-\tau/2)\cdot e^{-j2\pi t\eta}\cdot dt \qquad (2)$$

and $\Phi(\eta,\tau)$ is the kernel function which is usually a low-pass function and is used to mask out the interference. $x(t)$ is the analytic process under consideration obtained from the real recording, $x^*(t)$ is the complex conjugate, t is the time, f the frequency, τ is the time-lag and η is the frequency-lag. Since the $\Phi(\eta,\tau)$ kernel does not depend on t and f, the resulting distribution is time and frequency shift invariant [10]. This characteristic is of paramount importance when correlating the time-frequency representation with physical or physiological phenomena and makes Cohen class distributions particularly suitable to study muscle fatigue.

If the function of kernel is equal 1 the resulting distribution is referred to as Wigner–Ville distribution [10]. The Wigner–Ville is optimal to analyze signals constituted by a single component. However, it is not well suited for application to multicomponent signals, since the bilinearity of the transform induces the presence of interference terms [10]. In the following study we adopted the kernel based on Choi–Williams distribution function to suppress the cross-term. The kernel of Choi–Williams distribution is defined as follows:

$$\Phi(\eta,\tau) = \exp\left[-\alpha(\eta\tau)^2\right] \qquad (3)$$

where α is an adjustable parameter chosen equal to 1 for processing myoelectric data. In order to minimize the sensitivity of the instantaneous frequency parameter estimation to additive noise we adopted an algorithm previously suggested by D'Alessio [15] to estimate the upper frequency of the power density spectrum. The estimation procedure may be therefore summarized as follows:

I. Time-frequency spectrum estimation using the discrete time counterpart of (1).
II. Average over short time intervals of N samples to decrease the variability of the time-frequency spectrum.
III. Compute the upper frequency according to D'Alessio's algorithm.
IV. Estimate the instantaneous median (4) and mean (5) frequency defined as follows:

$$\sum_{i=1}^{If_{med}} P_i = \sum_{i=If_{med}}^{Mf} P_i \qquad (4)$$

$$If_{mean} = \frac{\sum_{i=1}^{Mf} f_i P_i}{\sum_{i=1}^{Mf} P_i} \qquad (5)$$

Where Mf denotes the upper frequency extracted with D'Alessio's algorithm, P_i is the time averaged estimate of the time-frequency spectrum, f_i is the frequency interval between the samples of the time-frequency spectrum. Other features were extracted and quantified by monitoring amplitude and spectral variables as well as the conduction velocity. The most commonly used estimators of amplitude features are the average rectified value (ARV) and the root mean square value (RMS) which are expressed by the following equations:

$$ARV = \frac{1}{N}\sum_{i=1}^{N}|x_i| \qquad\qquad RMS = \sqrt{\frac{1}{N}\sum_{i=1}^{N}x_i^2} \qquad (6)$$

where x_i are the signal samples, and N is the number of samples in the epoch considered.

3.2.6 The Decision Support System

After the features extraction in frequency and time domain a dataset is created and then analyzed by a decision support system which incorporates existing medical knowledge [16] as shown in Figure 27.

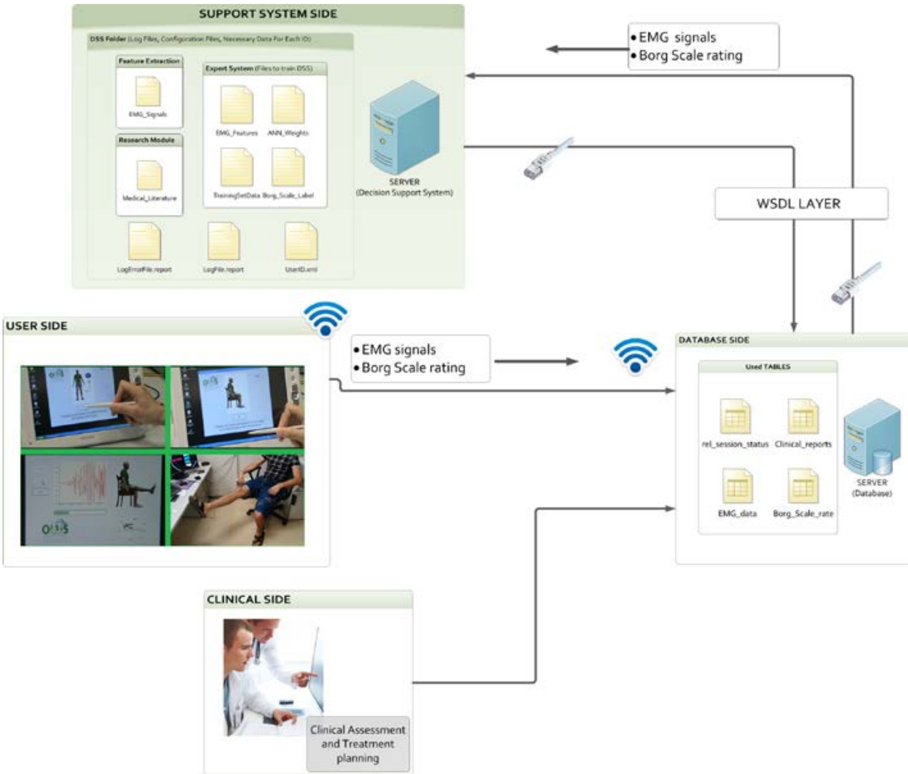

Figure 27 The Support system

It integrates knowledge based capable of analyzing complex physiological data, exploiting meaningful relationships in a data set to help physicians in the diagnosis, treatment and recognition of clinical outcomes. In this study an Artificial Neural Network (ANN) was developed for muscular fatigue prediction, providing a feedback to the patients in terms of fatigue levels (none, weak, moderate, strong, very strong, extremely strong). To test classification performance we compared 6 different types of classifiers integrating for validation the supervised labeling step performed using the Borg ratio scale of perceived exertion during exercise [8]. The first algorithm was the Instance Based Learning (IBL) [17]. IBL is based on the nearest neighbor approach. It uses Euclidean distance to find the closest training instance to the given test instance and determine the class. Contrary to the nearest neighbor approach, IBL classifier is based on specific instances of the training dataset rather than the entire dataset which makes them relatively faster. The second type of classifier we used was the Naïve Bayes (NB) [18]. NB is a simple probabilistic classifier based on the assumption that the features for a given class are mutually independent, which means that the decisions are made as if all features are equally important. The third classifier we used was the J48 (a version of C4.5) decision tree [19]. We used the J48 algorithm with reduced error pruning using a 10-fold cross-validation. The fourth classifier is the Multilayer Perceptron (MLP) [18]. MLP is based on the backpropogation technique and is one of the most common neural network structures as they are simple and effective. The hidden layers were determined automatically by the algorithm and all the nodes were sigmoid. The fifth classifier is Random Forest (RF) [20]. Random forests are ensembles of weakly correlated decision trees that “vote” on the correct classification of a given input. These ensembles minimize the risk of over-fitting the training set, a significant and well-known problem with individual decision trees. For our algorithm we used populated our RF with 10 trees. The sixth classifier is a Support Vector

Machine (SVM) [21] with a radial basis function kernel. The SVM estimates a hyperplane as a decision surface
that maximizes the margin of separation between samples belonging to two classes defined as δ in Figure 28 [22].

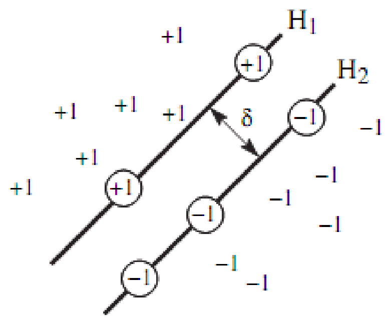

Figure 28 Maximum separation hyperplane

The hyperplane H_1 represent the border with the objects of class +1, while H_2 is the border with the examples having class -1. The two objects belonging to class +1 defining the hyperplane H_1, and the three objects with class -1 defining the hyperplane H_2 represent the support vectors. The solution of a classification problem is represented in this case by identifying the support vectors that maximize the distance between H_1 and H_2, and thus δ. Thus, an SVM training algorithm builds a model that predicts whether a new example falls into one category or the other. New examples are then mapped into that same space and predicted to belong to a category based on which side of the gap they fall on. SVM can be also applied for classifying examples that cannot be separated by a line, as reported in Figure 29. In these cases the coordinated of each examples are located in the feature space using non-linear functions Φ. The feature space is represented by an high number of dimensions, in which the two groups of examples can be linearly differentiated, as represented in Figure 29.

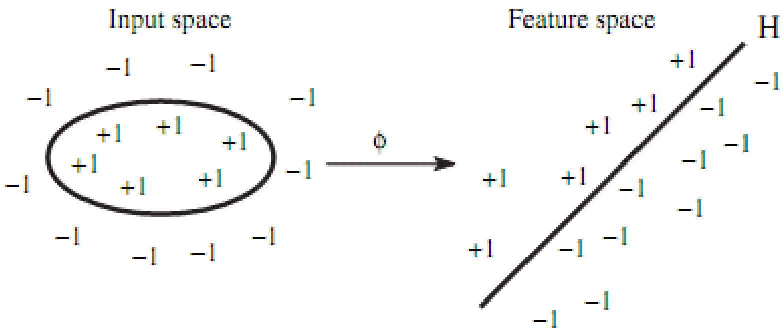

Figure 29 Linear separation in feature space

As reported in Figure 29, the non-linear function Φ maps each example into the features space, characterized by an extremely high or theoretically infinite number of dimensions. Due to the high number of dimensions characterizing the features space, ad-hoc non-linear functions called “kernel”

are employed to compute the classification hyperplane, which are more practical than directly using Φ functions. We determined, empirically, that a Gaussian radial basis function kernel (gamma = 0.01, misclassification cost C = 1) performs best for our data set. Classification was performed by two methods 1) 10-fold cross validation and 2) Leave one subject out. By using a 10-fold cross validation approach we basically divide the data from a single subject into 10 subsets. Every iteration we take 9 subsets as the training set and use the remaining 1 subset as a testing set. A 10-fold cross validation approach evaluates the performance of a classifier when it has been trained

using subject specific information. Leave one subject out is an approach where the data from 9 subjects is used as a training set and the data from the subject that is left out is used as a training set. This approach evaluates how effective a technique is to generalization. The last component developed in the decision module was the literature search module, used when a doctor wishes to consult the medical literature on any issue that comes up during his/her decision-making process. It searches multiple literature sources and employs multiple ontologies and other resources for annotation. It has a contextualization feature, which can refine a query by adding information derived from some relevant text. The text can come from any source, including electronic health records.

3.3 Results and Discussion

In this work we designed and tested and innovative non-invasive architecture based on a clinical decision support system in order to setup a procedure for the recognition of the level of perceived fatigue of the elderly users. Three series of measurements were performed for each subject one time per week for a total of 120 acquisitions. A window of 512 samples was applied in the middle of the myoelectric signal and the time and frequency features were extracted. The instantaneous median and mean frequency was obtained by computing the time-frequency spectrum utilizing the Choi–Williams transform and applying a time-averaging window of 32 samples to decrease the variability of the time-frequency spectrum estimated. Quasi-cyclostationarity was assumed over four consecutive repetitions (i.e., cycles) of the exercise and each sample was obtained as the average of four estimates of the instantaneous median and mean frequency reducing the standard deviation to almost half the value obtained before averaging. The sEMG monitoring system was used to monitor and infer features of muscular performance during exercises of the subjects at home, focusing on the analysis and investigation of the correlation between the extraction of sEMG parameters (ARV, RMS, IMDF, IMNF) and the level of muscular fatigue provided by the Borg ratio scale. In particular were applied and compared six classifiers described in detail in section 3.2.2.4 to assess six levels of muscular fatigue: none, weak, moderate, strong, very strong, extremely strong, respectively extracted from the Borg scale. In Table 5 we can see classification results for leave-one-subject-out and 10-fold cross-validation methods.

Table 5 Classification error (%)

Comparison of Classifier	10x Cross Validation	Leave-One-Subject-Out
IBL	2.36 (±0.52)	17.31 (±4.83)
NB	2.45 (±1.56)	24.28 (±13.27)
J48	7.82 (± 2.31)	26.45 (± 10.82)
MLP	3.26 (± 0.42)	21.13 (± 9.79)
RF	2.66 (± 0.54)	17.51 (± 7.21)
SVM	**2.61 (± 0.51)**	**11.83 (± 2.62)**

We can see that for a 10-fold cross validation most of the techniques perform comparably. The J48 classifier is performs poorly as compared to the others but the error is still pretty low. This suggests that high classification accuracy can be achieved using a subject specific training approach. The results for the leave one subject out approach show that the SVM classifier outperforms the others. The IBL and RF classifier perform well but they fall short of SVM. In table 1 we can see the confusion matrix for the leave-one-subject-out classification using a SVM classifier.

Table 6 Confusion matrix for classification of predicted fatigue using SVM classifier

% Correct		PREDICTED CLASS					
		None	**Weak**	**Moderate**	**Strong**	**Very Strong**	**Extremely Strong**
CLINICAL CLASS	**None**	**93,60 ± 0,4**	1,45 ± 0,63	1,83 ± 0,11	2,1 ± 0,12	0,78 ± 0,01	0,24 ± 0,02
	Weak	1,30 ± 0,34	**82,36 ± 0,11**	9,09 ± 0,43	1,35 ± 0,23	2,48 ± 0,26	1,42 ± 0,15
	Moderate	1,34 ± 0,56	5,41 ± 0,22	**88,52 ± 0,11**	2,5 ± 0,16	1,12 ± 0,11	1,11 ± 0,24
	Strong	0,73 ± 0,02	1,59 ± 0,11	5,68 ± 0,22	**85,79 ± 0,25**	3,41 ± 0,17	0,8 ± 0,18
	Very Strong	2,21 ± 0,03	1,17 ± 0,03	2,11 ± 0,11	3,8 ± 0,21	**87,51 ± 0,14**	3,21 ± 0,5
	Extremely Strong	1,25 ± 0,23	2,85 ± 0,08	1,84 ± 0,02	1,56 ± 0,19	1,78 ± 0,21	**90,72 ± 0,19**

The rows are the clinical classes and columns are the predicted classes. The mean percentages of the confusion matrix as a result of the cross-validation procedure has shown that SVM is able to classify all the six classes with accuracy rates of 93.6%, 82.36%, 88.52%, 85.79%, 87,51%, 90.72%, respectively. We can see from the confusion matrix that None, moderate and very strong level of fatigue have been classified with a high degree of accuracy and most of the misclassifications come from levels of fatigue that are very close.

3.4 Conclusions

A pervasive activity and rehabilitation support system for the non-invasive evaluation of muscular fatigue and stimulation of activity-related changes in muscular strength was realized and integrated into a home-based mobile platform. The system consists of a wirelessly connected wearable platform for the acquisition of sEMG signals. Our aim was to gain a continuous evaluation of the user, to monitor and coach rehabilitation exercise, as well as to enable early detection of excessive fatigue and activity abnormalities minimizing the risk and maximizing the benefits for the user. This system could be useful for sEMG-related disorder recording, especially in the homecare and rehabilitation environments. No specific amount of time is recommended for muscle exertion, but muscle-strengthening exercises should be performed to the point at which it would be difficult to do another repetition without help. Development of muscle strength and endurance is progressive over time. This means that gradual increases in the amount of weight or the days per week of exercise will result in stronger muscles. This approach, even if applicable in clinical and home settings, strongly requires the collaboration of a subject who is aware of the task. In the case of pathologic neurological conditions, this approach fails and novel strategies must be achieved. The challenge is to gain a continuous evaluation of a subject, unobtrusively monitoring physical activities and their related muscular fatigue and avoiding to perform any task or exercise, as well as to let the subject aware of the measurements. Such novelty platform can enable an early detection of excessive fatigue and activity abnormalities minimizing the risk and maximizing the benefits for the user. The architecture developed in OASIS EU project will supports the elderly in physical activities to enhance their muscular strength, improve patient quality of life and will aids the clinician in the analysis of clinical parameters and in the decision making process.

3.5 References

[1]. Chaudhuri A, Behan PO. Fatigue in neurological disorders. Lancet 2004;363:978–88.

[2]. Merkies IS, Schmitz PI, Samijn JP, Van Der Meche FG, Van Doorn PA. Fatigue in immune-mediated polyneuropathies. European Inflammatory Neuropathy Cause and Treatment (INCAT) Group. Neurology 1999;53:1648–54.

[3]. Garber CE, Friedman JH. Effects of fatigue on physical activity and function in patients with Parkinson's disease. Neurology 2003;60:1119–24.

[4]. Gandevia SC. Spinal and supraspinal factors in human muscle fatigue. Physiol Rev 2001;81:1725–89.

[5]. Macaluso A, De Vito G. Muscle strength, power and adaptations to resistance training in older people. Eur J Appl Physiol 2004;91(4):450–72

[6]. US Department of Health and Human Services. Physical activity guidelines for Americans; 2008.

[7]. Levis P et al. TinyOS: an operating system for sensor networks ambient intelligence. In: Weber W et al., editors. Ambient intelligence. Berlin Heidelberg: Springer; 2005. p. 115–48.

[8]. Borg G. Psychophysical bases of perceived exertion. Med Sci Sports Exerc 1982;14(5):377–81.

[9]. Farina D, Merletti R. Comparison of algorithms for estimation of EMG variables during voluntary isometric contractions. J Electromyogr Kinesiol 2000;10:337–49.

[10]. L. Cohen, Time-Frequency Analysis: Prentice-Hall, 1995.

[11]. P. Bonato, G. Gagliati, and M. Knaflitz, “Analysis of surface myoelectric signals recorded during dynamic contractions,” IEEE Eng. Med. Biol., vol. 15, pp. 102–111, 1996.

[12]. S. Karlsson, J. Yu, and M. Akay, “Time-frequency analysis of myoelectric signals during dynamic contractions: A comparative study,” IEEE Trans. Biomed. Eng., vol. 47, pp. 228–238, Feb. 2000.

[13]. M. Knaflitz and P. Bonato, “Time-frequency methods applied to muscle fatigue assessment during

dynamic contractions," J. Electromyogr. Kinesiol., vol. 9, pp. 337–350, 1999.

[14]. S. H. Roy, P. Bonato, and M. Knaflitz, "EMG assessment of back muscle function during cyclical lifting," J. Electromyogr. Kinesiol., vol. 8, pp. 233–245, 1998.

[15]. T. D'Alessio, "'Objective' algorithm for maximum frequency estimation in Doppler spectral analyzers," Med Biol. Eng. Comput., vol. 23, pp. 63–68, 1985.

[16]. Kim SY et al. Pre-operative prediction of advanced prostatic cancer using clinical decision support systems: accuracy comparison between support vector machine and artificial neural network. Korean J Radiol 2011;12(5):588–94.

[17]. D. Aha and D. Kibler, "Instance-based learning algorithms" Machine Learning, vol. 6, pp.37-66, 2001.

[18]. RO Duda, PE Hart, DG Stroke, "Pattern Classification", 2nd edition, Wiley Interscience, 2001.

[19]. Quinlan, J. R. "C4.5: Programs for Machine Learning", Morgan Kaufmann Publishers, 1993.

[20]. L. Breiman, "Random Forests," Machine Learning, vol. 45, pp. 5-32, 2001.

[21]. Vapnik, V., "The Nature of Statistical Learning Theory", Springer-Verlag, 1995.

[22]. W.H. Press, S.A. Teukolsky, W.T. Vetterling, B.P. Flannery, Section 16.5. Support Vector Machines.

Numerical Recipes: The Art of Scientific Computing (3rd ed.). New York: Cambridge University Press, 2007

Chapter 4

A wearable sensing chest belt: design and clinical assessment of the integrated ECG solution

There is an increasing need to find new ways of managing the European healthcare models due to the demographic and socio-economic challenges that result from the fast ageing of the population. In particular, the increasing

number of elderly people directly entails an increasing number of patients with cardiovascular diseases. This type of patients, usually with limited physical activity, remains at home, outside the hospital environment and their health status continues to worsen with episodes of crisis leading to acute deterioration. These episodes, which require emergency and long-time hospital admissions, are always preceded by noticeable changes in several physiological parameters. In this context, accurate and reliable remote monitoring solutions take a main role in order to predict cardiovascular risk of patients and improve their quality of life. To reach this goal in this chapter a prototype of an implemented non-invasive wearable sensor platform for cardiac monitoring is presented and described. The introduction is focused on the applications and clinical scenarios of ECG monitoring with one single lead and the importance of heart rate variability (HRV) analysis as predictive marker for the patient's risk clusterization to determine the best medical managing strategy. Then, the hardware ECG design and the customized firmware is presented. Finally, clinical assessment studies to compare the ECG prototype with a "gold standard" holter were performed and a study on HRV assessment in anorexia nervosa adolescents is presented.

4.1 Introduction

4.1.1 Related works about single lead ECG monitoring systems

Cardiac issues are one of the most frequent causes of death in European and Western countries, and for this reason monitoring of cardiac situation in at-risk patients gained a great importance in last decades. The need for unobtrusive, user-friendly, smart, easy-to-use devices useful for this purpose is always more important in clinical practice, but the challenges to get such systems more high performance are still hard. In fact, even if from one side small portable systems are smarter and easy-to-use, from the other side they do not assure comparable performances with respect to traditional 12-lead ECG systems. Focusing on general purpose of single lead ECG systems, the most important applications in clinical practice should be referred to cardiac rehabilitation supports, in order to restore an acceptable level of cardiac function after, for example, an intervention. This purpose is very well satisfied by using a single-lead system, with the advantages above mentioned, and good results on this subject have been found by Worringham et al. [1], that used a portable system based on ECG, Smartphone and GPS to remotely monitoring exercise-based cardiac rehabilitation. The components of this system are shown in Figure 30. Authors report a great importance to the main features of this system and underline the ease of use, also for those people not having a great knowledge of electronic devices. The monitoring of health conditions is anyway the most useful task that could be reached by using a similar approach. In this way it is possible, in fact, to change the planning of several important activities in the patient’s life, such as sleeping times, eating, physical exercise and many other. With the help of such instruments, the clinicians can monitor the health status of the patient, they can even change in almost real time the strategy to defeat the problem and to give patients better life conditions. Another purpose for which single-lead systems can be successfully used is the evaluation of pharmacological response in cardiac field. It’s well known, in fact, that drugs are largely used in this field, in particular beta blockers, cardiac glycoside, calcium channel blocker, ivabradine, and that pharmacologic treatment’s evaluation is a key feature for basic cardiac cares, but it’s also largely agreed that this particular evaluation is not always easy neither well accepted by the patients. For this reason, having an useful, unobtrusive tool to assess this process can be very important for patients and caregivers. In this field some works have been made employing simplified ECG systems, such as the one used in the work of Camarozano et al.[2], that employs a 3-lead ECG system to evaluate the effects of beta-blockers on dobutamine-atropine stress echocardiography and ECG signal. This study assessed the decrease of both hemodynamic and chronotropic response during Dobutamine Stress Echocardiography (DSE) with the use of beta-blockers, and also that the early administration of atropine optimized the hemodynamic response, reduced test time in patients with or without Beta-blockers and reduced the number of inconclusive tests in the early protocol.

A single-lead portable ECG system could be used with good success also in the detection of possible cardiac events in patients with specific symptoms, such as syncope, dyspnea, obstructive sleep apnea [3] and dizziness, that could be good early predictors of such events and could represent an alarm ring for at-risk patients, in order to provide early treatments and capable, in many cases, to save subject's life and to lower down the chance of developing later complications, as above mentioned.

Figure 30: Components of remote monitoring system [6]

A study having this aim is the one conducted by She et al. [4], in which a single-lead ECG system prototype has been realized in order to monitor the simple HR to provide alarms in the case that HR shows significant changes with reference to the baseline signal. In this work, in particular, the authors paid attention to the realization of a fast algorithm to detect the R wave, starting with the differentiation of possible R waves, proceeding then with a thresholding to separate the real R wave from noise, extracting then the peak of R wave and finally calculating the heart rate. Moreover, the authors presented in this paper a low-cost portable ECG monitor capable to work for hours without requiring any kind of external power supply and also able to show the signal caught by the ECG single-lead system and to save it into an SD card.[4] This aim could be reached in some way also with another chance given by the single-lead system, that is to say the detection of possible cardiac arrhythmias with an asymptomatic patient. In fact, possible sinus tachycardia or bradycardia could be detected by simply using a single-lead system, allowing these problems to be discovered and properly treated in time. An interesting work mixing molecular basis, ECG evaluation and arrhythmias is the one of Farwell et al.[5], in which a very large investigation of the problem has been conducted. Obviously, it should be remarked that not every problem in cardiac field should be detected and solved by using the simple single-lead ECG, otherwise it should not have sense to use traditional 12-lead ECG tools. In fact, single-lead systems are not capable to prevent stroke, one of the most burdensome problems concerning cardiac world, and also they cannot prevent myocardial ischemia.

Monitoring of valvulopaties, pericardial effusion and pulmonary congestion is also impossible with a similar approach and requires more accurate and, unluckily, less unobtrusive, systems. Other attentions that the patient should pay to the employment of single-lead system refer to the need for periodic visits to the cardiologist, absolutely to not underestimate: in fact the wearable system should represent a very important aid for the patient itself but should not replace the periodic clinical visit, especially for people at-risk for such events. This is important also in order to discuss with the caregiver about the feedbacks given by the portable systems, that should be compared also to the health status of the patient and to his other physiological parameters, in order to get a proper care to overcome the problem. Anyway, a general overview of the possible real clinical applications of the single lead ECG wearable system is shown in the Table 7 below.

Table 7: Possible real scenarios of wearable ECG single-lead

Use Proposal	**YES**	**NO**
Post Acute Event Rehabilitation	X	
Pharmacological Response Evaluation and Monitoring	X	
Sinus tachycardia /bradycardia	X	
Supraventricular, ventricular arrhythmias	X	
Cardiac events during selected activities (sleeping, eating,exercise etc.)	X	
Cardiac events during specific symptoms (syncope, dyspnea,dizziness)	X	
Chronotropic competence	X	
Sympathovagal effects	X	
Myocardial Ischemia		X
Valvulopaties		X
Pericardial Effusion		X
Pulmonary Congestion (CHF)		X

Several types of systems for ECG recognition are available in the market used in different field, such as medicine, sport and research area, for monitoring of heart functionality, but most of them are not ergonomic and moreover it is not possible customize their functionalities.

Several wireless ECG monitoring systems have been proposed [6], [7], [8], [9], [10], [11]. All of them use conventional “wet” ECG sensors. For data sampling and wireless transmission, they use either existing standard wireless interfaces or general-purpose wireless sensor nodes. This combination results in many system-level drawbacks such as big form factor, low transmission speed, short battery lifetime, and lack of wearability.

4.1.2 The prognostic value of HRV assessment

Heart rate is by itself of prognostic importance and the knowledge of the mean, minimum (resting) and maximal (exercise) heart rate may help in the decision making for optimal therapeutic strategies. But another important aspect of ECG monitoring is represented by the assessment of heart rate variability (HRV), which can be extrapolated from ECG. HRV helps to identify the neuro-hormonal balance which has significant prognostic implication. It reflects behavior of both parts of autonomous nervous system: sympathetic and parasympathetic. It is widely used for quantifying neural cardiac control [12], and low variability is particularly predictive of death in patients after myocardial infarction [13]. In fact, patients with lower HRV values show the highest mortality rate compared with patients with higher HRV values. A number of earlier studies of HRV have shown significant prognostic information in chronic heart failure (CHF). The United Kingdom Heart Failure Evaluation and Assessment of Risk Trial [14] (in 433 outpatients) found that reduced SDNN (SD of the normal-to-normal R-R interval) from 24-hour Holter ECG predicted death from progressive heart failure but failed to predict sudden cardiac death. It might be expected that increased sympathetic activity would be accompanied by a relative predominance of LF oscillations in frequency-domain analysis of HRV [15]. However, both increased [16] and reduced [17] LF power were found to be associated with an increased risk of cardiac death. Data from Galinier et al. [18] showed that reduced daytime LF power from 24-hour Holter recording independently and significantly predicted sudden death, although very few other parameters were included in the analysis. La Rovere et al. [19] demonstrate how reduced 24-hour time and frequency-domain measures of HRV identify CHF patients at increased risk of death. In the present study is shown that a simple bedside ECG recording of <10 minutes of duration and an LF power analysis of HRV obtained during controlled breathing provides additional important prognostic information. Moreover Vazir et al. [20] sustain that in the majority of congestive heart failure patients with mild-to-moderate symptoms, the analysis of nocturnal heart rate variability by spectral analysis is a quick, easy and a promising screening tool for sleep-disordered breathing. Setting the per cent very low frequency index at 2.23% provided a high negative predictive value that was necessary for a rule-out test for sleep-disordered breathing both for central and obstructive sleep apnea. Finally several recent studies demonstrates that HRV parameters continuously measured from invasive and non-invasive cardiac devices reduce patients' mortality and hospitalization risk [21], [22], [23], [24].

4.2 Material and methods

4.2.1 Requirements of the wearable ECG system

Heart functionality of patients is usually controlled by the analysis of the electrocardiogram (ECG). It is one of the most important clinical investigations in cardiac diagnosis. Thanks to information provided by ECG, it is possible to detect the presence of alterations of cardiac rhythm, alterations in the propagation of electric impulses (conduction alterations) or myocardial alterations as a consequence of an ischemia (coronary diseases). In Figure 31 is shown the anatomy of the human heart and the waveform of the ECG signal.

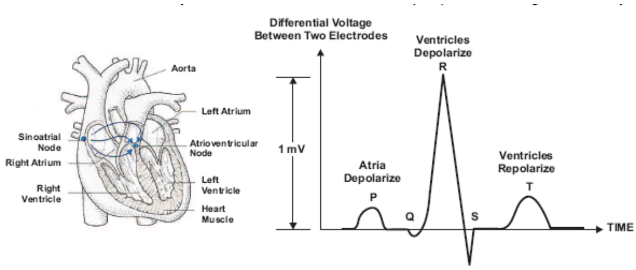

Figure 31: Human heart anatomy on the left side, and ECG waveform on the right.

The typical amplitude of the R wave component of the ECG signal is approximately 1 mV. This peak is located within a group of peaks known as the QRS complex and represents the electrical pulse flowing through the ventricles. As this pulse travels via the blood stream, it can be detected at various points on the body. The extremities and the chest have become the standard locations for placing electrodes for acquiring the ECG signal. In addition to the clinical functions that traditional ECG equipment provides, the wireless ECG chest belt has to incorporate portability without compromising performance. This translates to the following design considerations:

- The sensor interface must be able to pick up sub-millivolt level ECG signals from two spaced electrodes on the chest, and apply bandwidth conditioning and data quantization locally. A low noise front-end amplifier with sufficient gain and built-in filtering function is thereby required.
- Wireless transmission and local storage are both determining factors for portability and versatility in a multi-

sensorial platform. The wireless ECG sensor should be small in size, and cause minimal discomfort to patients to guarantee continuous health monitoring.

- For the ease of use, a fully integrated, “plug-and-play” type of design that requires few or no external wirings is preferred.
- Negligible artifact rate in extreme dynamic conditions.
- Highly configurable software, multi-functional sensing platform for wireless sensor network /ad-hoc wireless network

4.2.2 Hardware of the wearable ECG system

Taking into consideration of above requirements, the activity carried out in this study was focused on the development of a non-invasive wearable chest strap able to extract one-lead ECG signal customizing the functionality. The wearable sensing set for the measurement of the ECG signals was developed re-designing the ECG Shimmer based-platform. It includes the signal conditioning, the SD card and the low-power Bluetooth modules. The light weight (~80 g) and compact form factor of the sensor makes it very suitable for physiological sensing applications. The electronic board and his enclosure was redesigned to collect one lead ECG and to be easily plugged on the common cardio-fitness chest straps (i.e. Polar®, Adidas®), which are fully washable, integrate dry electrodes applied directly to the patient's skin for single-lead acquisitions without skin preparation, gels, or adhesives as showed in Figure 32. Moreover it guarantees an optimal and comfortable contact with the thorax for a long-term monitoring, adapting itself to the body shape.

Figure 32 Customized wearable ECG chest strap

The electronic board includes a low-power standard Bluetooth and 802.15.4 communications, three axis accelerometer, transduction, amplification and signal pre-processing blocks. The module collect the ECG signal from sensors and send the data to a mobile platform by means of Bluetooth connections. Bluetooth is a proper solution for sensor communication as most mobiles integrate it. Bluetooth capabilities for sensors are provided by Shimmer modules, which are an adequate choice as they provide internal accelerometers together with standard digital (I2C, SPI) communication buses for new potential sensors [25]. The noise signals picked up by the human body (such as the 50 to 60-Hz line frequency) pose a serious problem to detecting the low-frequency low-magnitude ECG signal. An analog front end with a high gain with low cutoff filter frequency is necessary to condition this signal for digital conversion and processing. Figure 33 below demonstrates the block diagram with the main modules of the ECG endpoint architecture. The first block of the ECG daughterboard is the low power front-end data acquisition circuit composed by analog amplifiers and filters able to reduce the artifacts of movement, breath and muscle contraction and to reach the desired dynamic range. The frequency response is 0.05 to 150 Hz with an ECG amplifier gain of 175. The collected analog signal is then sampled through an A/D converter of 12-bit accuracy. The digitized data are passed to a microcontroller for processing and storage. To maintain the low-power usage capabilities of the electronic board a power management system optimizes the power utilization by putting un-used circuits into sleep mode. Current consumption of the board is 18 mA. The core element of the system is the low power microcontroller (MSP430 family made by Texas Instrument) [25] which has been widely used in wireless sensors. The SHIMMER platform uses a Roving Networks™ RN-41 Class 2 Bluetooth® module to communicate via an integrated 2.4 GHz antenna. This module contains a full version 2 Bluetooth® Protocol Stack and supports the Serial Port Profile which facilitates rapid application development. The Bluetooth® module is connected to the MSP430 directly via the USART1 serial connection.

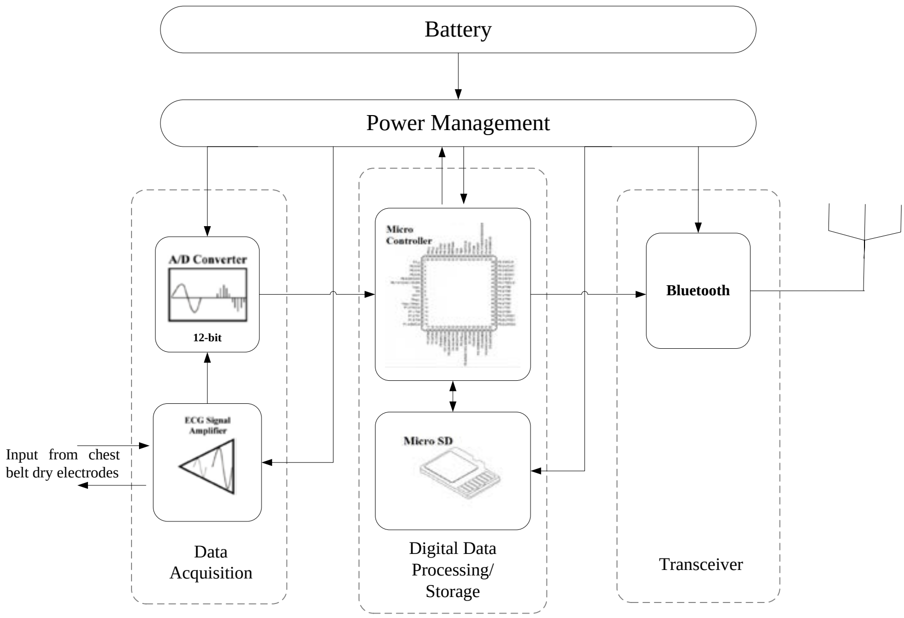

Figure 33: Block diagram of ECG architecture

The differential amplifier used in the front end of ECG platform is an instrumentation amplifier that remove the common-mode and amplifies the input differential ECG signal. In Figure 34 is shown the analog front-end of the ECG module developed.

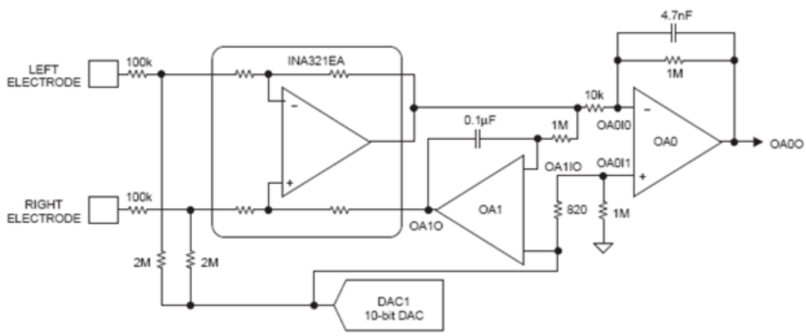

Figure 34 ECG front-end amplifier circuit diagram

The amplified ECG signal is internally digitized using the on-chip analog-to-digital converter available in the microcontroller. The core of the system, in fact, is a low power microcontroller (MSP430 family made by Texas Instrument). It is designed for low cost, low power consumption embedded applications. The MSP430 is particularly well suited for wireless RF or battery powered applications. The electric current drawn in idle mode can be less than 1 microamp. The top CPU speed is 25 MHz. It can be throttled back for lower power consumption. The MSP430 also utilizes six different Low-Power Modes, which can disable unneeded clocks and CPU. This allows the MSP430 to sleep, while its peripherals continue to work without the need for an energy hungry processor. Additionally, the MSP430 is capable of wake-up times below 1 microsecond, allowing the microcontroller to stay in sleep mode longer, minimizing its average current consumption. In Figure 35 is reported the ECG module with real dimensions of the electronic board.

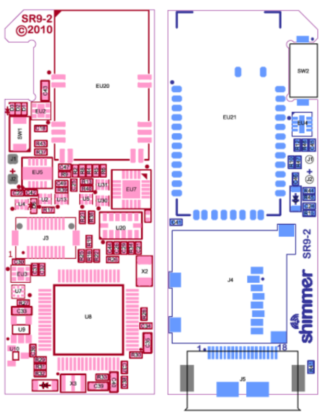

Figure 35:Schematics of the ECG module

4.2.3 Software architecture of the ECG system

The device uses TinyOS, an open-source research platform for the design, implementation, testing and validation of the embedded firmware. TinyOS provides off-the-shelf components to interface with the hardware at higher abstraction level and is optimized for limited resources of wireless nodes, in terms of memory and CPU. Firmware running on the sensor platform provides local processing of the sensed data, local storage of the data when required and communications of that data to a higher level application for advanced signal processing, display and data persistence. The operating system manages each hardware peripheral using different functions on the sensor node. The SD File-system component manages the storage on the SD card creating and naming files and folders. Sensor node communication is facilitated by the Radio Manager component, which manages the Bluetooth radio. The implemented firmware assumes that radio is turned on when ECG device is connected to the docking station. When the user wears the chest belt, it is possible to start the real-time acquisition and logging data on SD card. In the last case the Bluetooth is turned off and it is reactivated only when it is reconnected to the docking station to download collected data. Such intermittent operation ensures that the battery is not depleted rapidly by the radio. In Figure 36 is illustrated the block diagram of ECG firmware implementation.

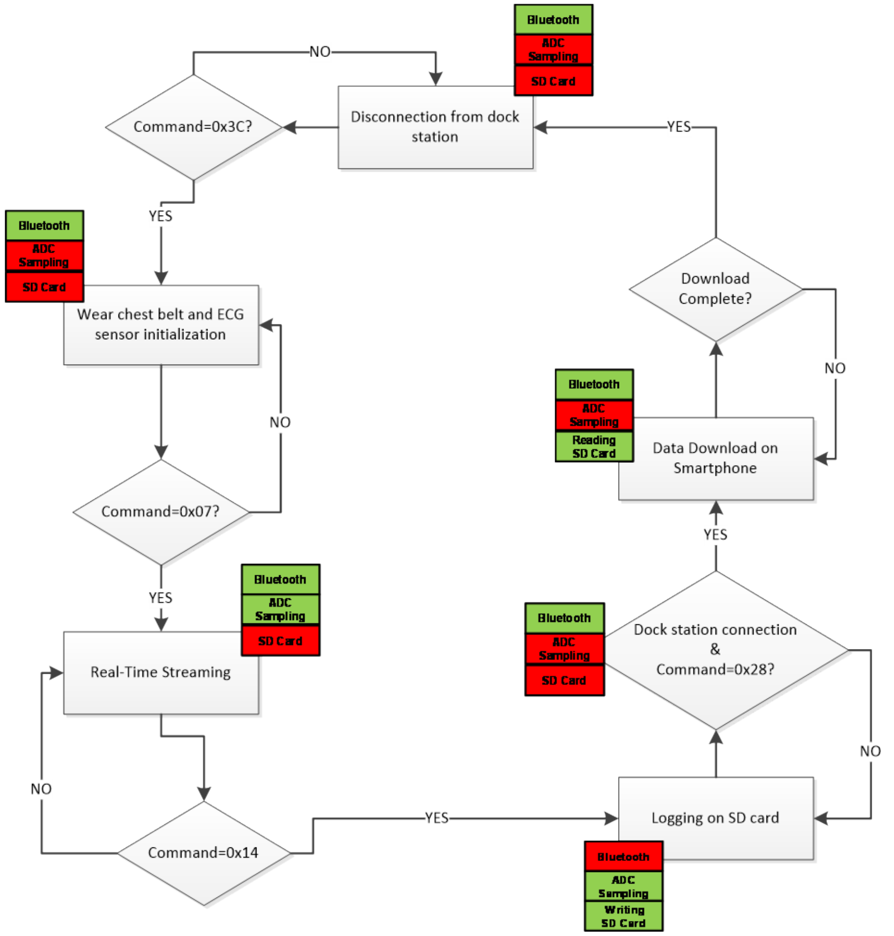

Figure 36: Block diagram of ECG firmware implementation

The Sensors Manager manages the external ECG daughterboard. It samples values from the AD converter at 500Hz and manipulates them so that they are ready to be stored on the micro-SD allowing a long-term local recording and ensuring no loss of data. The Commands Manager handles the commands reported in Table 8, sent to the sensor node by the smartphone.

Table 8 ECG Commands

Command	Function	Description
0x14	Start Logging SD card	Device start to acquire and save ECG data on SD Card and switch Bluetooth OFF.
0x28	Start download from SD card	Device start to send raw data to the master; this command works only when the Bluetooth is switched ON
0x07	Real-time ECG streaming	Device start to send real-time ECG data
0x3C	Delete ECG file	Device delete ECG file on SD card

The communication protocol is realized through a serial communication using packets delimited by header characters. The sensor transmits the data saved on SD card to the smartphone once a time interval of 50ms.The protocol is designed to be robust against wireless communication errors. In particular when the smartphone send the request of data to the ECG device, the first packet sent by the client is a 32 bit unsigned which represents the number of ECG packets saved on SD card. The frame format is based on 128 bytes as shown in Figure 37.The BOF (Beginning of Frame, hex byte “0xC0”) and EOF (End of Frame, hex byte “0xC1”) are used as header characters while the ECG packet payload is composed by 126 bytes. It is expected that when transmission is done with packets instead of continuously, the power consumption can be reduced, thus increasing operation time. This is because a large portion of the power is being consumed by the RF part of the wireless module, and packet transmission allows for this part to be switched off in the durations between successive packet transmissions.

128bytes

	BOF	ECG#1	ECG#2	ECG#3	…	ECG#63	EOF
	0xC0	16bits	16bits	16bits		16bits	0xC1
bytes	1	2-3	4-5	6-7		126-127	128

Figure 37: ECG Packet Format

4.2.4 The algorithm for QRS detection

The QRS detection is the starting point of an ECG analysis. This first stage of the ECG analysis will provide features as well as HR detection, RR interval, Heart Rate variability (HRV) recognition for a further ECG examination. From the existing literature several algorithms are used today to perform the QRS detection. Several ones are based on a first stage of linear filtering used to enhance a specific feature in the ECG signal, followed by a threshold crossing procedure [26] and others based on more complex signal processing tools, mainly the “Pan-Tompkins“ algorithm [27] and wavelet analysis tool [28],

[29], [30]. Once we get the QRS complex location, some additional processing modules may be required at the output of the detector to correctly locate the R wave. This is particularly needed for the beat detection standard validation procedure [31]. The digital signal passes, through a sequence of processing steps that includes three linear digital filters. First is a Bandpass Filter composed of cascaded low-pass and high-pass filters. Its function is noise rejection. Next is a filter that approximates a derivative. After an amplitude square process, the signal passes through a moving-window integrator as shown in Figure 38. Adaptive thresholds then discriminate the locations of the QRS complexes [27]. Bandpass Filter reduces the influence of muscle noise, baseline wander, and T-wave inference (5-11 Hz). Derivative filter is applied to provide QRS-complex slope information. After differentiation, the signal is squared point by point. This makes all of data points positives and does nonlinear amplification of the output of the derivative, emphasizing the higher frequencies. The purpose of Moving-Windows Integration is to obtain waveform feature information in addition to slope of the R wave. The windows samples number N is important. Generally, the width of the windows should be approximately the same as the widest possible QRS complex. If it’s too wide, the integration waveform will merge the QRS and T complexes, if it’s too narrow, some QRS complexes will produce several peaks in the integration waveform [27].

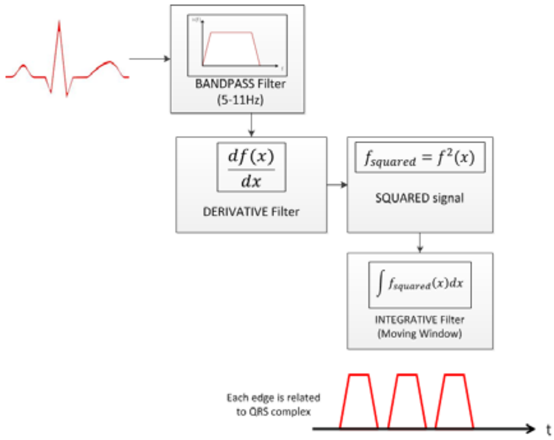

Figure 38: Pan-Tompkins QRS detection algorithm

4.2.5 Clinical assessment

The clinical assessment of the wearable ECG chest strap from a medical perspective was realized through clinical studies and its performance was evaluated in comparison with a “gold standard” holter. Tests and results were obtained from healthy subjects enrolled at the Institute of Clinical Physiology.

The performance of the system was evaluated at the bedside, outside the hospital, at home and during a marathon. In all the scenarios, the chest strap and the gold standard device (holter ELA used in the clinical activities at the Institute of Clinical Physiology) simultaneously recorded the ECG. The clinical assessment was performed collecting and synchronizing both the ECG from the chest belt and the clinical holter ELA on subjects at rest and during daily activities. The algorithm for QRS detection was applied on both signal extracting the sensitivity Se and specificity Sp with the following formulas:

Se = TP/(TP+FN)   Sp = TP/(TP+FP)

Where if the R peak detected is within this temporal window, it is considered as a true positive (TP). Any additional peaks revealed in the valid interval are treated as false positive (FP). If the algorithm fails to assert that a QRS complex has occurred a false negative (FN) is declared. The Bland-Altman plot and the mean error distribution of tachograms was applied to evaluate the absence of differences between the extracted time series of two system. The relative percentage error between the HR of the ECG chest belt and the gold standard system was extracted according to the formula:

$$\mathrm{HR\_err}(\%) = E\left[\frac{\left(HR_{holter}(n) - HR_{ChestStrap}(n)\right)}{HR_{holter}(n)} * 100\right] \tag{1}$$

Finally, we compared the information extracted from spectral analysis for heart rate variability assessment.

4.2.6 Subjects selection and experimental procedure

In order to test the performance of the ECG chest strap 10 healthy volunteers (age 30 ± 3 years) were enrolled in the study.

The ECG was acquired from 5 freely moving nurses at work and 5 subjects at bedside for 3 hours. All the subjects were monitored collecting data from simultaneous ECG recordings obtained by ECG chest strap and the clinical ELA holter whose good performances are well-known being its normal employment in a clinical setting. In Table 9 are reported the technical features of both devices.

Table 9: Features of the chest strap and the holter ELA

Technical features	**ECG Chest strap**	**Holter ELA**
Acquisition sampling rate	500 Hz	1000 Hz
Resolution A/D	10 bit	15 bit
Dimensions	50 x 25 x 23 mm	97 x 54 x 23 mm
Weight	~80 Grams	~300Grams
Power supply	3V Li-ion battery 450mAh	1.5V alkaline battery
Data Transmission	Bluetooth/802.15.4/SD Card	SD Card
Leads	One	Three

The main differences between chest strap and holter ELA are due to the sampling rate i.e. ECG chest strap were sampled at 500 Hz, while ELA data were sampled at 1000 Hz. Moreover, also the data transmission, the number of leads and dimensions are different. Filtered data were analyzed by employing methods suggested by scientific community standards and commonly accepted.

4.2.7 Features extracted for HRV assessment

HRV analysis is one of the most important application of the wearable ECG chest strap. It is based on evaluation of consecutive RR intervals extracted applying the algorithm of QRS detection described in section 4.2.4. HRV belongs to a group of non-invasive prognostic methods as described in section 4.1.2. It reflects behavior of both parts of autonomous nervous system: sympathetic and parasympathetic. It is well accepted that conditions such as assuming an upright position, mental stress, and exercise are associated with an increase of the sympathetic tone. In contrast, vagal tone is high during resting conditions. In normal subjects, both sympathetic and parasympathetic tones fluctuate throughout the day. [32] Numerous data, collected in various experimental conditions involving human and animal studies, support the assumptions that 1) the respiratory rhythm of heart period variability (HF) is a marker of vagal modulation (an issue widely accepted); 2) the rhythm corresponding to vasomotor waves and present in heart period and arterial pressure variability (LF) is a marker of sympathetic modulation of, respectively, heart period and vasomotion; and 3) the reciprocal relation existing in the R-R variability spectrum between power LF band and power HF band is a marker of the state of the sympathovagal balance modulating sinus node pacemaker activity [33]. We extracted HRV parameters in time and frequency domain following the Heart Rate Variability Guidelines, in order to extract significant prognostic information for the prediction of cardiac risk. In Figure 39 and Figure 40 are reported all the HRV features extracted.

Time Domain HRV Parameters

Parameters HRV	Description
Mean_RR	The mean of RR intervals
Std RR	Standard deviation of RR intervals
Mean HRV	The mean heart rate
Std HRV	Standard deviation of intravenous heart rate
RMSSD	Square root of the mean squared differences between successive RR intervals
NN50	Number of successive RR interval pairs that differ more than 50 ms
SDANN	Standard deviation of the averages of NN intervals in all 5 min segments of the entire recording
SDNN HRV	Standard deviation of all NN intervals
Poincare SD1	The standard deviation of the Poincaré plot perpendicular to the line-of-identity
Poincare SD2	The standard deviation of the Poincaré plot along the line-of-identity

Figure 39. Time Domain HRV Parameters

Frequency Domain HRV Parameters

Parameters HRV	Description	Parameters HRV	Description
FFT VLF peak	Band peak in frequency range 0Hz –0.04Hz	AR LF peak	Band peak in frequency range 0.04Hz –15Hz
FFT LF peak	Band peak in frequency range 0.04Hz –0.15Hz	AR HF peak	Band peak in frequency range 0.15Hz –0.4Hz
FFT HF peak	Band peak in frequency range 0.15Hz –0.4Hz	AR VLF power	Absolute power of 0Hz –0.04Hz band
FFT VLF power	Absolute power of 0Hz –0.04Hz band	AR VLF power prc	Relative power of 0Hz –0.04Hz band
FFT VLF power prc	Relative power of 0Hz –0.04Hz band	AR LF power	Absolute power of 0.04Hz –0.15Hz band
FFT LF power	Absolute power of 0.04Hz –0.15Hz band	AR LF power prc	Relative power of 0.04Hz –0.15Hz band
FFT LF power prc	Relative power of 0.04Hz –0.15Hz band	AR LF power nu	Powers of 0.04Hz –0.15Hz band in normalized units
FFT LF power nu	Powers of 0.04Hz –0.15Hz band in normalized	AR HF power	Absolute power of 0.15Hz –0.4Hz band
FFT HF power	Absolute power of 0.15Hz –0.4Hz band	AR HF power prc	Relative power of 0.15Hz –0.4Hz band
FFT HF power prc	Relative power of 0.15Hz –0.4Hz band	AR HF power nu	Powers of 0.15Hz –0.4Hz band in normalized units
FFT HF power nu	Powers of 0.15Hz –0.4Hz band in normalized units	AR LF/HF power	Ratio between LF and HF band powers
FFT LF/HF power	Ratio between LF and HF band powers		

Figure 40. Frequency Domain HRV Parameters

Variations in heart rate may be evaluated by a number of methods. Perhaps the simplest to be performed are represented by the time domain measures. With these methods either the heart rate at any point in time or the intervals between successive normal complexes are determined. In a continuous electrocardiographic (ECG) record, each QRS complex is detected, and the so-called normal-to-normal (N2N) intervals (that is all intervals between adjacent QRS complexes resulting from sinus node depolarization), or the instantaneous heart rate is determined. Simple time–domain variables that can be calculated include the mean N2N interval, the mean heart rate, the difference between the longest and shortest N2N interval, the difference between night and day heart rate, etc. (Hea). The main time domain feature extracted from the developed ECG chest strap for long-term monitoring of patients are reported below:

- RR mean: This feature is the standard statistical indicator. Mean is a parameter of distribution random variable, which is defined as a weighted average this distribution. The mean of all RR intervals is denumerable by following equation (Ond):

$$RR = \frac{RR_1 + RR_2 \dots RR_N}{\mathrm{N}} = \frac{1}{N}\sum_{i=1}^{N} RR_i \qquad (1)$$

where N is total number of all RR intervals.

- Std RR: Std RR is counted like standard deviation of the temporal differences of consecutive RR intervals. We can formalize it with following formula:

$$Std\ RR = \sqrt{\frac{1}{N-1}\sum_{i=1}^{N-1}(|RR_i - RR_{i+1}| - RRdif)^2} \qquad (2)$$

- Mean HR: It is mean of heart rate. Mean of heart rate is similar like RR mean described in subsection

$$HR = \frac{1}{N}\sum_{i=1}^{N} HR_i \qquad (3)$$

where N is total number of all RR intervals.

- RMSSD: is the root mean square of successive differences of RR intervals and it is described by following equation:

$$RMSSD = \sqrt{\frac{1}{N-1}\sum_{i=1}^{N-1}(RR_{i+1} - RR_i)^2} \qquad (4)$$

where N is total number of all RR intervals in segment.

- NN50: This feature is based on computing count of adjacent RR intervals differing by more than 50 ms in the entire analysis interval. It's used for classification of the segment longer or at least 5 minutes. We can describe this feature as:

$$NN50 = \sum_{i=1}^{N}\{|RR_{i+1} - RR_i| > 50ms\} \qquad (5)$$

where N is total number of all RR intervals in segment.

- SDANN: is the standard deviation of the averages of RR intervals in all 1 minute section which they divide selected segments of long term signal:

$$SDANN = \sqrt{\frac{1}{N}\sum_{i=1}^{N}(RR_i - RR)^2} \qquad (6)$$

  where N is total number of 1 minute sections RR intervals in selected segment, RR_i is mean of RR intervals in 1 minute section, RR is mean of all means of RR intervals in all 1 minute sections.
- SD1-SD2: Another important analysis is the Poincarè plot, a nonlinear method created by plotting all RR intervals in two dimensional system. SD1 and SD2 are two standard Poincarè and plot descriptors. SD2 is defined as the standard deviation of the projection of the Poincarè and is plot on the line of identity (y = x), and SD1 is the standard deviation of projection of the Poincarè on the line perpendicular to the line of identity (y=-x). Both parameters we may define as:

$$SD1 = Var\left(\frac{1}{\sqrt{2}}RR_n - \frac{1}{\sqrt{2}}RR_{n+1}\right) = \frac{1}{2}SDSD^2 \qquad (8)$$

$$SD2 = 2SDRR^2 - \frac{1}{2}SDSD^2 \qquad (9)$$

As regards the study of HRV in the frequency domain, this post elaboration is accomplished with power spectrum analysis, which, in principle, requires rigorous stationary conditions that, in strict terms, are unknown to biology. Thus a practical compromise must be found, and this consists of defining as adequate conditions those characterized by the absence of slow trends or step changes in the tachogram. Using the Power Spectral density (PSD) we can observe the distribution of power signal in the characteristic band of frequencies. In ECG chest belt we extracted PSD using a parametric approach. This method assumes the time series under analysis to be the output of a given mathematical model, and no drastic assumptions are made about the data outside the recording window. The parametric approach of signal PSD is completely independent of the physiologic, anatomic and physical properties of the biologic system under consideration, but provides a simple input-output relationship of the process (black-box approach). A critical point of this method is choosing the appropriate model to represent the data sequence. The more general case of the parametric estimator is the autoregressive moving average model (ARMA Auto-Regressive Moving Average), represented by the following linear equation:

$$y(k) = -\sum_{i=1}^{p} a_i y(k-i) + \sum_{j=1}^{q} b_j w(k-j) + w(k) \qquad (10)$$

where w(k) is the input white noise of the system (mean value zero and variance equal to λ2), p and q are, the orders of auto-regressive (AR) and moving average (MA) parts, respectively, and a_i and b_j are the coefficients. The ARMA model may be reformulated as an AR or MA model where the coefficients a_i

and b_j are, respectively, set to zero. Since the estimation of the AR parameters results in liner equations, the AR model is usually employed in place of ARMA or MA models. An autoregressive process of order p is described by the following equation:

$$y(k) = -\sum_{i=1}^{p} a_i y(k-i) + w(k) \qquad (11)$$

z-domain transfer function of the system:

$$H(z) = \frac{Y(z)}{X(z)} = \frac{1}{A(z)} = \frac{1}{1-\sum_{i=1}^{p} a_i z^{-i}} = \frac{1}{\prod_{m=1}^{p}(1-\frac{zm}{z})} \qquad (12)$$

where the coefficients characterize the identification and zm are the poles of the corresponding model. Since the power spectral density of y (k) is:

$$P_y(f) = |H(\exp(j2\pi f \Delta T))|^2 P_u(f) \qquad (13)$$

where ΔT is the sampling interval and $P_y(f)$ is the spectral density of input power, then it follows that:

$$P_y(f) = \frac{\lambda^2 \Delta T}{\left|1-\sum_{i=1}^{p} a_i z^{-i}\right|^2_{z=\exp(j2\pi f \Delta T)}} \qquad (14)$$

Looking at the last formula is understood that the estimate of the PSD in the case of autoregressive models, is reduced to the calculation of the AR itself [34]. This assessment can be carried out in various ways, including resolution of equations of Yule-Walker and least squares estimation methods. In particular, the Yule-Walker method involves calculating the autocorrelation values and then solve a system of linear equations for estimating the parameters. The parametric spectral estimation is generally more complex than non-parametric. In addition, it requires an a priori choice of the structure and order of the model of signal generation. From each power spectral estimation, we extracted the spectral indexes in order to evaluate the involvement of autonomic system:

- Total Power (TP) (from 0.03 Hz to 0.4 Hz)
- Low frequency component (LF) (from 0.03 Hz to 0.15 Hz)
- High frequency component (HF) (from 0.15 Hz to 0.40 Hz)
- Low to high frequency component ratio (LF/HF)

All the described parameters were developed on a GUI for the HRV assessment as showed in Figure 41 to perform the sympatho-vagal analysis.

Figure 41 GUI for HRV assessment

The GUI is divided into three sections: 1) ECG with QRS recognition (identified with red stem) and extraction of RR interval series; 2) RR series pre-processing, where artifact can be removed automatically or after manual selection by an expert user; 3) Feature extraction section reporting statistical time domain parameters (mean, standard deviation, variance coefficient, maximum, minimum, dynamic range, percentiles, etc.) and frequency domain parameters for each frequency band, low frequency (LF: 0.03-0.15 Hz) and high frequency (HF: 0.15-0.40 Hz), included absolute powers, peak frequencies (Max LF and Max HF) and the LF/HF power ratio. These features can be extracted using PSD analysis according to three different spectrum estimation options: the Welch transformation [35], the Lomb-Scargle periodogram [36], [37], and the Burg spectral estimation [38]. The power of each band is normalized in respect to the total power of the spectrum. Another relevant feature can be extracted: the respiratory sinus arrhythmia (RSA). RSA refers to the periodic fluctuations in heart rate that are linked to breathing. RSA is largely determined by vagal influences on the heart, and as such provides a noninvasive index of parasympathetic activity, social functioning and cognitive performances. A growing body of theory and research suggests that RSA figures prominently in emotional responding, even if its exact role remains unclear [39], [40]. Moreover, other nonlinear parameters can be extracted, i.e. the Poincaré Plot, a graphical representation created by plotting all RR(n) on the x-axis versus RR(n+1) on the y-axis. Then, the data are fitted using an ellipse projected according the line of identity and extracting the two standard deviations (SD) respectively [41]. Another index reported that measures the global sympathetic-parasympathetic equilibrium in the analyzed portion of tachogram is the ratio of areas extracted from LF/HF ratio curve. The marked line is an equilibrium threshold, which indicates where the LF/HF ratio equals the identity. Above this line, the curve reveals sympathetic dominancy. Below the threshold, the parasympathetic influence is dominant as showed in Figure 42.

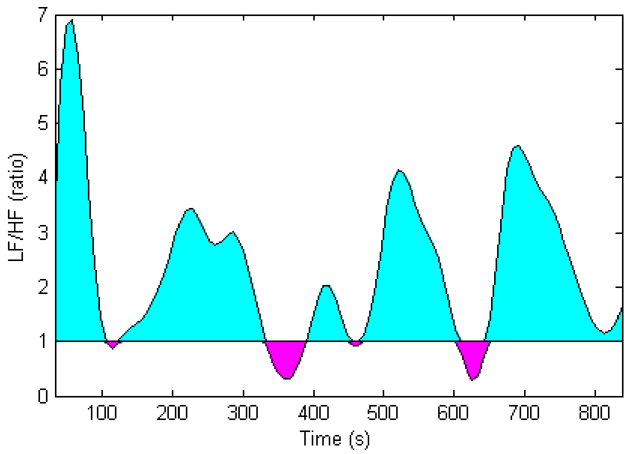

Figure 42 Curve of LF/HF ratio to evaluate the sympathetic and parasympathetic dominancy

The Poincaré Plot could be also an useful tool to investigate and combine the differences of the cardiac rhythms during the performed tasks of the subject as shown in Figure 43. Looking at the standard deviations (SD) of the points perpendicular to the line of identity two different dispersions can be observed.

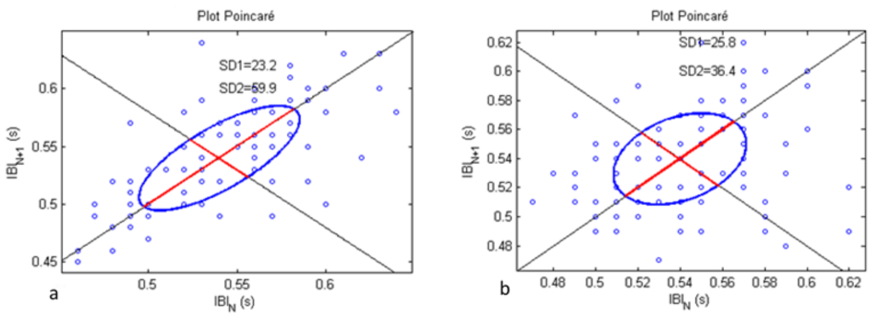

Figure 43 Poincarè plot parameters extracted during two different subject conditions

4.2.8 Subject selection and experimental procedure of HRV study in young anorexia nervosa adolescents

All the parameters of HRV described above were monitored for a study of young adolescents with anorexia nervosa (AN) as compared to controls by means of the developed wearable chest strap. 27 adolescent girls (mean age: 14.6 ± 2.2 years) with ANR complete form in line with DSM-4TR standards were consecutively enrolled to be part of the experimental group in the Child and Adolescent Eating Disorders Unit of the IRCCS Stella Maris. All patients showed typical psychiatric comorbidities on Axis I, such as Major Depressive Episode (59.23%), Dysthymic Disorder (37%), Generalized Anxiety Disorder (11.11%), Oppositional Defiant Disorder (3.7%). Data collection was performed in all subjects within 3 days of patient hospitalization before any pharmacologic treatment was started. A sample of 15 healthy adolescent girls was enrolled as control group (mean age: 14.5 ± 1.5 years). The written informed consent from a parent or guardian of children was obtained. The research protocol was approved by the Institutional Review Board of the Clinical Research Institute for Child and Adolescent Neurology and Psychiatry. After the complete echocardiographic exam, the electrocardiographic signals were acquired with the developed and validated ECG chest strap for 15 min while the patients lay in a supine position on an ambulatory bed in a quiet, darkened room. The patients were asked to do nothing except to relax.

ECG signals were sampled at 250 Hz and pre-processed in Matlab removing common drift, line artifacts and DC components as proposed by Thankor et al. [42]. Once pre-processed, R waves were detected with the algorithm described in section 4.2.4 to obtain the tachogram, that is the series of the time intervals between the occurrence of two consecutive R peaks. Temporal and frequency domain features described above were extracted from tachogram. In particular the following parameters were extracted: mean HR, the mean RR intervals (RRmean), the standard deviation of RR intervals (RRdevstd), the difference between the longest and shortest RR interval (diffRR) and the root mean square of successive differences (RMSSD). The power spectrum density (PSD) was calculated using the parametric autoregressive Yule-Walker model of order 9 chosen by using the information criterion due to Akaike (AIC) [43]. The features extracted from the PSD and estimated for each frequency band, low frequency (LF: 0.03-0.15 Hz) and high frequency (HF: 0.15-0.40 Hz), included absolute powers, peak frequencies (Max LF and Max HF) and the LF/HF power ratio. The power of each band was normalized to the total power of the spectrum. Statistical comparisons of the autonomic function outcome measures were performed using SPSS software (SPSS Inc, Chicago, IL, USA) [44]. The Shapiro-Wilk test was applied to test the normality of the variables. Type I error for statistical tests of hypothesis was equal to 0.05. When the variables had non-normal distribution data they were compared using the

Kolmogorov-Smirnov non-parametric test for independent samples. No adjustments for multiple comparisons were made [45]. A comparison between patients and controls was performed. The AN patients and the control girls were described in terms of demographic, personal and outcome data. The analyses were repeated also using BMI as covariate in an ANCOVA test. When a non-parametric test was required variables and covariate were transformed in rank and an ANCOVA on ranks was performed. Bivariate correlations between the outcome measures and age, or BMI were also investigated using Pearson's correlation coefficient analysis in both AN patients and controls.

4.3 Results and Discussion

A comparison of the recordings at the bedside performed by expert cardiologists of the Institute of Clinical Physiology demonstrated that the chest strap recordings with respect to the traditional ECG electrode placements and recordings have a similar waveform as shown in Figure 44.

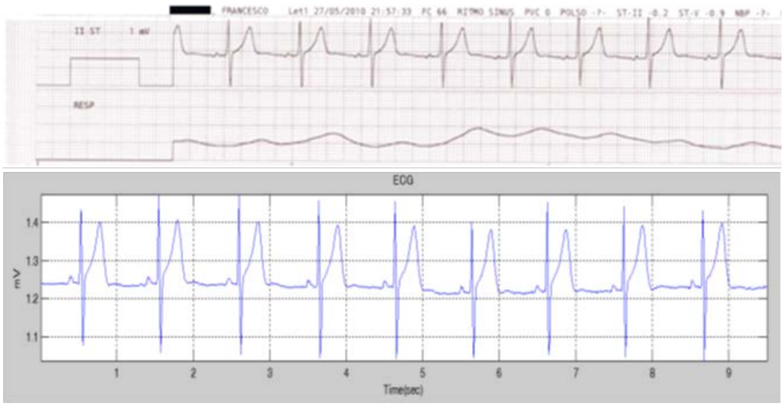

Figure 44: Comparison of ECG chest strap recordings with a clinical electrocardiograph at bedside

Moreover the chest strap was also used by runners during a marathon; the ECG signal appears really stable and with a negligible number of artifacts, as reported in Figure 45.

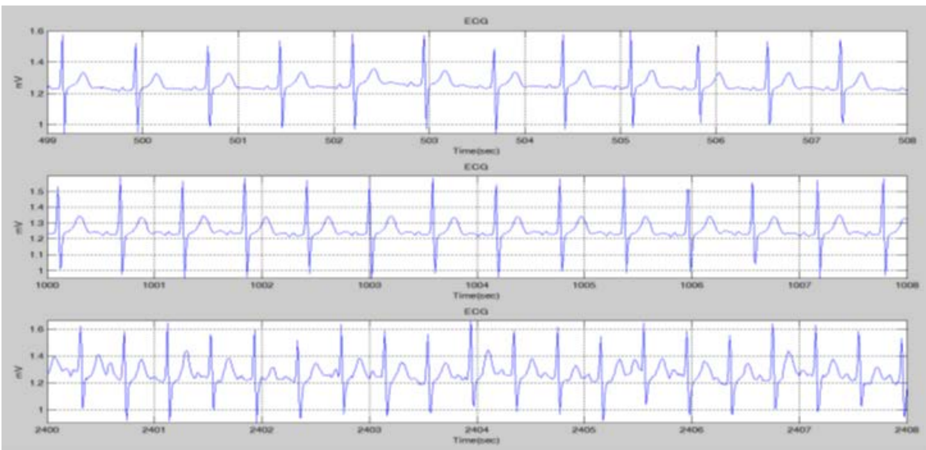

Figure 45 Three phases of ECG chest strap recordings on runner during a marathon

In particular, in the first two plots of the Figure 45 is shown the ECG signal acquired before the start of marathon, while in the third plot is reported the ECG signal acquired during running phase. In Figure 46 the mean HR is reported.

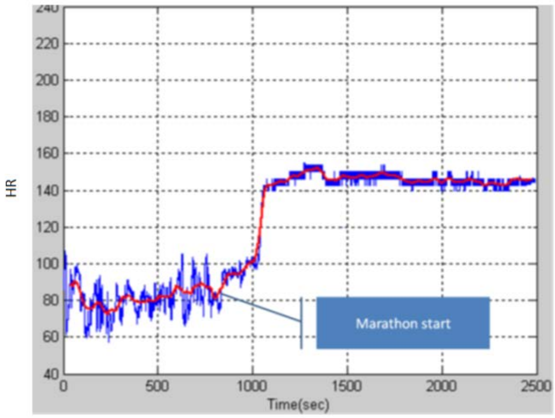

Figure 46: HR values extracted from ECG signal, before and during marathon

Different experiments were performed in order to evaluate the R peak detection to validate the wireless ECG system and to investigate the feasibility of using the sensor in mobile environment. The algorithm has been assessed on the signal collected from the healthy subjects wearing both ECG chest strap and Holter ELA during working activities. The R peak detected, using the developed algorithm, were compared to the ones annotated in different report provided by ELA Holter. In Table 10 the results of the evaluation of the 10 ECG signals collected and analyzed with the developed algorithm are reported. 151 false positive (FP) beats (Sp =99.26 %) and 8 false negative (FN) beats (Se =99.97 %) were obtained. It is worth mentioning that the FN values are very low (range 0÷2);

this is mainly related to the capability of the proposed algorithm to correctly detect any QRS complex and to the negligible number of artifacts of the ECG signal collected from the wearable chest belt. Moreover, the ECG chest strap provided readable signal for more than 95% and 99% of the time of acquisition while the subjects were working and lying supine at bedside respectively.

Table 10: Sensitivity and specificity extracted from collected ECG signals

Tape N°	**Total Beats**	**FN (beats)**	**FP (beats)**	**Sen (%)**	**Spec(%)**
1	2273	0	0	100	100
2	1865	0	4	100	99,78
3	2084	0	1	100	99,95
4	2229	1	17	99,95	99,24
5	2572	0	38	100	98,54
6	2532	1	2	99,96	99,92
7	2124	1	1	99,95	99,95
8	2539	1	1	99,96	99,96
9	1795	2	67	100	96,40
10	1879	2	20	99,89	98,94
Total tape	**21892**	**8**	**151**	**99,97**	**99,26**

The good performances of the ECG chest strap were confirmed by the data shown in Figure 47. The resulting waveform confirmed the signal quality was comparable to that acquired by the ELA holter. It can be noticed that the tachogram of the ECG chest belt (black line) closely follows the tachogram of holter ELA (red line).

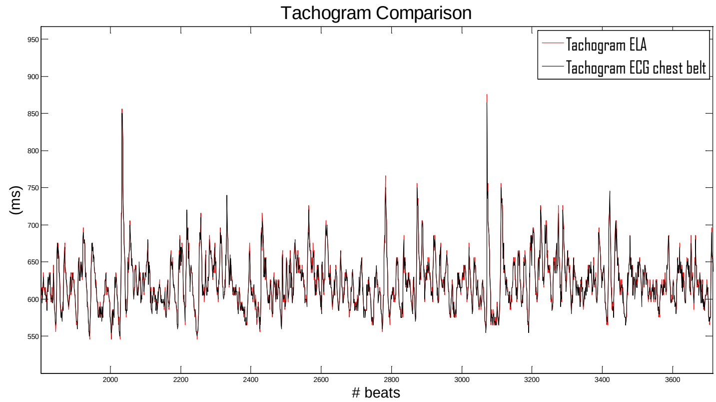

Figure 47: Tachogram comparison between ECG chest strap and ELA holter

The mean percentage of HR measurements was lower than the 10% (maximum value established by the CEI ISO60601-2-47 about HR calculation) during the whole validation. Moreover, statistical parameters of the tachogram error distribution are extracted and shown in Figure 48. The low value of mean error distribution (~0.01 sec) confirms the absence of differences between the two signals analyzed.

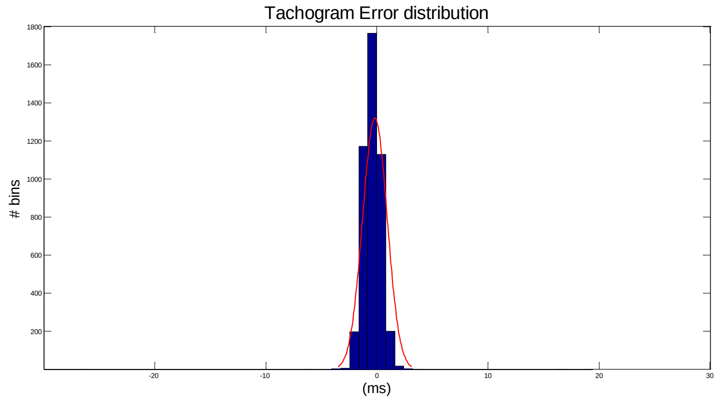

Figure 48: ECG chest strap tachogram error distribution with respect to the gold standard ELA holter

Another analysis aiming to assess performances of a system with respect to a gold standard method is the Bland-Altman plot, often employed for this purpose [46], [47]. In Figure 49, the Bland-Altman plot for comparison between the two methods is displayed. It's evident that the ECG chest strap is coherent with the holter ELA, confirming once again the validity of the approach proposed. It's evident that the greater part of data are contained into a small dispersion around the zero value of the difference between holter and sensor.

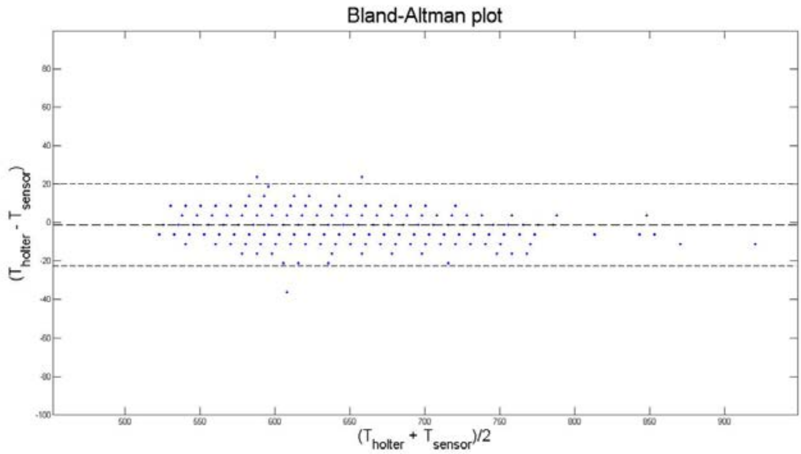

Figure 49: Bland-Altman plot for the comparison of ECG chest strap and ELA holter tachogram.

Finally we observed that the information provided by the power spectral analysis, are equal as the one reported in Figure 50. This important result confirms that the ECG Chest Strap System has a high accuracy in terms of HRV assessment, and then it can be effectively used to investigate the autonomic function.

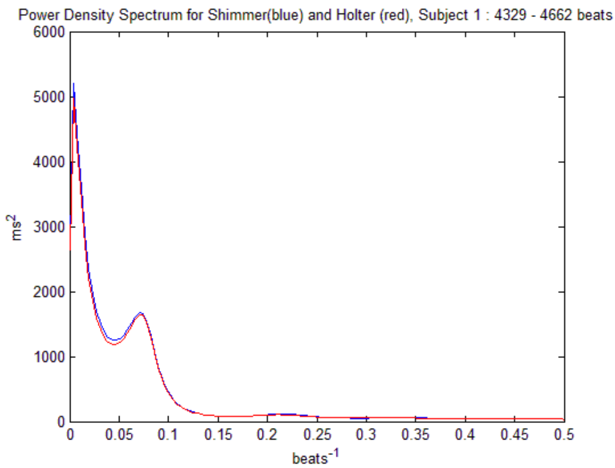

Figure 50: Spectral Power Density of ECG Chest Strap and Holter ELA from the same time of acquisition.

After validation of the wearable ECG system, an HRV study was conducted on AN adolescents. Data were collected and analyzed offline as described in section 4.2.8. The comparison of the individual temporal features showed that in AN patients mean HR was decreased (AN mean: 62.05 ± 13.84, controls mean: 77.97 ± 10.31, $p < 0.001$). RRmean (AN mean: 1000 ± 250 ms, controls mean: 790 ± 90 ms, $p = 0.002$), diffRR (AN mean: 270 ± 70 ms, controls mean: 210 ± 30 ms, $p = 0.006$), RMSSD (AN mean: 130 ± 110 ms, controls mean: 50 ± 20 ms, $p = 0.008$) and RRdevstd (AN mean: 77(45-13) ms, controls mean: 60(40-70) ms, $p = 0.028$) were increased in AN with respect to controls. The comparison between AN and controls of the frequency features showed a decreased normalized LF power (mean: 0.42 ± 0.18, vs 0.62 ± 0.19, $p = 0.001$) and an increased normalized HF power (mean: 0.62 ± 0.17 vs 0.46 ± 0.18, p = 0.001). Overall, the ratio between LF and HF was lower in AN than in controls (AN mean: 0.69(0.43-0.27), controls mean: 2.07(0.85-5.29), p = 0.002). All these comparisons were significant after BMI correction except for RRdevstd as showed in Table 11.

Table 11. Outcome measures of heart rate (HR) and heart rate variability (HRV) analysis on AN vs control subjects, with and without BMI correction

	AN group N=27	**Control group N=15**	**Test significance**			**Test significance (with BMI correction)**		
			ANOVA	**MW**	**p-value**	**ANCOVA**	**ANCOVA on ranks**	**p-value**
HRmean	62.05 (13.84)	77.97 (10.31)	15.5	na	<0.001*	7.61	na	0.002*
RRmean (ms)	1000 (250)	790 (90)	10.7	na	0.002*	6.09	na	0.006*
RRdevst (ms)	77 (45-13)	60 (40-70)	na	133.5	0.028*	na	2.72	0.07
diffRR (ms)	270 (70)	21 (0.03)	8.4	na	0.006*	5.05	na	0.011*
RMSSD (ms)	130 (110)	50 (20)	7.6	na	0.008*	4.64	na	0.015*
LFnorm	0.42 (0.18)	0.62 (0.19)	12.3	na	0.001*	5.58	na	0.007*
HFnorm	0.58 (0.18)	0.37 (0.19)	12.3	na	0.001*	5.58	na	0.007*
LF/HF	0.69 (0.43-1.27)	2.07 (0.85-5.29)	na	93.5	0.002*	na	5.25	0.009*
MaxLF (Hz)	0.03 (0.01-0.07)	0.06 (0.03-0.08)	na	166.5	0.14	na	1.27	0.29
MaxHF (Hz)	0.23 (0.18-0.28)	0.19 (0.17-0.23)	na	174.5	0.23	na	2.21	0.12

*: $p < 0.05$

The developed ECG monitoring system was selected by EU CHIRON project to be integrated also in a wearable chest strap for continuous monitoring of relevant parameters of CHF patients during daily activities. A literature research was performed resulting in a long list of parameters, which were classified in short-term and long-term together with its relevance as potential risk factors. The present solution focuses on the short-term parameters: electrocardiogram (ECG), potassium blood content (obtained from ECG), average energy expenditure evaluation through activity recognition, skin and ambient temperature, sweating and ambient humidity. This solution differs from other remote monitoring systems for healthcare as it is specifically designed for CHF patients. It comprises the components that are in charge of concentrating the data, extracting the proper features and sending them to the hospital servers. All the parameters will be analyzed to design a complete and personalized health monitoring system. Related to CHIRON project architecture, the main data analysis will be performed using all parameters (physiological and behavioral) stored on the database acquired during the observational study. The wearable platform comprises two different straps: one placed at the chest, which collect ECG, skin temperature, sweat index and acceleration data and a second one at the thigh collecting extra acceleration data for accurate activity recognition.

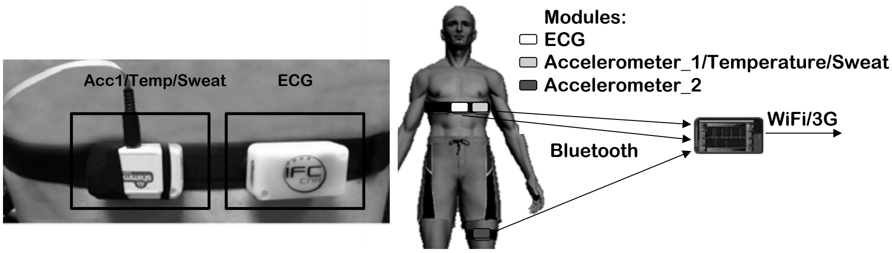

Figure 51: Diagram and prototype implementation of the wearable sensor platform

Figure 51 shows a scheme of the system. The modules collect the parameters from sensors and send the data to a mobile platform by means of Bluetooth connections. In order to perform the observational study in the most comfortable way for the users all the devices were integrated in a chest wrapper. Moreover to guarantee the maximum comfort and performance of the humidity/sweat sensor also the probe was shrouded using a thin textile as shown in Figure 52.

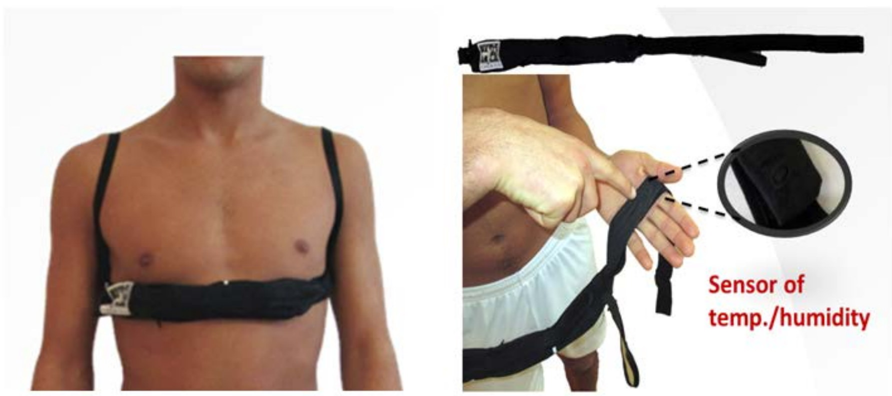

Figure 52 Integrated multi-sensorial chest belt with ECG, accelerometer for activity recognition and sensor of temperature/humidity

4.4 Conclusions

In this document a detailed description of software and a characterization of the novel ECG chest strap designed has been reported. The developed wearable chest straps can be used for continuous monitoring and may be a form of management that allows daily monitoring of symptoms and signs measured at home while allowing patients to remain under close supervision.

The system offers a unique opportunity for a structured follow-up with patient education, optimization of medical treatment, psychosocial support and a close cross-talk with nurses and physicians for their well-being. To reach this ambitious goal the ECG module was designed taking into account the main characteristic such as usability, comfort, and reducing skin irritability and physical constraint typical of conventional holter ECG, without leaving out the importance to achieve reliable and robust parameters. The ideal setting of the wearable system includes scenarios such as long-term monitoring in chronic cardiovascular diseases, the assessment of sympatho-vagal function and stress level. In this work the clinical assessment was focused on the analysis of the developed solution in comparison with holter ELA as gold standard equipment. Preliminary results have shown high hardware performances in terms of usability, the integrated algorithm allowed to detect reliable QRS complex, showing very good results in terms of sensibility and specificity of R peak detection. A negligible number of artifacts and comparable results for the analysis of HRV parameters were obtained, allowing to gain high correlation values around 98%. After the characterization of the wearable device, a study was conducted on HRV indexes extracted both in time and frequency domain as useful biomarker of autonomic function in young adolescents with anorexia nervosa (AN) compared to controls in a resting condition. The results of this study showed that compared to controls, young ANR adolescent girls have significantly lower heart rate (HR) and higher heart rate variability (HRV), lower low-frequency components, elevated high-frequency components, and decreased low- to high-frequency power ratio when compared to controls. Therefore, AN patients showed a reduced cardiovascular sympathetic nervous responsiveness and an increased parasympathetic responsiveness when compared with healthy controls. The results of the this study confirmed previously published data obtained by means of conventional recording techniques in AN adolescents or young adult patients, which showed that in AN the physiological balance of cardiac vagal and sympathetic activities is mostly shifted towards a parasympathetic over-reactivity [48]. However, at present, changes in the autonomic nervous system in AN are not univocally reported as parasympathetic/sympathetic imbalance with parasympathetic dominance and decreased sympathetic modulation; some studies have described sympathetic dominance; and a small but not negligible group of papers could not identify any autonomic differences in comparison to control samples [49]. Since HRV assessment still represents a tool for evaluation of AN patients who are at increased arrhythmic risk, potential methodological problems that can explain these controversial results need to be resolved. In fact, recent papers warrant the use of new methodological approaches for a more thorough comprehension of the autonomic system in this specific high-risk group of patients [50]. In this respect, the use of wearable technology may offer a completely new approach for HRV assessment in AN. Results of this study, obtained at present in a quiet ambulatory room, may indicate the use of wearable systems for signal acquisition of physiological parameters in the home setting, without interference and possible pitfalls due to the use of wires. This technical opportunity could also provide better understanding of the physiological phenomenon, since a large amount of data (more than with conventional ECG recording) can be collected, providing the substrate for a more extensive medical interpretation and possibly offering a personalized therapeutic model of intervention. In the specific setting of young AN adolescents, the assessment of HR and HRV by wireless technology appears to be of real clinical importance, not only to overcome any lack of compliance with conventional technologies but particularly for the opportunity to transfer this modality of acquisition to a more “natural” environment. The promising results obtained in this study in resting conditions could direct future research on shifting from invasive approaches (e.g., multi-electrode ECG Holters) to minimally invasive methods for extraction of physiologic parameters during daily life. To get best results from wearable chest strap in patients the first important step is communication. In fact, explain to the patients what these devices are made for, what they can do, what is the possible advantage for their clinical status and the information they can provide is very useful for the spread of this approach. This is a critical issue because the patient needs to be fully aware that ECG monitoring may not save his life but may help in modulating the medical therapies and have impact on his/her overall well-being. It is necessary to ensure that this monitoring does replace visits with physicians. These obtained results have fostered the selection and integration of ECG chest strap in CHIRON platform with accelerometers for activity recognition and energy expenditure evaluation, skin temperature and sweating index. The platform communicates sensor parameters to a mobile platform by means of Bluetooth communications using the store-and-forward principle that preserves the platform autonomy. Future steps comprise the integration of collected data with those available in the Hospital Information System in order to build a physiological model (Alter Ego).

4.5 References

[1]. Worringham C, Rojek A, Stewart I. Development and Feasibility of a Smartphone, ECG and GPS Based System for Remotely Monitoring Exercise in Cardiac Rehabilitation. PLoS ONE 6(2): e14669. doi:10.1371/journal.pone.00146.

[2]. Camarozano AC, et al. The effects of beta-blockers on dobutamine-atropine stress echocardiography: early protocol versus standard protocol. Cardiovascular Ultrasound 2006, 4:30 doi:10.1186/1476-7120-4-30.

[3]. De Chazal P, et al. Automated Processing of the Single-Lead Electrocardiogram for the Detection of Obstructive Sleep Apnoea. IEEE Transactions On Biomedical Engineering, Vol. 50, No. 6, June 2003.

[4]. She LH, Zhao JS, Zhang S, Wang GH, Wang G. A Novel Portable One Lead ECG Monitor with Low-Cost and Long-Time Recording Based on NUC501. 2010 Chinese Control and Decision Conference.

[5]. Farwell D, Gollob MH. Electrical heart disease: Genetic and molecular basis of cardiac arrhythmias in normal structural hearts. Can J Cardiol 2007;23(Suppl A):16A-22A.

[6]. C. Otto, A. Milenkovic, C. Sanders, and E. Jovanov. Final results from a pilot study with an implantable loop recorder to determine the etiology of syncope in patients

with negative noninvasive and invasive testing. The American Journal of Cardiology, 82:117–119, 1998.

[7]. Victor Shnayder, Bor-rong Chen, Konrad Lorincz, Thaddeus R.F. Fulford-Jones, and Matt Welsh. Sensor networks for medical care. Technical report, Harvard University, 2005.

[8]. B. Lo, S. Thiemjarus, R. King, and G.Z. Yang. Body sensor network - a wireless sensor platform for pervasive healthcare monitoring. In Adjunct Proceedings of the 3rd International Conference on Pervasive Computing, May 2005.

[9]. Joshua Proulx, Ryan Clifford, Sarah Sorensen, Dah-Jye Lee, and James Archibald. Development and evaluation of a Bluetooth EKG monitoring sensor. In Proceedings of the IEEE International Symposium on Computer-Based Medical Systems (CBMS), 2006.

[10]. Rune Fensli, Einar Gunnarson, and Torstein Gundersen. A wearable ECG-recording system for continuous arrhythmia monitoring in a wireless tele-home-care situation. In Proceedings of the IEEE International Symposium on Computer-Based Medical Systems (CBMS), 2005.

[11]. Eugene Shih, Vladimir Bychkovsky, Dorothy Curtis, and John Guttag. Continuous medical monitoring using wireless microsensors. In Proceedings of SenSys, page 310, November 3–5 2004.

[12]. Task Force of the European Society of Cardiology and the North American Society of Pacing and Electrophysiology. Heart rate variability: standards of measurement, physiological interpretation and clinical use. Circulation. 1996;93: 1043–1065.

[13]. La Rovere MT, Bigger JT, Marcus FI, et al. Baroreflex sensitivity and heart rate variability in prediction of total cardiac mortality after myocardial infarction. Lancet. 1998;351: 478–484.

[14]. Nolan J, Batin PD, Andrews R, et al. Prospective study of heart rate variability and mortality in chronic heart failure: results of the United Kingdom Heart Failure Evaluation and Assessment of Risk Trial (UK-Heart). Circulation. 1998;98: 1510–1516.

[15]. Malliani A, Pagani M, Lombardi F, et al. Cardiovascular neural regulation explored in the frequency domain. Circulation. 1991;84: 482–492.

[16]. BM, van Veldhuisen DJ, van der Veer N, et al. Prognostic value of heart rate variability in chronic congestive heart failure secondary to idiopathic or ischemic dilated cardiomyopathy. Am J Cardiol. 1997;79: 978–980.

[17]. Ponikowski P, Anker SD, Chua TP, et al. Depressed heart rate variability as an independent predictor of death in chronic congestive heart failure

secondary to ischemic or idiopathic dilated cardiomyopathy. Am J Cardiol.

[18]. Galinier M, Pathak A, Fourcade J, et al. Depressed low frequency power of heart rate variability as an independent predictor of sudden death in chronic heart failure.

[19]. La Rovere MT, Pinna GD, Maestri R, et al. Short-term heart rate variability strongly predicts sudden cardiac death in chronic heart failure patients. Circulation 2003;107:565–570.

[20]. A. Vazir, M. Dayer, Hastings, et al. Can heart rate variation rule out sleep-disordered breathing in heart failure? EurRespir J. 2006;27:571-577.

[21]. Continuous Autonomic Assessment in Patients With Symptomatic Heart Failure: Prognostic Value of Heart Rate Variability Measured by an Implanted Cardiac Resynchronization Device Circulation. 2004;110:2389-2394.

[22]. Device diagnostics and long-term clinical outcome in patients receiving cardiac resynchronization therapy Europace. 2009;11:1647-1653.

[23]. Chronic vagus nerve stimulation: a new and promising therapeutic approach for chronic heart failure Eur Heart J. 2011;32:847-855.

[24]. Home monitoring for heart failure management. J Am Coll Cardiol. 2012;59:97-104.

[25]. Shimmer research, http://www.shimmer-research.com.

[26]. Vahanian A, Camm J, De Caterina R, Dean V, Dickstein K, Filippatos G, Funck-Brentano C, Hellemans I, Kristensen SD, McGregor K, Sechtem U, Silber S, Tendera M, Widimsky P, Zamorano JL ESC Committee for Practice Guidelines.

[27]. J. pan, W.J. Tompkins, “A real- time QRS detection algorithm”, IEEE Transaction on biomedical engineering, vol. 32, n°3, march 1985.

[28]. S. Kadambe, “Wavelet transform-based QRS complex detector”, IEEE.

[29]. C. Li, C. Zheng, C. Tai, “detection of ECG characteristic points using wavelet.

[30]. R. Murray, S. Kadambe, G. F. Boudreaux-Bartels,” Extensive analysis of a QRS.

[31]. American National Standard, “ Testing and reporting performance results of.

[32]. Jeffrey J. Goldberger, “Sympathovagal balance: how should we measure it?” Am. J. Physiol. 276 (Heart Circ. Physiol. 4), 1999, pp. H1273-H1280.

[33]. Alberto Malliani, The Pattern of Sympathovagal Balance Explored in the Frequency Domain. News Physiol. Sci., Volume 14, June 1999.

[34]. Mainardi L. T., Bianchi A. M., Cerutti S., 2000. Digital Biomedical Signal Acquisition and Processing. In:

The Biomedical Engineering Handbook: Second Edition, Vol. 2, Bronzino J. D., CRC Press Inc., 983-985.)

[35]. P. D Welch, “The Use of Fast Fourier Transform for the Estimation of Power Spectra: A Method Based on Time Averaging Over Short, Modified Periodograms,” IEEE Trans. Audio Electroacoustics, Vol. 15, no. 2, pp. 70-73, Jun. 1967.

[36]. N. R. Lomb, “Least-squared frequency analysis of unequally spaced data,” Astrophys. Space Sci., vol. 39, pp. 447–62, Feb. 1976.

[37]. J. D. Scargle, “Studies in astronomical time series analysis: II. Statistical aspects of spectral analysis of unevenly spaced data,” Astrophys. J., vol. 263, no. 1, pp. 835–853, Dec. 1982.

[38]. J. P. Burg “Maximum Entropy Spectral Analysis” in Proc. 38th Annu. Int. Meeting Sot. Of Explor. Geophys, 1975, vol. 6.

[39]. M. A. Patriquin, J. Lorenzi, A. Scarpa, M. A. Bell, “Developmental trajectories of respiratory sinus arrhythmia: Associations with social responsiveness,” Dev. Psychobiol., Jan. 2013.

[40]. M. A. Patriquin, A. Scarpa, B. H. Friedman, S. W. Porges, “Respiratory sinus arrhythmia: a marker for positive social functioning and receptive language skills in children with autism spectrum disorders,” Dev. Psychobiol., vol. 55, no. 2, pp. 101-112, Mar. 2013.

[41]. M. Brennan, M. Palaniswami, P. Kamen, “Do existing measures of Poincaré plot geometry reflect nonlinear features of heart rate variability,” IEEE Trans Biomed Eng, vol. 48, no. 11, pp.1342–1347, Nov. 2001.

[42]. N.V. Thakor, J.G. Webster, W.J. Tompkins, Optimal QRS detector. Med.Biol. Eng. Comput. vol 21, 343-350, 1993.

[43]. Akaike, Hirotugu (1974), "A new look at the statistical model identification", IEEE Transactions on Automatic Control 19 (6): 716–723, doi:10.1109/TAC.1974.1100705, MR 0423716. 29, 30.

[44]. IBM Corp. Released 2012. IBM SPSS Statistics for Windows, Version 21.0. Armonk, NY: IBM Corp.

[45]. Rothman K J 1990 No adjustments are needed for multiple comparisons Epidemiology 1 43-6.

[46]. J. M. Bland and D. G. Altman, “Statistical methods for assessing agreement between two methods of clinical measurement,” The Lancet, vol. 327, no. 8476, pp. 307–310, 1986.

[47]. O. P. Heikkinen, J. A. Lipponen, O. Tikkanen, and M. P. Tarvainen, “Development and validation of an ambulatory HRV measurement system,” in XI Annual Seminar of the Finnish Society for Medical Physics and Medical Engineering, Turku, Finland, 2012.

[48]. Ishizawa T, Yoshiuchi K, Takimoto Y, Yamamoto Y and Akabayashi A 2008 Heart rate and blood pressure

variability and baroreflex sensitivity in patients with anorexia nervosa Psychosomatic Medicine 70 695– 700.

[49]. [Mazurak N, Enck P, Muth E, Teufel M and Zipfel S, Heart Rate Variability as a Measure of Cardiac Autonomic Function in Anorexia Nervosa: A Review of the Literature. Eur. Eat. Disorders Rev. 2011 19 87–99.

[50]. Mazurak N, Enck P, Muth E, Teufel M and Zipfel S, Heart Rate Variability as a Measure of Cardiac Autonomic Function in Anorexia Nervosa: A Review of the Literature. Eur. Eat. Disorders Rev. 2011 19 87–99.

Chapter 5

A novel wearable sensing technology for long-term monitoring of knee kinematics during ambulatory activities

Long-term unobtrusive monitoring of biomedical signals is a key component in proactive healthcare. It can provide valuable information about health status and recovery assisting in the provision of a continuum of care for subjects with chronic conditions and older adults in the home and community settings. Many orthopedic and physical therapy techniques aim to restore joint motion and hence promote rehabilitation of functional activities. These techniques are designed to restore pain free and unrestricted movement to joints on the assumption that patients will subsequently exhibit better functional ability and less impairment and disability. The most common approach to monitor these functional capability is based on the clinical use of stero-photogrammetric systems which are very expensive and are suitable only for short sessions. In this chapter, a wearable sensing system for long term monitoring of activity and knee range of motion developed at Spaulding Rehabilitation Hospital at Harvard Medical School is presented. The aim of the novel unsupervised therapeutic system is to detect changes of parameters that would suggest a decline or improvement of knee functions contextualized with daily activities of the subject. The introduction is focused on the state of art of methods of human movement analysis and related works for models of activity daily recognition with inertial sensors. A description of the system based on an innovative mechanical design with an embedded tri-axial accelerometer and electro-goniometer equipped with a wireless unit able to rely data to a smartphone is presented. In the second part, is described the software architecture. Experimental measures gathered with the developed system demonstrates the reliability of a model based on artificial neural network for the automatic recognition of ambulatory activities and the characterization of knee kinematic data compared with the gold standard stereo-photogrammetric system.

5.1 Introduction

5.1.1 Related works of human movement analysis and activity recognition

Acquisition of quantitative information about the mechanics of the musculo-skeletal system during the execution of a motor task is the main goal of the human motion analysis. In particular, information is sought concerning the movement of the whole-body centre of mass; the relative movement between

adjacent bones, or joint kinematics; the forces exchanged with the environment; the resultant loads transmitted across sections of body segments or between body segments, or transmitted by individual body tissues such as muscles, tendons, ligaments, and bones; and body segment energy variation and muscular work. Traditionally to evaluate the dynamic behavior of a joint the motion analysis is performed in clinical laboratory using sophisticated camera-based motion capture systems (i.e. stereo-photogrammetric systems). Gait analysis is generally carried out by mounting retro-reflective markers on the skin surface of the subjects and reconstructing their 3D position using video-based optoelectronic systems as shown in Figure 53. Retro-reflective markers and infrared illumination produced by light-emitting diodes (LEDs) around the lens of the cameras are used for the 3D reconstruction. By adjusting the camera thresholds, reflective markers are sampled and the recognition of the markers in the video frames is performed.

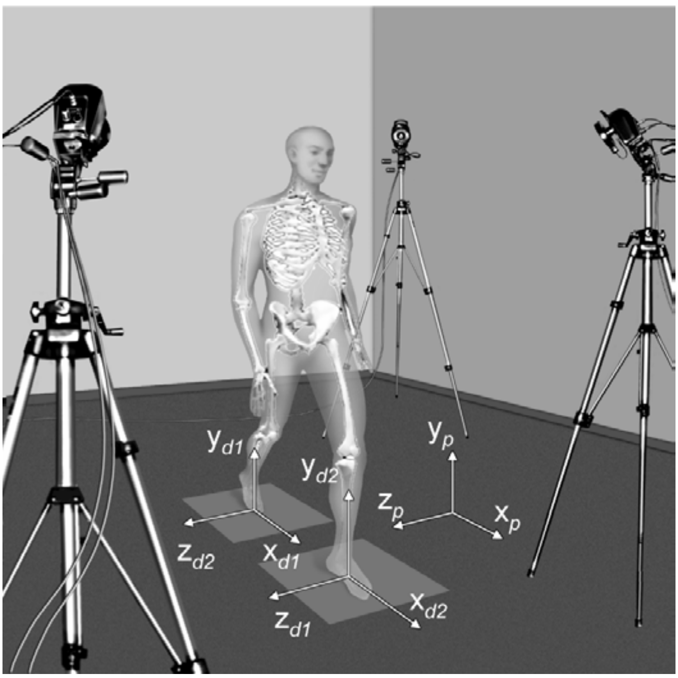

Figure 53 The human movement analysis laboratory with basic measurement instruments, with their systems of axes (p: photogrammetry; d: dynamometry). When level walking is analysed, the motor task frame may overlap with the frame of one of the two force plates [1]

Such systems are capable of providing a full biomechanical model of motion including predictions of joint loads, but they are expensive and can be used only in limited spaces for very short periods of assessment (1-2 hrs). To address this issue recent studies have shown that inertial sensors provide the ability to capture human body orientation [2], knee joint range [3] and posture [4]. Several groups have worked on capturing the body position of a human [5], [6] and detecting the knee angles [7] via inertial sensors. Recent approaches concerning knee motion using inertial sensors [8], [9] achieve good results under lab conditions, but face practicability challenges when transferred to a real life setting with patients. Therefore, they have not yet been validated in clinical practice. However, these systems are not yet suitable for long-term monitoring of daily activities due to large errors resulting from gyroscope drift and positioning of the IMUs [10], [11]. Besides, gyroscopes and magnetometers are power hungry, which imposes a major limitation on the battery life of the wearable system for long term monitoring. Flexible electrogoniometry solutions [12], [13], offers the opportunity to investigate joint kinematics during a number of functional activities routinely in the clinical environment. This method is inexpensive, portable, comfortable to wear and relatively simple to operate [13.] but has received little attention as a potential tool for wearable systems because it is affected by crosstalk errors related to endblocks rotation (general crosstalk) and to the characteristics of each sensor (individual crosstalk) that has to be compensated [14]. Other groups [15], [16], have explored the possibility of using sensors integrated in form fitting textiles to monitor joint kinematics. These systems are simple and easy to wear but they require complex calibration, special manufacturing techniques and can be susceptible to errors due to changes in the garment fit or properties of sensing material [11]. About models of activity recognition, it has recently gained attention as a research topic because of the many potential applications. Some of the earliest work in accelerometer based activity recognition focused on the use of multiple accelerometers placed on several parts of the user's body. In one of the earliest studies of this topic, Bao & Intille [17] used five biaxial accelerometers worn on the user's right hip, dominant wrist, nondominant upper arm, dominant ankle, and non-dominant thigh in order to collect data from 20 users. Using decision tables, instance-based learning, C4.5 and Naïve Bayes classifiers, they created models to recognize twenty daily activities. Their results indicated that the accelerometer placed on the thigh was most powerful for distinguishing between activities. This finding supports our decision to have our test subjects wear the knee tracker with accelerometer in the most convenient location of right thigh. Other researchers have, like Bao & Intille, used multiple accelerometers for activity recognition. Krishnan et. al. [18] collected data from three users using two accelerometers to recognize five activities: walking, sitting, standing, running, and lying down. This paper claimed that data from a thigh accelerometer was insufficient for classifying activities such as sitting, lying down, walking, and running, and thus multiple accelerometers were necessary (a claim our research contradicts). In another paper, Krishnan et. al. [19] examined seven lower body activities using data collected from ten subjects wearing three accelerometers. This method was tested in supervised and semi-naturalistic settings. Tapia et. al. [20] collected data from five accelerometers placed on various body locations for twenty-one users and used this data to implement a real-time system to recognize thirty gymnasium activities. A slight increase in performance was made by incorporating data from a heart monitor in addition to the accelerometer data. Mannini and Sabatini [21] used five tri-axial accelerometers attached to the hip, wrist, arm, ankle, and thigh in order to recognize twenty activities from thirteen users. Various learning methods were used to recognize three “postures” (lying, sitting, and standing) and five “movements” (walking, stair climbing, running, and cycling). Foerster and Fahrenberg [22] used data from five accelerometers in one set of experiments and from two of those accelerometers in another for activity recognition. Thirtyone male subjects participated in the study and a hierarchical classification model was built in order to distinguish between postures such as sitting and lying at specific angles, and motions such as walking and climbing stairs at different speeds. Researchers have used a combination of accelerometers and other sensors to achieve activity recognition.

Parkka et. al. [23] created a system using twenty different types of sensors (including an accelerometer worn on the chest and one worn on the wrist) in order to recognize activities such as lying, standing, walking, running, football, swinging, croquet, playing ball, and using the toilet in specific locations. Lee and Mase [24] created a system to recognize a user's location and activities, including sitting, standing, walking on level ground, walking upstairs, and walking downstairs using a sensor module that consisted of a biaxial accelerometer and an angular velocity sensor worn in the pocket combined with a digital compass worn at the user's waist. Subramayana et. al. [25] addressed similar activities by building a model using data from a tri-axial accelerometer, two microphones, phototransistors, temperature and barometric pressure sensors, and GPS to distinguish between a stationary state, walking, jogging, driving a vehicle, and climbing up and down stairs. While these systems using multiple accelerometers or a combination of accelerometers and other sensors were capable of identifying a wide range of activities, they are not very practical because they involve the user wearing multiple sensors distributed across their body. This could work for some short term, small scale, highly specialized applications (e.g., in a hospital setting) but would certainly not work for the applications that we envision. Some studies have also focused on combining multiple types of sensors in addition to accelerometers for activity recognition. Maurer et al. [26] used "eWatch" devices placed on the belt, shirt pocket, trouser pocket, backpack, and neck to recognize the same six activities that we consider in our study. Each “eWatch” consisted of a biaxial accelerometer and a light sensor. Decision trees, k-Nearest Neighbor, Naïve Bayes, and Bayes Net classifiers with five-fold cross validation were used for learning. Choudhury et. al [27] used a multimodal sensor device consisting of seven different types of sensors (tri-axial accelerometer, microphone, visible light phototransitor, barometer, visible+IR light sensor, humidity/temperature reader, and compass) to recognize activities such as walking, sitting, standing, ascending stairs, descending stairs, elevator moving up and down, and brushing one’s teeth. Cho et. al. [28] used a single tri-axial accelerometer, along with an embedded image sensor worn at the user’s waist, to identify nine activities. Although these multi-sensor approaches do indicate the great potential of mobile sensor data as more types of sensors are being incorporated into devices, our approach shows that only one type of sensor (an accelerometer) is needed to recognize most daily activities. Thus our method offers a straightforward and easily-implementable approach to accomplish this task. Other studies, like our own, have focused on the use of a single accelerometer for activity recognition. Long, Yin, and Aarts [29] collected accelerometer data from twenty-four users using a triaxial accelerometer worn without regard for orientation at the user’s waist. Data was collected naturalistically, and decision trees as well as a Bayes classifier combined with a Parzen window estimator were used to recognize walking, jogging, running, cycling, and sports. Lee et. al. [30] used a single accelerometer attached to the left waists of five users. Standing, sitting, walking, lying, and running were all recognized with high accuracies using fuzzy c-means classification. However unlike these studies, our work is the first that propose the use of a wearable knee tracker with an accelerometer integrated placed on the thigh with the objective to contextualize the knee joint kinematics during the most important ambulatory activities as “standing”, “sitting”, “walking”, “upstairs”, “downstairs”. This ergonomic system interfaced with a smartphone enables make a practical real-world application for long-term monitoring and patient rehabilitation.

5.2 Materials and Methods

5.2.1 Requirements of the wearable knee tracker

The main hardware requirements are that it has to be easy to use, unobtrusive, reliable and accurate for long-term monitoring applications. The aim of the system is to monitor the knee flexion/extension functions and activities of daily living to contextualize the knee angle measurements. In addition to ensure good data quality also the subject compliance should be monitored. The system must be wireless, interfaced with different type of sensor and have large local storage to log sensor data for several days. To reach this goal, strategies to optimize power consumption such as putting the sensor nodes in sleep mode during periods of inactivity and minimizing the radio transmissions are implemented. During monitoring scenario, the user manages the wearable system using an application developed on smartphone. It acts as a gateway for data collection and streaming to an electronic health record (EHR). It is able to check the correct status of the wearable system, providing alert messaging in case of malfunctions and questionnaires to collect qualitative information from the subject.

5.2.2 Hardware of the wearable knee tracker

The hardware selected is based on Shimmer platform [31]. The proposed multi-sensorial platform is attached to the knee sleeve made of breathable material with magnetic buttons to simplify the design and to make it very easy to wear in long-term monitoring applications as shown in Figure 54.

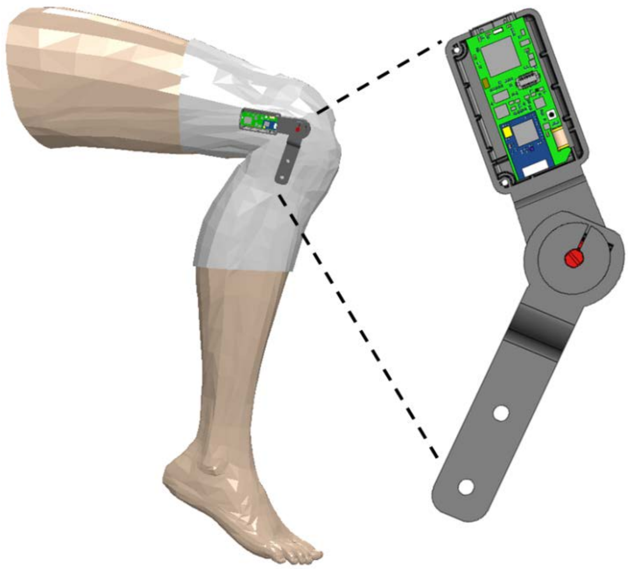

Figure 54 The wearable knee tracker

The package is made of thermoplastic material flexible on the frontal plane and rigid on the sagittal plane. The platform integrates the triaxial accelerometer for the identification of ambulatory activities and a daughter board which connects a potentiometer to evaluate the knee angle and a strain gauge sensor for compliance monitoring to ensure data reliability as shown in Figure 55.

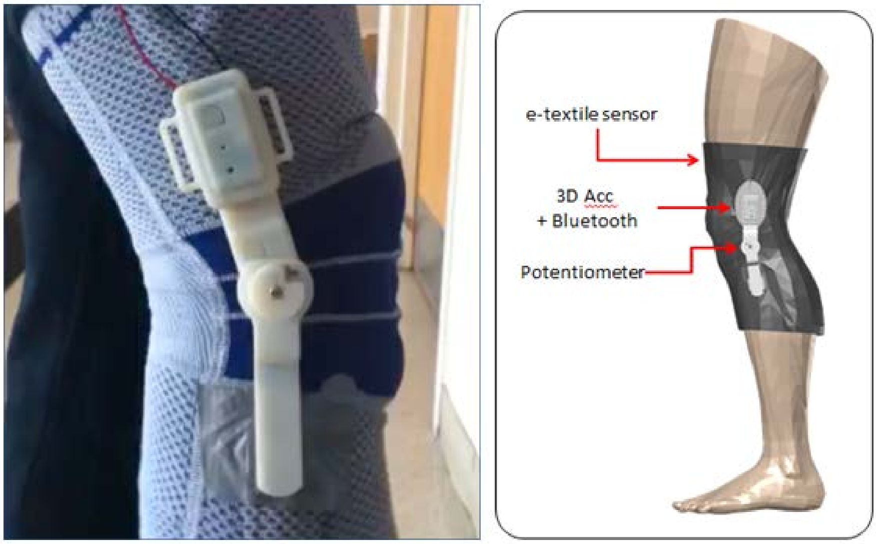

Figure 55 Knee tracker prototype with integrated sensors

We choose a potentiometer for monitoring of knee angles instead of inertial sensors because it is the most suitable solution for long-term monitoring. It is low power consumption, low cost and more ergonomic than the use of inertial sensors which requires at least two sensors node for analysis of the knee joint's motion: one on the thigh and one on the shank [32].

5.2.3 Software architecture of the wearable knee tracker

The software architecture is composed of two main components: 1) the firmware of the sensor and 2) the smartphone application as is shown in Figure 56.

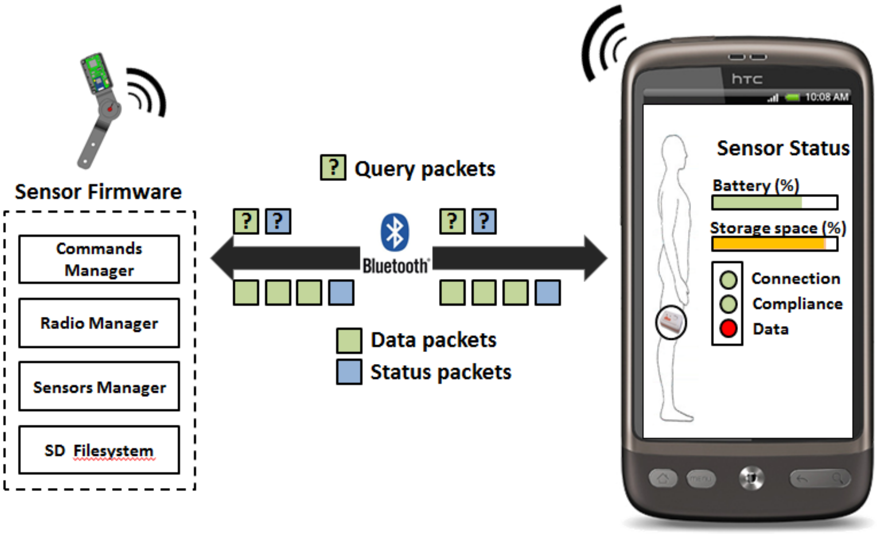

Figure 56 Software architecture of wearable knee tracker

These two components interacts using Bluetooth communication. The developed knee tracker is based on Shimmer platform and uses TinyOS [33], which is coded in a C-derived programming language called nesC. This programming language was designed specifically for TinyOS and its main purpose is to somehow modularize the firmware. TinyOS programs are built out of *components* and component behavior is specified in terms of a set of *interfaces*. When two components are linked through an interface, one component takes the role of provider, while the other one will be the interface user. Depending on implementation, there are two component types: configuration and module. In the first one, you must indicate all components required for the application, and then proceed to wire them. The second one contains the particular program code. The main application component is a module-type. Inside it, events, functions and tasks are implemented. In particular the function_SD manages the data logging on SD card. It creates naming files and folders. The function_BT manages the Bluetooth radio and the protocol of communication. The radio is turned on when the sensor node is transmitting alerts or during the sensor calibration process. Such operation saves the power and guarantee the duration until one week without recharge the device. The function_ext_sensor handles the interrupt for data sampling of external sensors and manipulate them to be stored on SD card. Moreover it manages an integrated tilt sensor during which the sensor nodes is put into a sleep state during periods of inactivity. In this condition the sensor node stops sampling and logging sensor data enabling longer battery lifetime. To increase the battery performances, instead of a continuous writing to the SD card, we buffered data and wrote every few seconds. Finally the function_Command manages the commands sent to the sensor node by the smartphone application. The GUI developed using android operating system performs real-time data visualization and data storage for offline analysis. It also receives status/alert messages from sensor node, performs sensor calibration and sends configuration commands to the sensor node. The ability to perform spot checks is important to ensure high-quality data in long-term monitoring scenarios.

5.2.1 The gait cycle study

The novel knee tracker was validated analyzing the gait cycle and in particular focusing on knee kinematics. In studies of human locomotion, a walking cycle is typically broken down into two phases, the stance phase (60%) and the swing phase (40%) (Figure 57). The gait cycle for the right side begins with heel strike of the right foot. At this point, both feet are on the ground. This is known as the initial double support phase. This sub-phase of the gait cycle is also known as weight acceptance as the body weight is shifted to one leg. Forward advancement begins when the left foot leaves the ground (ie. left toe-off). During the single support phase of stance, the right leg supports the body weight while the left leg advances forward. When the left foot hits the ground, it is the beginning of a second double support phase. As the right leg comes off the ground (toe-off), the body transitions into swing phase. During this phase, the limb advances forward in preparation for the next contact with the ground [34].

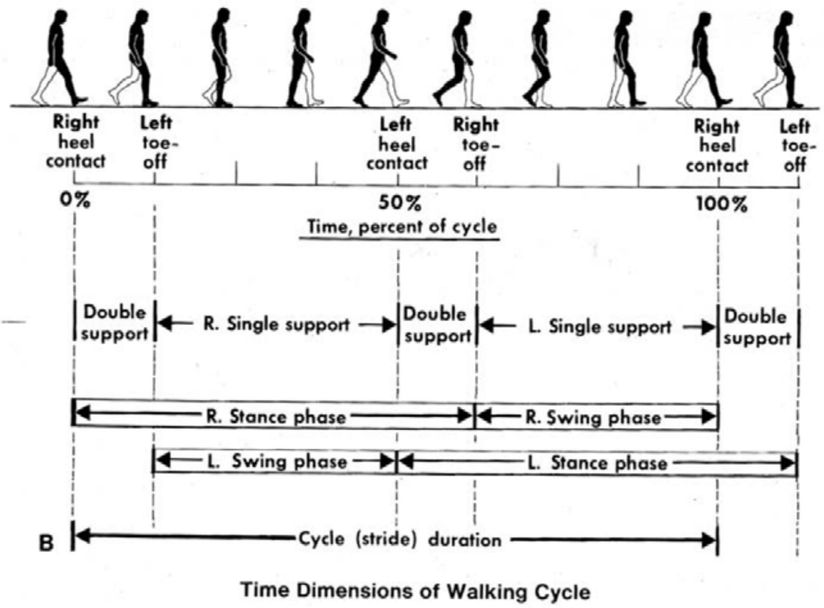

Figure 57 The gait cycle [35]

Characterization of the ankle during level walking was done in three parts, as described by Palmer [36]. The first period of stance was controlled plantar flexion (CP). This phase began at foot strike (FS) and ended at the point where the minimum ankle position was reached. This position was referred to as foot flat (FF). The second period of stance was controlled dorsiflexion (CD), which lasted from FF until the point where the power became positive. In this project, the end of controlled dorsiflexion was detected by identifying the occurrence of the maximum value of angular position. This point corresponds to that chosen by Palmer (zero crossing of power trajectory) since the velocity at a maximum is zero, and power is the product of moment and velocity. The third period that was studied was powered plantar flexion (PP). This began the instant the power became positive and lasted until the foot came off the ground (FO).

5.2.2 Clinical validation of knee angle

MATLAB software programs were developed to perform statistical data analysis. We used standard biomechanical methods which allow us to extract information about various aspects of gait. These methods take the data captured by Vicon cameras and convert it into joint angle trajectories, peak flexion/extension angles and range of motion. We also extracted the same set of parameters from the knee sensor for comparison. The comparison between knee sensor data and Vicon data was performed by calculation the root mean squared error (RMSE).

5.2.3 Subject selection and experimental procedure

Six healthy young adults participated in this research. The subjects had a mean age of 25 (range 23 to 29), a mean body mass of 63 kg (range 52.3 to 73.4), and a mean height of 170.6 cm (range 160 to 182.5). Subjects had no neurological, musculoskeletal, chronic knee problems or gait disorder that results in an abnormal gait pattern. Prior to participation in the study, written informed consent was obtained from each subject.

Subjects must be able to walk at comfortable walking speeds for 2 minutes without interruptions on a treadmill. The subject was asked to wear shorts and sneakers to setup the lower body marker configuration on the skin. The testing session took place in the Motion Analysis Lab and last up to 3 hours for each subject to observe effects due to knee sleeve migration. At the beginning of the lab testing session the subject was asked to walk at three speeds on the treadmill:

- Self-selected comfortable walking speed (CWS)
- Slow speed (30% less than CWS)
- Fast speed (30% more than CWS)

We placed small reflective markers on the subject's lower body for gait analysis by Vicon motion analysis system. The subject was asked to also wear the knee sensor. During each testing session, subjects walked on a treadmill at the speeds listed above for a period of 2 minutes each. For each participant 3 testing sessions were performed. Data from Vicon Motion Capture System and knee sensor were collected simultaneously during the testing sessions. The session was videotaped as well by the Vicon system. The lab was equipped with an 8-camera motion analysis system (Vicon 512, Vicon Peak, Oxford, UK) was used to collect kinematic data for each lower limb during the walking trials. The camera system measured the three-dimensional position of reflective markers, at 120 frames per second. Markers were attached to the pelvis (bilateral anterior superior iliac spines and posterior superior iliac spines), knee (lateral femoral condyles), ankle (lateral malleolus), forefoot (base of the second metatarsal), and heel as shown in Figure 58.

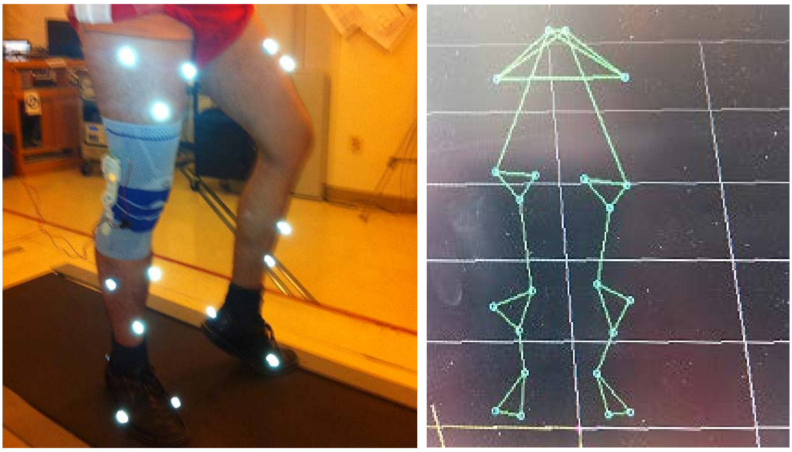

Figure 58 Technical markers positioned for gait analysis

Kinematics were described from the trajectories of reflective markers attached to the lower limbs of the subject. In particular a set of "technical" marker clusters was attached to the skin over bony landmarks of the pelvis and each foot, and the anterior aspects of each thigh and shank. Additional "anatomical" markers were attached to specific anterior bony landmarks of the pelvis and proximal and distal bony landmarks of each femur, tibia and fibula before each block of walking trials for the respective conditions. The technical and anatomical markers were coincidental for the feet. The relative position and orientation of the "technical" marker clusters on the segments defined by the "anatomical" markers was recorded via a static standing calibration trial. The "anatomical" markers for each thigh and shank were then removed prior to the walking trials. Translation-rotation matrices of the respective marker clusters defining each segment were used to quantify the kinematics of the knee of each lower limb during the dynamic walking trials. Moreover the following anthropometric measures were collected, along with motion analysis measures to calculate kinematics and kinetics: body weight, height, leg length (measured from medial malleolus to anterior superior iliac spine), knee width, and ankle width.

5.2.4 Ambulatory activity recognition to contextualize knee angle measurements

At the end of Vicon validation session, each subject was asked to wear the knee tracker system and two times per day he/she had to follow a script with a defined protocol of five different ambulatory activities: “standing”, “sitting”, “walking”, “upstairs”, “downstairs”, as showed in Figure 59.

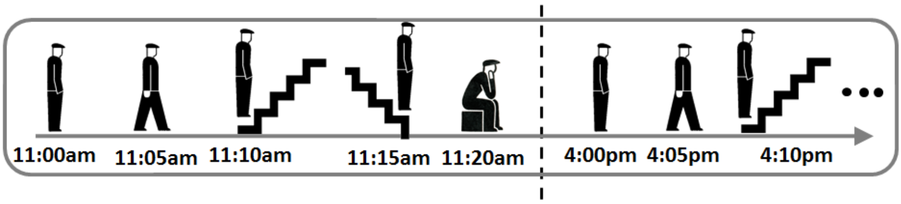

Figure 59 Example of protocol to follow to perform the five ambulatory tasks

During the performed activities, data were collected from the integrated tri-axial accelerometer placed on the right leg and a hierarchical model of activity recognition to contextualize the knee angle measurements was developed. The selected inertial sensor was a MMA7260Q made by Freescale and capable of sensing accelerations ranging from ±1.5g, ±2g and ±6g where g = 9.8m/s^2. The acceleration was sampled at 25 Hz, stored on the SD card on board and the data collection was managed by the application developed on smartphone. The subjects were trained on the use of data collection application. Each subject then collected the activity data in the motion analysis laboratory with the researchers' supervision. We collected approximately 6 hours of the activity data, i.e., 1 hour per subject. Data were collected and processed from the tri-axial accelerometer, features were extracted and a machine learning model was implemented and validated.

5.2.5 Pre-processing and feature extraction

Collected data of accelerometer were digitally filtered (5th order elliptical low-pass, fc = 12 Hz, transition bandwidth 1 Hz, passband tolerance 0.5 dB, minimum stopband attenuation 20 dB, non-causal implementation) to remove high-frequency noise. Further, to separate components related to applied accelerations from those related to body segment orientation changes, a high-pass digital filter was applied (2nd order elliptical, fc = 0.5 Hz, transition bandwidth 0.5 Hz, passband tolerance 0.5 dB, minimum stopband attenuation 20 dB, non-causal implementation). Extraction of epochs for further analysis was performed by sliding a 6s window through the recording to extract the epochs. This resulted in a 50% overlap between successive epochs. Then the following features were extracted per epoch for each axes of accelerometer. The features were chosen to represent characteristics such as orientation, variability, intensity, coordination and signal complexity. The mean value extracted prior to high-pass filtering was calculated as a measure of limb orientation and/or posture (all other features were derived from the high-pass filtered data). The RMS energy for each channel was calculated as a measure of intensity of the overall acceleration applied to each body segment. The modulation of the output of each sensor was used to represent dynamic characteristics of the tasks, and was calculated as the variance and 25th, 75th percentile of each

channel. Large values of this feature were indicative of intervals of rapid movements interspersed with intervals of slow movements. Range was calculated as the maximum peak-to-peak signal value. Large values of range indicated high activity with significant movement of a body segment. An estimate of entropy was calculated as in indicator of the signal complexity. Entropy captures the amount of randomness or the level of unpredictability of a signal. Correlation
coefficient at zero lag between X, Y and Z (two axes at a time) was calculated as an indicator of the coordination of movement. Spectral features extracted were the dominant frequency component (i.e. 0.5 Hz bin with greatest energy) between 0.5 and 12 Hz and the ratio of energy in dominant frequency component to the total energy below 12 Hz, which provide an estimation of how much the signal is dominated by a particular frequency, i.e. its periodicity. The features were extracted for each of the axes (i.e. X, Y and Z). In total we had 30 features extracted summarized in Table 12.

Table 12 Features extracted from accelerometer values

No.	Features Extracted	Description	Measure of
1	*MeanX, MeanY , MeanZ*	Mean acceleration on x, y, z	Orientation
2	*RMSX,RMSY ,RMSZ*	Root-mean-square acceleration on x, y, z	Intensity
3	*VarX, VarY , VarZ*	Variance acceleration on x, y, z	Variability
4	*Perc25thX, Perc25thY ,*	Percentile 25th acceleration	Variability

	Perc25thZ	on x, y, z	
5	*Perc75thX, Perc75thY , Perc75thZ*	Percentile 75th acceleration on x, y, z	Variability
6	*PP_X, PP_Y , PP_Z*	Peak-to-peak acceleration on x, y, z	Smoothness
7	*EntropyX, EntropyY, EntropyZ,*	Entropy acceleration on x, y, z	Complexity
8	*CorXY , CorYZ, CorXZ*	Correlation of acceleration for pairs of xy, yz, xz	Coordination
9	*DomFreqX, DomFreqY, DomFreqZ*	Dominant frequency acceleration on x, y, z	Smoothness
10	*EnRatioDomFreqX, EnRatioDomFreqY, EnRatioDomFreqZ*	Energy ratio dominant frequency acceleration on x, y, z	Smoothness

5.2.6 Classification

The classification of ambulatory activities was performed implementing the artificial neural network (ANN) multilayer perceptron (MLP) [37]. MLP is based on the back-propagation technique and is one of the most common neural network structures as they are simple and effective. The structure of the developed multilayer perceptron consists of three levels or neuron layers: the input level, the level of hidden layers and the output level as showed in Figure 60.

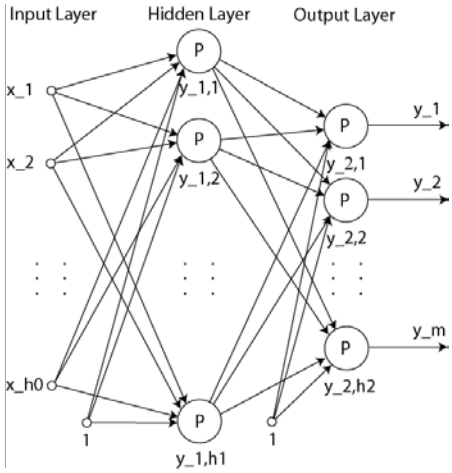

Figure 60. ANN graphical scheme

The network adapts the different weights during its learning process. The changes during the learning process are: the destruction, modification and creation of connections between neurons. In the biological systems exists a continuous process of creation and destruction of connections between neurons. In ANN a creation of a connection is equivalent to giving its weight a value different from zero. When a weight with a non-zero value is substituted with a zero, a connection is destroyed. The problem of building a neural network can be, in short, formulated as follows: given a set of input data with dimension n within a domain D_{in} and a set of output data with dimension m within a domain D_{out}, a neural network is a function:

$$f^n : D_{in} \rightarrow D_{out}$$

in such a way that an error function is minimum for that training data set. We aim to create a non-linear functional mapping between spaces of many dimensions. MLP was consisting of 30 input neurons, 18 hidden neurons and 5 output neurons. All neurons used sigmoid functions. Initial parameters were learning rate 0.3 and momentum 0.2. A momentum based weight update was used in training performed for 500 epochs.

5.3 Results and Discussion

Before start with the data collection from Vicon system and the wearable knee sensor, the first step for clinical validation of the device was the characterization of the integrated electro-goniometer. The knee tracker device was attached to the arms of a plastic protractor using double-sided tape on the base of the end pieces and single-sided tape around the end plate and protractor arm. The calibration of the plastic goniometer had been checked previously using an accurate vernier scale metal protractor and was found to be accurate to less than a degree. The continuous voltage that varies with electro-goniometer angles was stored on SD card. In order to test the system's stability the protractor was set to 0° and the electro-goniometer was zeroed in that position. The output from the electro-goniometer was recorded for 5 seconds at 50 hertz (250 readings) for each position, in ten degrees of increment until the maximum range of rotation of 160 degrees. The precision of the electro-goniometer, defined as ‘the repeatability with which a measured value can be obtained’, was determined at each increment by calculating the standard deviation of the 250 readings around the mean value for that increment. The device was found to exhibit a high level of precision throughout the range with a maximum standard deviation of less than 0.4% of the measurement range (equivalent to 0.25°).The experiment was repeated with the sampling taking place over one hour and similar results were obtained. The response of the sensor was measured monitoring the change of voltage value, related to the selected angles. The calibration curve was determined by plotting the average voltage values against the angle value increments from -20 to 140 degrees. The best fitting was obtained using a polynomial curve of third order as shown in Figure 61.

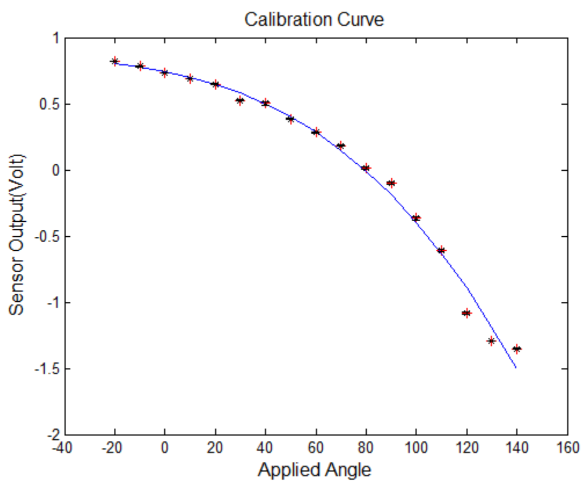

Figure 61 Relationship between angle applied and sensor Output

The equation of this line was $Y = -2.77 \cdot 10^{-7}X^3 - 4.96 \cdot 10^{-5}X^2 - 0.0037X + 0.7427$. The model showed a highly significant correlation between the applied angle and sensor output. Given the limitations of the plastic protractor these results seem acceptable for clinical use of the electro-goniometer. The experiment was repeated a further four times and a little variation was found. Maximum absolute residual errors were equivalent to less than 3° with the average error below 1° in all five tests. It appears from these results that the calibrated response of the system is repeatable over time. After tests of calibration, data were collected from the enrolled subjects performing the tests sessions described above on treadmill with Vicon motion capture system and wearing the novel knee tracker. During the acquisition, both the systems were synchronized to compare the signals. Vicon data were processed applying the model for the lower extremity and extracting the knee angles of gait cycle. In figure Figure 62 is shown the comparison between the mean knee angle trace recorded by the knee tracker and mean knee angle recorded by the Vicon System for the right knee.

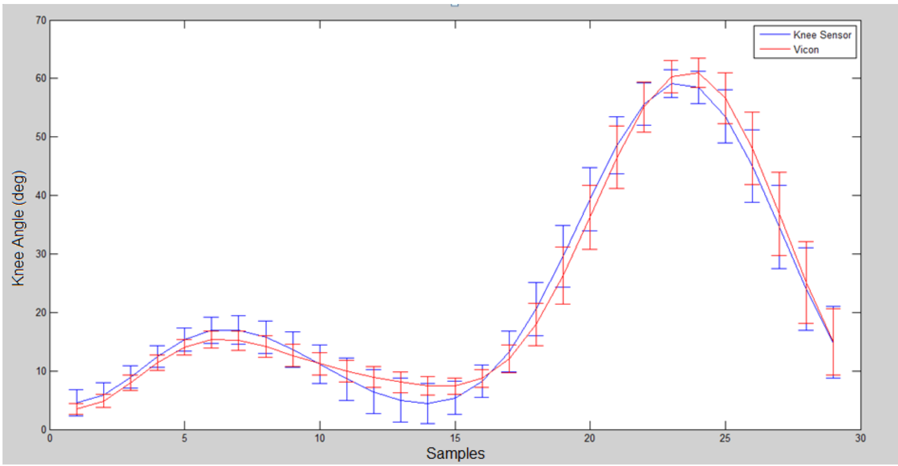

Figure 62 Comparison of mean knee angle Vicon vs wearable knee tracker

The plot showed that there was a good agreement between the two systems in terms of the pattern, timing and range of joint angles used. An important clinical parameter extracted from the knee angle was the range of motion (RoM) as showed in Figure 63. The mean difference was 1.5° with a standard deviation of 2.8°. Slight differences were due in the definitions of joint axes, differences in soft tissue movements between the electro-goniometers and the markers or the effect of the curve smoothing routines and filters incorporated into the Vicon data capture process. The overall correlation of all angular measurements was 0.99 and the overall RMSE was 2.72.

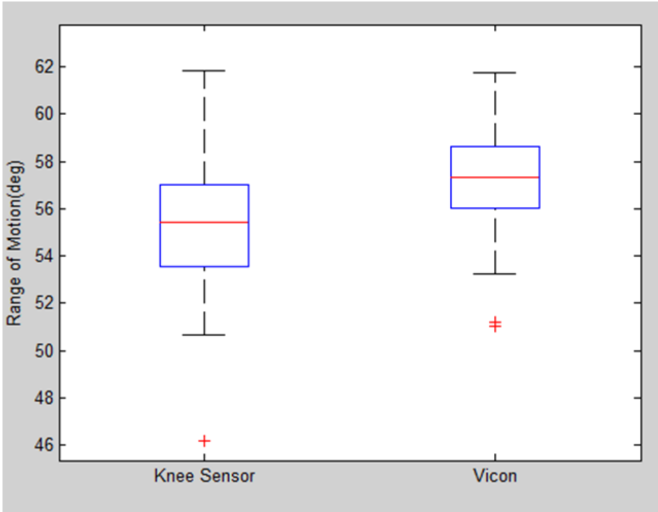

Figure 63 Box plot Range of motion of knee sensor and Vicon

After validation of the knee angle extracted from the wearable knee system, data collected from the tri-axial accelerometer were pre-processed and features were extracted as described in section 5.2.5. The labeled raw accelerometer data were transformed into examples containing 30 features and covering 6 healthy subjects. This formed a balanced dataset subsequently used for training and testing. The only exception was for the postures standing and sitting because as one would expect, these postures do not exhibit any regular periodic behavior and all of the acceleration values are relatively constant. As mentioned earlier, the primary differences between these activities is the relative magnitudes of values for each axis, due to the different orientations of the device with respect to the Earth when the user is sitting and standing. Thus it appears easy to differentiate between sitting and standing, even though neither involves much movement. For this reason at the top level of the hierarchy the set of 5 classes was split into 2 categories (posture and activity) using a simple threshold-based approach similar to that of Mathie et al. [38]. For all six subjects, 100% sensitivity and 0% misclassification were achieved by the following criteria:

1. If root mean square of right thigh accelerometer (anteroposterior axis) is greater than 0.08, task is activity; otherwise, task is posture.
2. If task is posture and mean of right thigh accelerometer (up-down axis) is high (e.g. greater than 0.6 g), subject is standing; otherwise, subject is sitting.

The three remaining tasks of activities: “walking”, “upstairs” and “downstairs” were classified applying the MLP described in section 5.2.6. The confusion matrix is reported in Table 13. Each activity is classified applying the leave one subject out cross validation.

Table 13 Confusion matrix obtained using all 30 features and applying the leave one out cross validation

			CLASSIFIED AS		
			Walking	**Up_Stairs**	**Dwn_Stairs**
ACTUAL CLASS	Subject 1	**Walking**	193	0	0
		Up_Stairs	0	158	0
		Dwn_Stairs	0	2	149
	Subject 2	**Walking**	173	0	0
		Up_Stairs	0	161	0
		Dwn_Stairs	0	0	154
	Subject 3	**Walking**	188	0	0
		Up_Stairs	0	156	0
		Dwn_Stairs	0	0	140
	Subject 4	**Walking**	131	0	0
		Up_Stairs	0	164	1
		Dwn_Stairs	0	0	156
	Subject 5	**Walking**	168	0	0
		Up_Stairs	0	173	0
		Dwn_Stairs	0	1	162
	Subject 6	**Walking**	159	0	0
		Up_Stairs	0	146	0
		Dwn_Stairs	0	0	151

Using all the 30 features we achieved accuracies above 99%. Walking appears easier to identify than upstairs and downstairs. It seems to make sense, since walking shows different patterns changes in acceleration. Even if appears much more difficult to identify the two stair climbing activities, simply because those two activities are very similar sometimes, we were able to obtain a very encouraging percentage of classification of more than 98% for both tasks. We obtained this result also because we estimated an appropriated window length for feature extraction. So far we have used a 6 sec window length for feature extraction based on empirical observation. In Figure 64 we can see a bar plot of MLP classification error for window lengths from 1s to 12s.

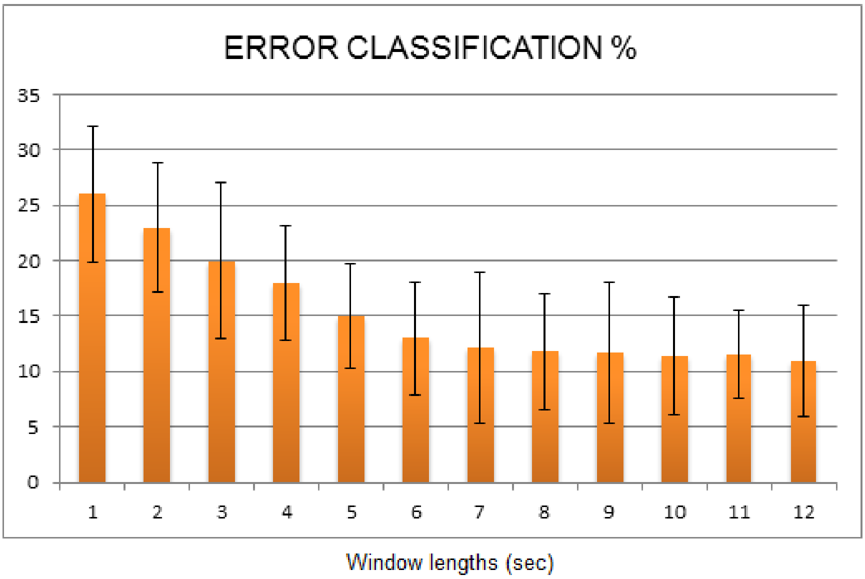

Figure 64 MLP Classification error for variable window lengths

There is ~2% gain as we go from 6s to 7s, but after 7s we do not gain much in terms of classifier accuracy by increasing the window length. This result is close what was earlier reported by Bao et al [39]. After this analysis, we tried to simplify the model and reduce the computational costs for a possible development of an embedded software with a good accuracy of activity recognition. In particular features were selected applying the Relief Ranking method [40] and applying the Davies Boulding

(DB) index [41] by incrementally adding each ranked feature. The DB index was extracted and reported in Figure 65.

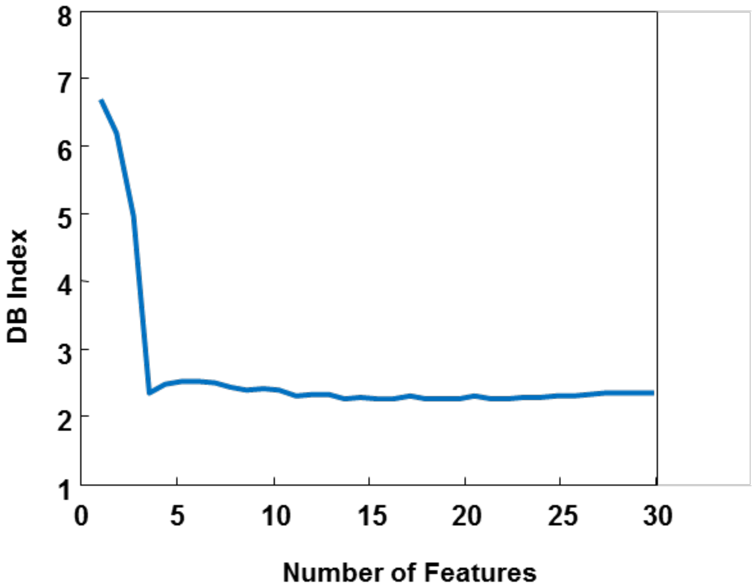

Figure 65 Extraction of DB index

Thus, the application of the DB index for the ranked features yielded the reduction of the feature space, by the elimination of redundant or less significant features. This method provided an ordered list of inclusion from the most to less discriminant features. We choose to include in the following step of classification the minimum number of features yielding the lowest DB index. Thus, the input feature vector for classifiers was Xi = [Mean_X, Correlation_XY, RMS_Y, Entropy_Y], that is the mean value of the acceleration of the anterior/posterior axes, the correlation between anterior/posterior and up/down axes and the root mean square of up/down axes. In Figure 66 we performed a visual inspection of the selected feature space. To perform this operation was necessary to reduce the dimensionality by selecting features that captured the characteristic accelerometer patterns associated with different tasks. Principle Component Analysis (PCA) is one of the most popular dimensionality reduction techniques. In order to reduce computational complexity and minimize the influence of redundant features, a PCA was applied to the feature set, and the first 2 PCs were used for performing scatter plots as shown in Figure 66.

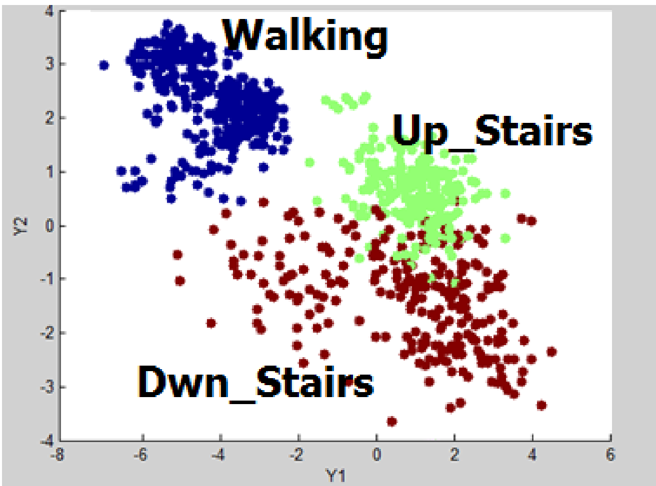

Figure 66 Scatter plot of the 1st and the 2nd principal components

We can clearly see that points belonging to the same task tend to cluster together. The task down_stairs has a larger spread. This higher variability implies that some examples overlap with the class up_stairs. In Table 14 we can see the results of multilayer classification provided with the confusion matrix and using the leave-one-subject-out validation.

Table 14 Confusion matrix obtained using the 4 selected features and applying the leave one out cross validation

			CLASSIFIED AS		
			Walking	**Up_Stairs**	**Dwn_Stairs**
ACTUAL CLASS	Subject 1	**Walking**	193	0	0
		Up_Stairs	0	157	1
		Dwn_Stairs	0	4	147
	Subject 2	**Walking**	173	0	0
		Up_Stairs	0	159	2
		Dwn_Stairs	0	1	153
	Subject 3	**Walking**	188	0	0
		Up_Stairs	0	156	0
		Dwn_Stairs	0	4	136
	Subject 4	**Walking**	131	0	0
		Up_Stairs	0	154	11
		Dwn_Stairs	0	6	150
	Subject 5	**Walking**	168	0	0
		Up_Stairs	0	157	16
		Dwn_Stairs	0	1	162
	Subject 6	**Walking**	159	0	0
		Up_Stairs	0	143	3
		Dwn_Stairs	0	14	137

The mean classification was less than the previous model, but more than 90%. This error was mainly due to the high similarity of upstairs and downstairs patterns and the reduced resolution obtained reducing the number of features.

5.4 Conclusions

The design, software architecture and human testing of a novel wearable system for monitoring a patient's knee function during daily activities over extended periods of time has been developed and evaluated in this work. The key features of the system include: a compact, lightweight design integrated in a knee sleeve solution with knee flexion/extension monitoring capabilities through a low cost electro-goniometer, a strain gauge sensor to guarantee the correct position and the reliability of gathered data, a triaxial accelerometer to contextualize the knee kinematics with daily activities. The integrated electrogoniometer validated with Vicon system proved to be a useful measurement system which gave joint angles of similar magnitude to those reported for gait and stair climbing. Minor differences were observed between the results of the electrogoniometer and Vicon systems in terms of the mean range of motion, the mean maximum and mean minimum angles, and the mean pattern calculated for individual cycles. Whatever the cause of the errors, the differences in calculated angle were small, of the order of two or three degrees, which is acceptable for the clinical evaluation of patients with musculoskeletal problems. The results of this experiment indicate the two systems show a high degree of concurrent validity. It should be remembered however that both systems measure intersegmental motion using surface attachments. If soft tissue movement is a significant factor then the results of both systems may be invalid measures of the true angulation of the underlying bones. In this experiment the markers were attached to prominent bony landmarks on the lower limb in an established fashion and the wearable knee tracker was attached to the knee sleeve running down the limb segments. In summary, the results of this study indicate that the integrated electrogoniometer is stable, precise, accurate and repeatable in performance when tested on the laboratory bench. Small hysteretic effects and inaccuracies are present in the devices but these are of the order of 1° or 2°. Moreover we demonstrated that implementing an artificial neural network with the integrated tri-axial accelerometer we achieved the classification of physical activities with accuracy more than 90% also with the selected feature subset. This means that the choice of Relief method and DB index was appropriate for the feature selection. In the next future the developed model will be integrated in the wearable system. The integrated strain gauge is capable of giving meaningful clinical data with a high degree of cost and time efficiency. The system would appear to be a scientific and cost effective method of carrying out this type of investigation. This system will provide possibilities for identifying problems that may not be easily recognizable during supervised lab inspections or clinical visits. This applies e.g. to changes in gait symmetry, compensation movements during prolonged walking as caused by tiring as well as changes in activity level. Our approach has the potential to provide outside the lab, unconstrained measurements of knee function during challenging activities. We expect to observe differences in situations where stability of the knee with an endoprosthesis is limited and to measure gait activities of everyday life including stair ascent and descent as a useful supplement to the medical examination. This system may be also an useful tool for long-term gait monitoring during appropriate exercise programmes of gait re-education in stroke patients.

5.5 References

[1]. Cappozzo A, Della Croce U, Leardini A, Chiari L: Human movement analysis using stereophotogrammetry. Part 1: theoretical background. Gait and Posture 2005, 21:186-196.

[2]. H. J. Luinge, P. H. Veltink, “Measuring orientation of human body segments using miniature gyroscopes and accelerometers,” Med Biol Eng Comput, vol. 43, no. 2, pp. 273-282, 2005.

[3]. N. Yaikwawongs, N. Limpaphayom, V. Wilairatana, “Reliability of Digital Compass Goniometer in Knee Joint Range of Motion Measurement,” J Med Assoc Thai, vol. 92, no. 4, pp. 517-522, 2009.

[4]. R. Takeda, S. Tadano, A. Natorigawa, M. Todoh, S. Yoshinari, “Gait posture estimation using wearable acceleration and gyro sensors,” J Biomech, vol. 42, no. 15, pp. 2486-2494, 2009.

[5]. B. Kemp, J. M. W. Janssen, B. van der Kamp, “Body position can be monitored in 3D using miniature accelerometers and earth-magnetic field sensors, ” Electroencephalogr Clin Neurophysiol, vol. 109, no. 6, pp. 484-488, 1998.

[6]. A. M. Sabatini, “Quaternion-Based Extended Kalman Filter for Determining Orientation by Inertial and Magnetic Sensing,” IEEE Trans Biomed Eng, vol. 53, no. 7, pp. 1346-1356, July 2006.

[7]. R. Williamson, B. J. Andrews, “Detecting absolute human knee angle and angular velocity using accelerometers and rate gyroscopes,” Med Biol Eng Comput, vol. 39, no. 3, p. 1-9, 2001.

[8]. J. Favre, X. Crevoisier, B. M. Jolles, K. Aminian, “Evaluation of a mixed approach combining stationary and wearable systems to monitor gait over long distance,” J Biomech, vol. 43, no. 11, pp. 2196-2202, 2010.

[9]. L. Kun, Y. Inoue, K. Shibata, C. Enguo, “Ambulatory Estimation of Knee-Joint Kinematics in Anatomical Coordinate System Using Accelerometers and

Magnetometers," IEEE Trans Biomed Eng, vol. 58, no. 2, pp. 435-442, February 2011.

[10]. C. Peng and B. Oelmann, "Joint-Angle Measurement Using Accelerometers and Gyroscopes. A Survey," Instrumentation and Measurement, IEEE Transactions on, vol. 59, pp. 404-414, 2010.

[11]. P. H. Veltink and D. De Rossi, "Wearable technology for biomechanics: e-textile or micromechanical sensors? [Conversations in BME]," Engineering in Medicine and Biology Magazine, IEEE, vol. 29, pp. 37-43, 2010.

[12]. Rowe P. The evaluation of the functional ability of total hip replacement patients. University of Strathclyde, Glasgow UK. 1990: PhD Thesis., Nicol AC. A new flexible electrogoniometer with widespread applications. Biomechanics XB, Human Kinetics, 1987, 1029–34.

[13]. Rowe PJ, Nicol AC, Kelly IG. Flexible goniometer computer system for the assessment of hip function. Clinical Biomechanics award paper. Clin Biomech 1989;4:68–72.

[14]. Sato, T.O.; Hansson, G.A.; Coury, H.J.C.G. Goniometer crosstalk compensation for knee joint applications. Sensors 2010, 10, 9994–10005.

[15]. P. T. Gibbs and H. H. Asada, "Wearable Conductive Fiber Sensors for Multi-Axis Human Joint

Angle Measurements," J Neuroeng Rehabil, vol. 2, p. 7, Mar 2 2005.

[16]. A. Tognetti, et al., "Body segment position reconstruction and posture classification by smart textiles," Transactions of the Institute of Measurement and Control, vol. 29, pp. 215-253, August 1, 2007.

[17]. Bao, L. and Intille, S. 2004. Activity Recognition from User- Annotated Acceleration Data. Lecture Notes Computer Science 3001, 1-17.

[18]. Krishnan, N., Colbry, D., Juillard, C., and Panchanathan, S. Real time human activity recognition using tri-Axial accelerometers. In Sensors, Signals and Information Processing Workshop, 2008.

[19]. Krishnan, N. and Panchanathan, S. 2008. Analysis of Low Resolution Accelerometer Data for Continuous Human Activity Recognition. In IEEE International Conference on Acoustics, Speech and Signal Processing, (ICASSP 2008). Pages 3337-3340.

[20]. Tapia, E.M., Intille, S.S. et al. 2007. Real-Time recognition of physical activities and their intensities using wireless accelerometers and a heart rate monitor. In Proceedings of the 2007 11th IEEE International Symposium on Wearable Computers, 1-4.

[21]. Mannini, A. and Sabatini A.M. 2010. Machine learning methods for classifying human physical activity

from on body accelerometers. In Sensors 2010, 10, 1154-1175.

[22]. Foerster F. and Fahrenberg J. 2000. Motion pattern and posture: correctly assessed by calibrated accelerometers. In Behavior Research Methods, Instruments, & Computers, 32(3), 450–7.

[23]. Parkka, J., Ermes, M., Korpipaa, P., Mantyjarvi, J., Peltola, J., and Korhonen, I. 2006. Activity classification using realistic data from wearable sensors. In IEEE Transactions on Information Technology in Biomedicine, 10(1), 119-128.

[24]. Lee, S.-W. and Mase, K. 2002. Activity and location recognition using wearable sensors. In IEEE Pervasive Computing, 1(3):24–32.

[25]. Subramanya, A., Raj, A., Bilmes, J., and Fox, D. 2006. Recognizing activities and spatial context using wearable sensors. In Proceedings of the 22nd Conference on Uncertainty in Artificial Intelligence.

[26]. Maurer, U., Smailagic, A., Siewiorek, D., & Deisher, M. 2006. Activity recognition and monitoring using multiple sensors on different body positions. In IEEE Proceedings on the International Workshop on Wearable and Implantable Sensor Networks,3(5).

[27]. Choudhury, T., Consolvo, S., Harrison, B., LaMarca, A., LeGrand, L., Rahimi, A., Rea, A., Borriello, G., Hemingway, B., Klasnja, P., Koscher, K., Landay, J.,

Lester, J., Wyatt, D., and Haehnel, D. 2008. The mobile sensing platform: An embedded activity recognition system. In IEEE Pervasive Computing, 7(2), 32-41.

[28]. Cho, Y., Nam, Y., Choi, Y-J., and Cho, W-D. 2008. Smart-Buckle: human activity recognition using a 3-axis accelerometer and a wearable camera. In HealthNet.

[29]. Long, X., Yin, B., and Aarts, R.M. 2009. Single accelerometer- based daily physical activity classification. In 31st Annual International Conference of the IEEE EMBS, 6107-6110

[30]. Lee, M., Kim, J., Kim, K., Lee, I., Jee, S.H., and Yoo, S.K. 2009. Physical activity recognition using a single tri-axis accelerometer. In Proceedings of the World Congress on Engineering and Computer Science 2009, 1.

[31]. Shimmer research, http://www.shimmer research.com.

[32]. M. J. Mathie, A. C. Coster, N. H. Lovell, B. G. Celler, “Accelerometry: providing an integrated, practical method for longterm, ambulatory monitoring of human movement,” Physiol Meas, vol. 25, no. 2, pp. R1-20, 2004.

[33]. Levis P et al. TinyOS: an operating system for sensor networks ambient intelligence. In: Weber W et al., editors. Ambient intelligence. Berlin Heidelberg: Springer; 2005. p. 115–48.

[34]. Hamill, J.a.K., K., Biomechanical Basis of Human Movement. 2 ed. 2003, Philadelphia: Lippincott Williams & Wilkins.

[35]. Inman, V.T., H.J. Ralston, and F. Todd, Human Walking. 1981, Baltimore, MD.:Williams & Wilkins.

[36]. Palmer, M., Sagittal plane characterization of normal human ankle function across a range of walking gait speeds, Masters Thesis, Massachusetts Institute of Technology, 2002.

[37]. RO Duda, PE Hart, DG Stroke, “Pattern Classification”, 2nd edition, Wiley Interscience, 2001.

[38]. Mathie MJ, Celler BG, Lovell NH, Coster ACF: Classification of basic daily movements using a triaxial accelerometer. Medical & Biological Engineering & Computing 2004, 42:679-687.

[39]. L. Bao and S. S. Intille, "Activity recognition from user-annotated acceleration data," in Proceedings of PERVASIVE 2004, vol. LNCS 3001.

[40]. ReliefF M. Robnik-Sikonja and I. Kononenko, BTheoretical and empirical analysis of ReliefF and RReliefF, Mach. Learn. J., vol. 53,pp. 23–69, 2003.

[41]. J. C. Bezdek and N. R. Pal, BSome new indexes of cluster validity, IEEE Trans. Syst., Man, Cybern., vol. 28, pp. 301–315, 1998.

Final Remarks

The potential impact of PHS on the clinical practice of medicine and rehabilitation is remarkable. A significant shift in focus is possible thanks to wearable technology. While the main focus of clinical assessment techniques is currently on methods that are implemented in the clinical setting, wearable technology has the potential to redirect such focus on field recordings. This is expected to allow clinicians to eventually benefit from both data gathered at home and in the community settings during the performance of activities of daily living and data recorded in the clinical setting under controlled conditions. Complementarities are expected between field and clinical evaluations. Future research will surely address optimal ways to combine these two types of assessment to optimize the design of rehabilitation interventions. The purpose of this PhD work has been the development and characterization of PHS and soft computing models for early diagnosis and long term personalized treatment. In order to achieve this goal an innovative large scale screening methodology for heart sound classification, a wireless architecture and methodology to evaluate the muscular fatigue, novel ergonomic devices for long term monitoring of patients with cardiovascular diseases and lower limb injuries have been designed and characterized. The focus on enhanced body devices supported by soft computing approach represents an important milestone to gain the continuity of care and a new person centric model. During my PhD, my research activity was focused also on development of soft computing models to analyze pulmonary diseases, which results were reported in international medical journals. Finally, I actively participated as Co-investigator of EU-projects to develop PHS and advanced ICT solutions.

Publications

Most of the material of this thesis has been published in the following international journals:

- **G. Tartarisco**, L. Billeci, G. Ricci, L. Volpi, G. Pioggia, G. Siciliano, “A personal monitoring architecture to detect muscular fatigue in elderly”, Neuromuscular Disorder, vol. 22, pp. 192-197, Dec 2012.

- **G. Tartarisco**, G. Baldus, D. Corda, R. Raso, M. Ferro, A. Gaggioli, G. Pioggia, “Personal Health System architecture for stress monitoring and support to clinical decisions”, Computer Communications, vol. 35, pp. 1296-1305, June 2012.

- H. Solar, E. Fernández, **G. Tartarisco**, G. Pioggia, B. Cvetković, S. Kozina, M. Luštrek, J. Lampe, “A non-invasive, wearable sensor platform for multi-parametric remote monitoring in CHF patients”, Lect Notes Comput Sc, vol. 7251, pp.140-147, 2012.

- A. Gaggioli, G. Pioggia, **G. Tartarisco**, G. Baldus, M. Ferro, P. Cipresso, S. Serino, A. Popleteev, S. Gabrielli, R. Maimone, G. Riva, “A system for automatic detection of

momentary stress in naturalistic settings", Stud Health Technol Inform, vol.181, pp.182-6, 2012.

- M. Pifferi, A. Bush, G. Pioggia, D. Caramella, **G. Tartarisco**, M. Di Cicco, M. Zangani, I. Chinellato, F. Maggi, G. Tezza, P. Macchia, A. Boner, "Evaluation of pulmonary disease using static lung volumes in primary ciliary dyskinesia", Thorax, vol. 67, pp. 993-9, 2012.

- M. Pifferi, A. Bush, F. Montemurro, G. Pioggia, M. Piras, **G. Tartarisco**, MD. Cicco, I. Chinellato, AM. Cangiotti, AL. Boner, "Rapid diagnosis of primary ciliary dyskinesia: cell culture and soft computing analysis", Eur Respir J., in press, Aug 2012.

- A. Gaggioli, P. Cipresso, S. Serino, G. Pioggia, **G. Tartarisco**, G. Baldus, D. Corda, G. Riva, "An open source mobile platform for psychophysiological self-tracking", Stud Health Technol Inform, vol. 173; pp. 136-138, 2012.
- S. Serino, P. Cipresso, **G. Tartarisco**, G. Baldus, D. Corda, G. Pioggia, A. Gaggioli, G. Riva, "An Event-Driven Psychophysiological Assessment for Health Care", Proceedings 2nd International Workshop on Computing Paradigms for Mental Health, pp. 25-34, SciTe Press, 2012.

- G. Crifaci, **G. Tartarisco**, L. Billeci, G. Pioggia, A. Gaggioli, “Innovative technologies and methodologies based on integration of virtual reality and wearable systems for psychological stress treatment”, International Journal of Psychophysiology, vol. 85, pp. 402-6, 2012.
- L. Billeci, E. Brunori, G. Crifaci, **G. Tartarisco**, “Skin conductance monitoring during relaxation in anorexia nervosa adolescents by wearable sensors combined with wireless technologies”, International Journal of Psychophysiology, vol. 85, pp. 373-8, 2012.
- A. Gaggioli, G. Pioggia, **G. Tartarisco**, G. Baldus, D. Corda, P. Cipresso, G. Riva, “A Mobile Data Collection Platform for Mental Health Research”, Pers Ubiquit Comput, 2011.

And it has been presented and published on IEEE international conferences:

- G. Pioggia, N. Carbonaro, G. Anania, A. Tognetti, **G. Tartarisco**, M. Ferro, D. De Rossi, A. Gaggioli, G. Riva, “Interreality: The use of advanced technologies in the assessment and treatment of psychological stress”, in proceedings of 10th IEEE International Conference on Intelligent Systems Design and Applications (ISDA), pp. 1047 - 1051, Cairo, 2010.

- G. Pioggia, **G. Tartarisco**, G. Ricci, L. Volpi, G. Siciliano, S. Bonfiglio, "A wearable pervasive platform for the intelligent monitoring of muscular fatigue", in proceedings of 10th IEEE International Conference on Intelligent Systems Design and Applications (ISDA), pp. 132 - 135, Cairo, 2010.

And in deliverables of the following European project:

- **Tartarisco G.**, Tonacci A., Sicari R., Baldus G., Corda D., Gargani L., Pioggia G. (2012), "A wearable sensing set for the measurement of the ECG signals – Design and Clinical assessment" Deliverable 2.2.2, European Project CHIRON (FP7 n. 100228), WORKPACKAGE: WP2, Sensor nodes and multi-parametric monitoring.
- **Tartarisco G.**, Baldus G., Corda D., Ferro M., and Pioggia G. (2012), "Decision Support Processing Architecture", Deliverable 5.2, European Project INTERSTRESS (FP7 n. 247685), WORKPACKAGE: WP5, Decision Support System.
- **Tartarisco G.**, Baldus G., Corda D., Billeci L., Ruta L., and Pioggia G. (2012), "Report on Functional/Non Functional Requirements", Deliverable 1.2, European Project MICHELANGELO (FP7 n. 288241), WORKPACKAGE:

WP1, Requirement Gathering and Analysis – Design of the overall system architecture.

- Visintainer, F., **Tartarisco G.**, Muro, M., Carlino, A., Kalogirou, K., Contreras, J., Pioggia, G., and Ferro, M. (2010), “Two vehicle demonstrators for elderly drivers support”, Deliverable 3.4.1, European Project OASIS (FP7 n. 215754), WORKPACKAGE: WP3.4, Personal mobility, ACTIVITY: A3.4.2, Driver telematic support services; A3.4.3, Driver comfort support services.

Acknowledgements

During these three years I was very lucky. I had the opportunity to travel a lot discovering new places and to work with several researchers around the world, having a lot of advice, inspiration, support and fruitful discussions to became one day a researcher.
A special thanks is for my tutor Giovanni Pioggia who was not only an important scientific guidance but also a great friend. Since the first moment he was able to discover my skills to coordinate research activities, and involved me as co-investigator in several EU-project, giving me the opportunity to collaborate with important scientific research groups and industrial partners such as FIMI a division of Philips Medical Systems.
In this period I had also a great experience as a PhD visitor of six months in Boston at Harvard medical school, Spaulding Rehabilitation Hospital, where I had the opportunity to work with prof. Paolo Bonato and his team, leader of rehabilitation technology with special emphasis of wearable systems, learning a lot from their scientific research approach. A special thanks is for Alessandro who helped and inspired me to pursue this dream!
Many thanks to all the group that worked with me and in particular to Giovanni and Daniele, the two brothers of Sardinia always by my side!

Very special thanks to my family for their love and support. Finally I want to thanks my brother Antonio the best young qualified engineer and supporter of my career. Thanks to him most of time I find the strength to go on! “He just take a look to understand always what I mean!”.